2013-05-17

Isolation, Characterization and Synthesis of Asthma Inducing Fungal Glycolipid and Analytical Method Development for Novel Antimicrobial Peptide Mimics

Vinod Chaudhary
Brigham Young University - Provo

Isolation, Characterization and Synthesis of Asthma Inducing Fungal Glycolipid and Analytical Method Development for Novel Antimicrobial Peptide Mimics

Vinod Chaudhary

A dissertation submitted to the faculty of
Brigham Young University
in partial fulfillment of the requirements for the degree of

Doctor of Philosophy

Paul B. Savage, Chair
Steven L. Castle
Matt A. Peterson
Joshua L. Price
Steven G. Wood

Department of Chemistry and Biochemistry

Brigham Young University

May 2013

ABSTRACT

Isolation, Characterization and Synthesis of Asthma Inducing Fungal Glycolipid and Analytical Method Development for Novel Antimicrobial Peptide Mimics

Vinod Chaudhary
BYU, Department of Chemistry and Biochemistry
Doctor of Philosophy

NKT cells are an important part of human immune system and recognize a specific set of antigens called glycolipids. Only a handful of "natural" NKT cell antigens are known till date. Although NKT cells play a protective role against pathogenic organisms, imbalances in NKT cell functions are implicated in many diseases including asthma. Allergic asthma, a Th2 driven inflammation of airways, is primarily caused by inhalation of environmental allergens. In the last decade, inhaled allergen *Aspergillus fumigatus* has been under scrutiny for the presence of NKT cell antigens that might trigger asthma. We successfully isolated, characterized and synthesized a "natural" antigenic glycolipid which activates NKT cells in CD1d dependent manner. When this glycolipid is administered intranasally to mice, WT but not CD1d-/- mice developed airway hyperreactivity (AHR), which is a cardinal feature of asthma. Our results indicate that this glycolipid also triggers the production of key cytokines responsible for development of airway hyperreactivity, namely IL-4 and IL-13

Widespread use of antibiotics has convoluted the problem of antimicrobial resistance. Our research group has developed a novel class of antimicrobial peptide mimics called Ceragennins. These cholic acid based antimicrobial compounds have many desirable properties including low MICs, effectiveness against biofilms, and relatively low manufacturing cost. In order to advance the clinical development of Ceragennins, we developed analytical methods for qualitative and quantitative determination of these compounds in complex biological matrices. These methods were also used for carrying out the stability studies of Ceragenins under varying pH and temperatures.

Keywords: NKT cells, Aspergillus, Glycolipids, Antimicrobial peptide mimics, Analytical method development

ACKNOWLEDGMENTS

Firstly, I would like to thank Dr. Savage for the direction and vision he provided me during my PhD program. I will always remember him as an enthusiastic and motivated researcher. I am also very grateful to the Deartment of Chemistry and Biochemistry at BYU for their support.

I would like to express my gratitude towards my coworkers including Dr. Shenglou Deng, Yubo Li, Sara Mata, Jason Snaar, and Dr. Xiaobo Gu. I am also thankful for all the undergraduate students who worked with me during my stay at BYU. I would like to specially thank Brian Anderson for not only his advice and support in the lab, but also helping me understand the American culture. I would also like to thank our collaborators at Harvard Medical School, Scripps Research Institute, and University of Chicago. Their efforts and ideas made this dissertation more relevant and interesting.

I am always indebted to my parents for their love and support. I would especially like to thank my sister for giving me directions in life, whenever I felt lost, and for having faith in my abilities. Finally, I would like to thank my wife, Veena, for her love, support, belief, and sacrifice during this testing phase of my life. I am also thankful to my daughters Ishita and Shriya for the unconditional love and affection they have for me. When the time was testing my patience and abilities, their laughter, hugs and kisses kept me motivated and kept me sane.

Contents

List of Figures

List of Schemes

Chapter 1

Role of NKT cells in immune system

1.1 NKT cells and adaptive immune system

The immune system encompasses a powerful collection of defense mechanisms which are fundamental to our survival. Over the eons, the mammalian immune system has grown in sophistication to differentiate between self and non-self components. The immune system can be subdivided into two categories: the innate or natural immune system and the acquired or adaptive immune system. Although the innate immune system is the first responder to an infection, it is nonspecific and easier to evade. On the other hand, the adaptive immune system refers to the "antigen specific" defense mechanisms that eliminate or prevent microbial infections. Specificity and memory are the cardinal features of the adaptive immune system, which enables it to mount a more effective response to re-occurring infections.

Natural Killer T cells (NKT) are a subset of T lymphocytes that bridge the gap between

innate and adaptive immunity.[1] These cells are named NKT because they express surface markers characteristic of both, natural killer (NK) cell associated markers[2] (NK1.1 and CD161) and conventional T cell markers (such as TCR). NKT cells undergo selection in the thymus and are abundantly present in the spleen, liver, bone marrow and lungs.[3] These cells recognize CD1d, which is an antigen presenting molecule expressed on the surface of various antigen presenting cells and recognizes foreign lipid and glycolipid antigens. Once the CD1d presented ligands are recognized by the NKT cells, a cascade of events leads to rapid release of immunomodulating agents including interleukins and interferons.

NKT cells can be broadly classified into two categories: type-I and Type-II. Type I NKT cells expresses a T cell receptor (TCR) with an invariant Vα24-Jα18 TCRα chain (Vα-Jα18 in mice) paired with a restricted subset of TCR Vβ chains.[1] These cells are also called invariant NKT cells (*iNKT*) and recognize glycosphingolipid antigens. *iNKT* cells are highly conserved among mouse, non-human primates, and humans. On the other hand, type II or non-invariant NKT cells neither express the type 1-associated invariant TCRα chain nor recognize α-GalCer. These NKT cells express a range of TCRs and recognize a variety of lipid antigens, including glycolipids and phospholipids.[4,5]

When activated, *iNKT* cells rapidly produce both Th1-type cytokines including interferon (IFN-γ) and tumor necrosis factor (TNF) and Th2-type cytokines including interleukin (IL-4) and (IL-36). The fact that individual *iNKT* cell can produce both Th-1 and Th-2 type cytokines[6] seems paradoxical, as Th1 is a pro-inflammatory response and Th2 is an anti-inflammatory one. The mechanisms determining the cytokine polarity are just beginning to emerge and some include

pharmacokinetic properties of antigens[7], and translational regulations by p38MAPK.[8] Although the cytokine release by *iNKT* cells is rapid, it's not simultaneous. For example, when treated with α-GalCer, murine NKT cells first produce IL-4 which reaches its peak around two hours after the injection. Meanwhile, the IFN-γ is released in the second wave and peaks around 24 hours after the injection[5].

Research in the last decade has shown that *iNKT* cells are not only essential for defense against pathogens, but also for initiation and regulation of adaptive immune responses. Alterations in the number or function of *iNKT* cells has been linked with multiples sclerosis[9], diabetes mellitus[10], lupus, and asthma;[1] and in recent years there has been a great deal of research to harness the potential of *iNKT* cells into vaccines and vaccine adjuvants.

1.2 Role of *iNKT* cells in infectious disease

The ability of *iNKT* cells to influence the immune system and to promote Th1/Th2 development indicates a larger role of *iNKT* cells in immune responses to infectious agents. Research in the past decade has established that *iNKT* cells can play either beneficial or detrimental roles in the murine immune responses against a variety of pathogens including bacteria, viruses, fungal, and protozoan parasites[1,11,12]. The protective role is primarily carried out by neutrophil recruitment and enhancement of Th1 responses, while detrimental effects are mainly due to explosive cytokine secretion leading to septic shock. Although the specific antigens in most of these infections are unknown, the role of *iNKT* cells is confirmed by the use of either Jα18[13] knockout mice, which

Microorganism	NKT cell Function
Streptococcus spp	Neutrophil recruitment, IFN-g secretion
Borrelia burgdorferi	Prevention of possibly detrimental IgG2a
Pseudomonas Spp	Neutrophil recruitment, enhancement of alveolar macrophage
Leishmania major	NKT cell activation by IFN-g secretion
HSV-1 and HSV-2	Mechanism unknown
Leishmania donovani	Detrimental immune polarization, defective hepatic recruitment of CTL
Sphingomonas Spp	Explosive cytokine secretion leading to septic shock
Novobium aromaticum	Transactivation of autoreactive T cells and B cells causing primary billary cirrhosis
Hepatitis-B virus	Recognition of stress induced ligands on hepatocytes via the NKG2D receptor

Figure 1.1 Protective mechanisms are indicated in green, detrimental mechanisms are indicated by red. Bacterial species are indicated by blue, parasites by purple and virus by yellow

lack the Jα gene to form the invariant TCR or by CD1d[14] knockout mice, which lack the *iNKT* cell population.

1.2.1 Bacterial Infections

The role of *iNKT* cells in bacterial infections has been thoroughly investigated.[15–17] For example, significant deficiency of *iNKT* cells have been reported in pulmonary tuberculosis patients. A recent study demonstrated that administration of α-GalCer, a well-known antigen for *iNKT* cells, can improve the clinical outcome of Mycobacterium tuberculosis.[18] *iNKT* cells also play a critical role in the host defense against pulmonary infections with Pseudomonas aeruginosa. In the murine model, the bacterial burden was found to be 100 fold higher in the lungs of CD1d knockout mice,

which clearly established the protective role of *iNKT* cells in pneumonia.[19]

1.2.2 Parasitic and viral Infections

Involvement of *iNKT* cells in protection against hosts of other microbes has also been investigated. These studies demonstrated the involvement of *iNKT* cells in Plasmodium berghei (malarial parasite), Leishmania major, cytomegalovirus, Herpes simplex virus (HSV-1), hepatitis-B, respiratory syncytial virus (RSV) and many more. In most of these studies, mice were injected with α-GalCer and the protection was measured against a wild type (control) mice. Although in most of these cases, the specific antigens responsible for causing *iNKT* cell activation are not known, the role of *iNKT* cells are confirmed by comparisons with CD1d knockout mice.

1.2.3 Autoimmune diseases and HIV

Although *iNKT* cells are activated during microbial infection, the infection also has an impact on the function of *iNKT* cells. Research shows that the number of *iNKT* cells in HIV-1^+ individuals is significantly lower[20] with a specific depletion of the CD4+ *iNKT* subset compared to the CD4- subset.[21] In the non-human primates, reduced numbers of CD4+ *iNKT* cells are inversely correlated to the viral load and CD1d is also downregulated[22]. Although plenty of data is available to confirm the depletion and dysfunction of *iNKT* cells during HIV infection, impact of this depletion on the disease progression is not completely established. As the evidence in this field continues to point towards a critical role of *iNKT* cells, scientific community has increased its efforts in illuminating whether these cells can contribute towards protection from HIV infection.

1.3 *iNKT* cell activation pathways during microbial infections

To better understand the role of *iNKT* cells during infections, we need to understand their activation pathways. There exist two principal pathways of *iNKT* cell activation: direct and indirect. The direct activation starts with the acquisition and uptake of antigen by various components of the immune system. Some of these mechanisms include phagocytosis of microbes by dendritic cells (DCs) and macrophages, lipoprotein mediated uptake, or direct loading of antigen onto the surface of antigen presenting cell. All of these pathways deliver exogenous antigens to intracellular endocytic compartments (endoplasmic reticulum), where they are loaded into CD1d. After being loaded with antigens, these CD1 molecules traffic along the secretory route through the Golgi to the cell surface, where they are presented to *iNKT* cells by antigen presenting cells (APCs).

The indirect activation of *iNKT* cells is achieved through Toll like receptors which trigger the loading of CD1d with endogenous antigens like isoglobotrihexosylceramide (iGb3)[23,24]. Following the presentation of iGb3, dendritic cells secrete interlukin-12 (IL-12) which leads to the activation of *iNKT* cells. This phenomenon is also called the self-activation or autoreactivity of *iNKT* cells. These two mechanisms are illustrated in figure 1.2. This wide range of antigens and multiple modes of activation helps in explaining the existence of these highly conserved immunological cells and underscores their importance.

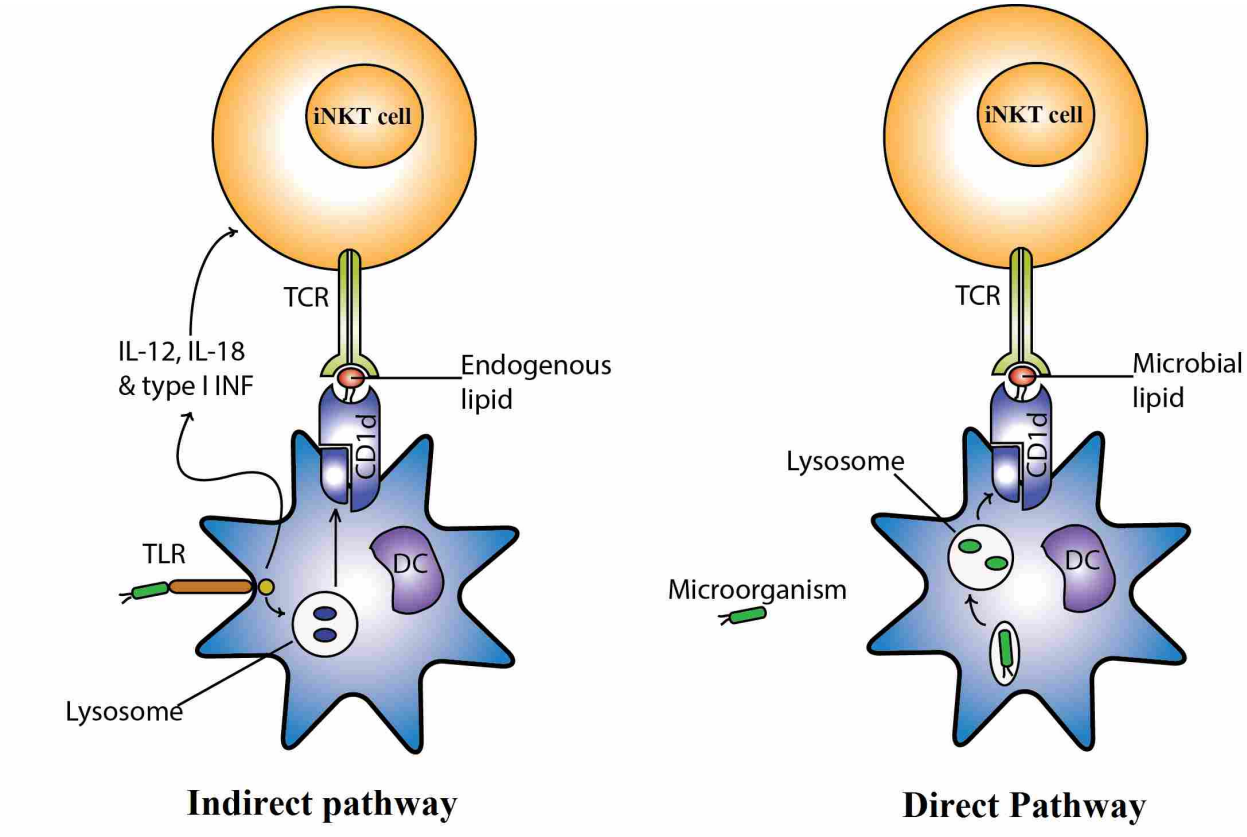

Figure 1.2 The direct and indirect mechanisms involved in the activation of *iNKT* cells

1.4 The *iNKT* cell antigens

As pharmaceutical researchers are starting to understand the therapeutic potential of *iNKT* cells, it is very important to understand the type of antigens recognized by *iNKT* cells. In this section, we will briefly cover natural, non-natural, and endogenous ligands and their importance.

1.4.1 α-GalCer- The famous antigen

The first major discovery in this context was made in 1995 when Koezuka et al. at Kirin pharmaceuticals isolated a group of α-monogalactosylceramides, from the marine sponge Agelas mau-

Figure 1.3 Chemical structure of Agelasphins (α-GalCer) with glycosidic bond in the α-orientation. Almost all of the NKT cell antigens are known to have α-glycosidic bond

ritianus. These compounds showed potent anticancer properties and were termed agelasphins (Fig.2). The most potent compound among agelasphins is commonly known as α-GalCer. Although, α-GalCer is a very potent agonist of *iNKT* cells, it's not a natural antigen.

1.4.2 Natural microbial antigens

After almost a decade following the discovery of α-GalCer, the first microbial antigen for *iNKT* cell was reported. In 2005, multiple groups[17,25,26] reported that Sphingomonas spp., a common environmental pathogen, possesses natural *iNKT* cell ligand called GSL-1. This compound is a glycosphingolipid and has a glucuronic acid connected to a sphingosine base via a α- linkage. In essence, the structure of GSL-1 is very similar to α-GalCer. After this discover, the structures of few other microbial antigenic lipids have been reported. These include α-galactosyldiacylglycerol from Borrelia burgdorfer[25], phosphatidylinositol-mannosidase from Mycobacterium bovis[27] and α-glucosyldiacylglycerol from Streptococcus pneumoniae[28]. Although these compounds belong to separate lipid classes and carry different lengths of lipid chains, all of them possess a striking similarity. In all these compounds, the lipid portions are connected to the carbohydrate moeity via

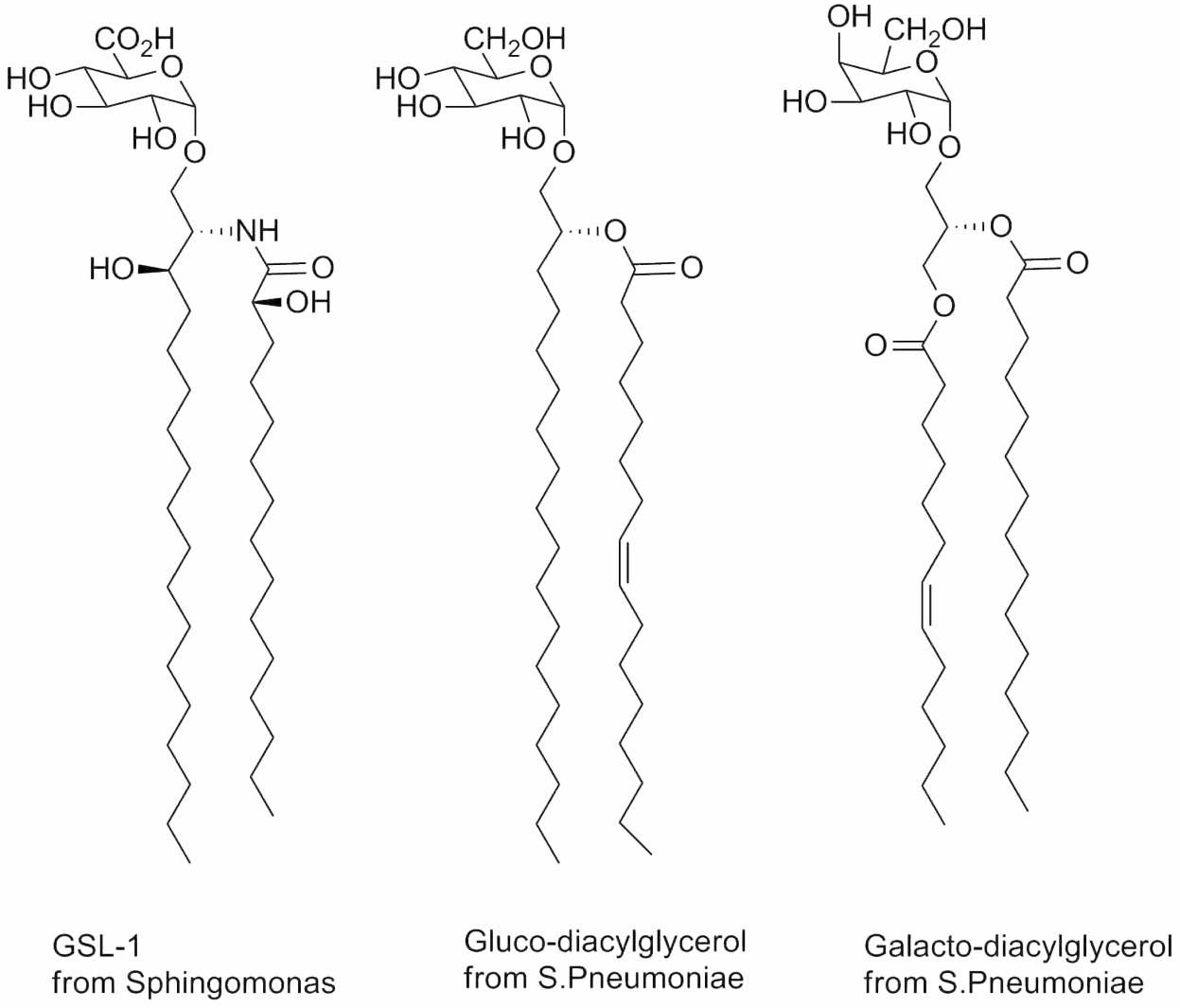

Figure 1.4 Pathogen derived *iNKT* cell antigens

the same α-anomeric linkage. A representative list of these compounds is provided in fig.1.4.

1.4.3 The endogenous antigen

Almost always, immunological cells have specific endogenous antigens that play a critical role in their development and function. The mouse and human *iNKT* cell are also known to be auto-

reactive[29] i.e, they react to self-lipid antigens presented by antigen presenting cells (APCs). So far, the search for endogenous *iNKT* cell antigens has led to only one molecule isoglobotrihexosylceramide (IGb3). Although IGb3 is not as strongly antigenic as α-GalCer, it can be recognized by *iNKT* TCR complex. The concept of endogenous antigen also becomes important because they are supposed to be involved in the positive selection of *iNKT* cells in thymus.[1]

1.5 The role of *iNKT* cells in asthma

As discussed in the previous sections, *iNKT* cells play a crucial role in the pathogenesis of many disease states. In the forthcoming chapters, we will be focusing on the role of *iNKT* cells in allergic asthma; therefore it's very important to understand the key attributes of this disease

1.5.1 Asthma and airway hyperreactivity

Asthma is a complex disease caused by a combination of genetic and environmental factors. Most common form of asthma, allergic asthma, is triggered by inhaled allergens and affects nearly 100 million people worldwide.[30] Other forms of asthma can be triggered by multiple causative agents including air pollution, ozone, viruses, and fungi[31]. These different pathways and triggers often coexist and act in synergy in asthma patients. At the molecular level, asthma is caused by a Th-2 driven inflammation of airways which elevates serum IgE (immunoglobulin E), a class of antibody that plays an essential role in hypersensitivity and airway hyperreactivity (AHR).[32],[33] AHR, a cardinal feature of asthma, is present in all forms of the disease and correlates to its severity. In

the murine model of asthma, AHR is the most important outcome and can be measured by the loss of pulmonary function with an increasing dosage of an inhaled allergen such as methacholine or histamine.

1.5.2 NKT cells and asthma

The role of antigen specific Th2 cells in the development of asthma has been thoroughly investigated. Although the presence of Th2 cells can explain many features of allergic asthma, other aspects including non-allergic asthma and the inability of anti Th2 antibody to alleviate AHR suggests that other immunological factors may also critically regulate asthma[34,35]. As *iNKT* cells are known to release large amounts of Th2 cytokine, their role in the development of asthma was also investigated. Using *iNKT* cell deficient mice, researchers have shown that allergen induced AHR failed to develop in these mice indicating that *iNKT* cells play a crucial role in the development of asthma[30]. Researchers have also demonstrated that IL-13, another cytokine released by *iNKT* cells, is also required for the development and action of Th2 biased OVA-specific T cells in the lungs, which drives the development of asthma[36]. Many years of research in this field has identified various mechanisms (fig. 1.5) by which, *iNKT* cells orchestrate the pathogenesis of asthma.

As shown in figure 1.5, NKT cells play a central role in the development of asthma. For example, the production of IL-17 by *iNKT* cells recruits neutrophils to the airways, which are polymorphonuclear leukocytes and have been linked to the development of severe chronic asthma and sudden asthma attacks[37]. NKT cells can also activate alveolar macrophages to produce IL-13, which then induces chronic lung disease. A few other important cytokine mediators released by

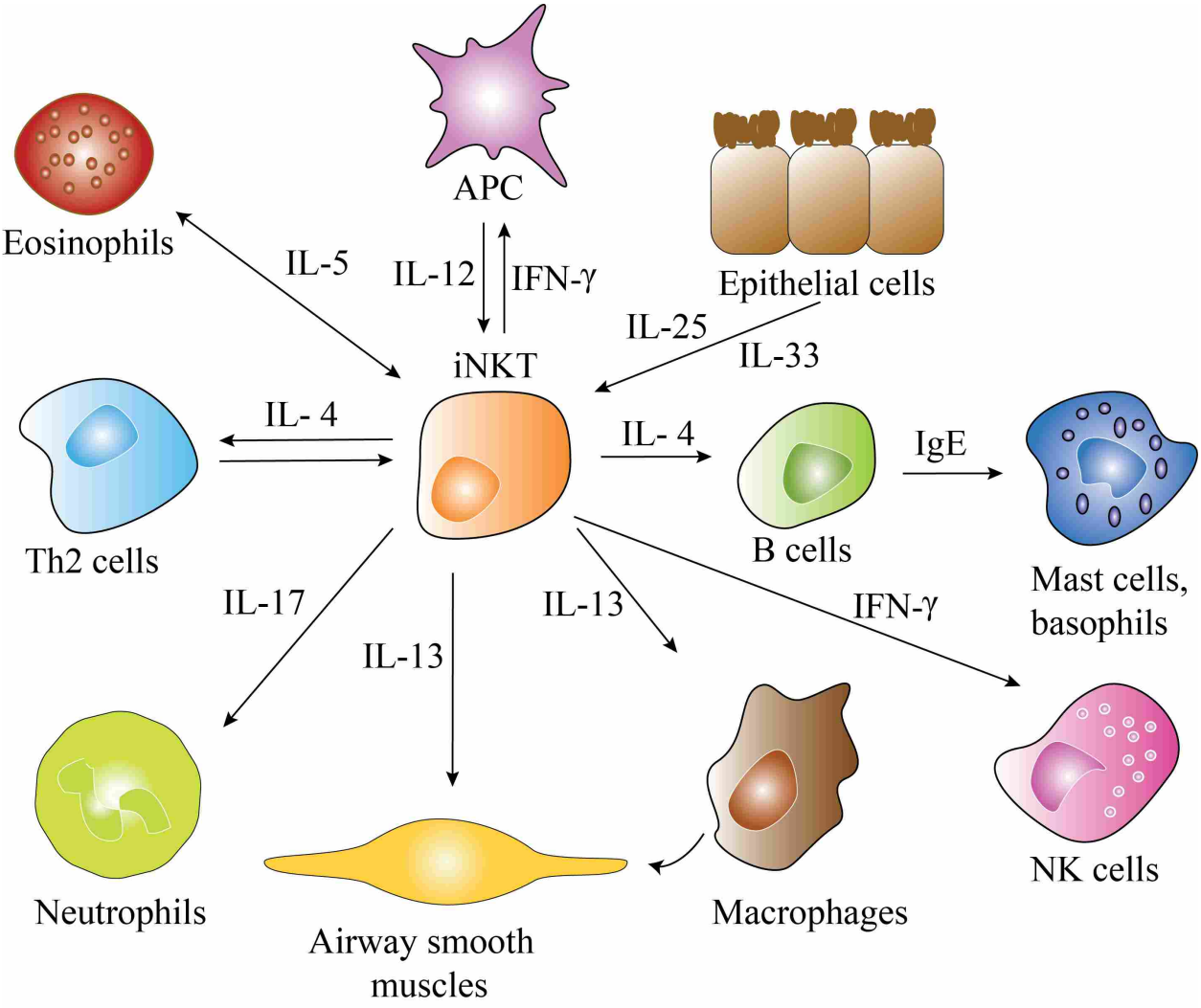

Figure 1.5 The central role of invariant NKT cells in the development of airway hyperreactivity (AHR). *iNKT* cells secrete various cytokines, including Th2 cytokines, which have direct effect on various pulmonary cells. *iNKT* cells also regulate other immunological cell types including Neutrophils, Eosinophils, and basophils that are known to trigger asthma

NKT cells are IL-25, which greatly enhances Th2 response and 1L-33 which induces AHR and goblet cell hyperplapsia.[33,38] In addition to cytokine production and monitoring the immunoglobulin recruitment, NKT cells have been shown to be cytotoxic to the regulatory T cells, which normally suppress airway inflammation.

In the last decade, immunologists have done very exciting research to establish the central role of NKT cells in the development of asthma, although a key question remains unanswered. What are the antigens that trigger pulmonary NKT cells? Is NKT cell activation exclusively driven by endogenous ligands or do pathogenic antigens play a key role? Throughout this dissertation, we have tried to answer these key questions which are critical in understanding the pathology of asthma and hopefully will lead to new drugs by targeting NKT cells for asthma therapy.

Chapter 2

Asperamide-B: The first fungal antigen for NKT cells

2.1 The importance of NKT cell response to fungi

A number of bacteria and parasites have been found to synthesize glycolipids that act as pattern recognition molecules for *i*NKT cells[1]. However, until now only a few "pathogenic" microbes are known to express antigens that can be directly recognized by the TCR of *i*NKT cells[23,39]. The high degree of conservation of the *i*NKT cell TCR across many mammalian species suggests that other types of pathogenic microorganisms including fungi, may also express specific antigens for these immunomodulatory cells. In support of this argument, researchers have shown that treatment of systemically infected mice with α-GalCer diminishes the fungal burden and promotes protective Th1 response. Another study indicated that the clearance of opportunistic fungal pathogen

Cryptococcus neoformans was delayed in *i*NKT cell deficient mice. Taken together, these studies underscore the importance of *i*NKT cells in mammalian antifungal responses. Although these studies undoubtedly establish a role of *i*NKT cells in fungal infections, the specific mechanisms involved remain completely unexplored.

Certain fungi, especially *Aspergillus fumigatus* are potent allergens and have been implicated in either triggering or enhancing allergic asthma[40,41]. *A. fumigatus* is a saprophytic fungus that is ubiquitous in the environment and its spores or conida are recovered at very high rates from within buildings, homes, and soil, resulting in daily respiratory exposure in most individuals[42,43]. Although *A. fumigatus* can cause invasive infections in immunocompromised hosts, in normal healthy individuals the conida is rapidly cleared by the immune system. However, in some individuals allergic sensitization to *A. fumigatus* may develop.[44] In patients with asthma, sensitization is associated with severe disease with reduced lung function. In patients of cystic fibrosis, a unique hypersensitivity to *A. fumigatus* known as allergic broncopulmonary aspergillosis (ABPA) develops.[31] Although the precise mechanism for innate immune recognition of *A. fumigatus* is not known, its association with allergic asthma and the potential role of the *i*NKT cells in asthma (reviewed in chapter-1) led us to investigate whether *A. fumigatus* could activate *i*NKT cells. These studies were performed in collaboration with the research group of Dr. Dale Umetsu at Harvard Medical School.

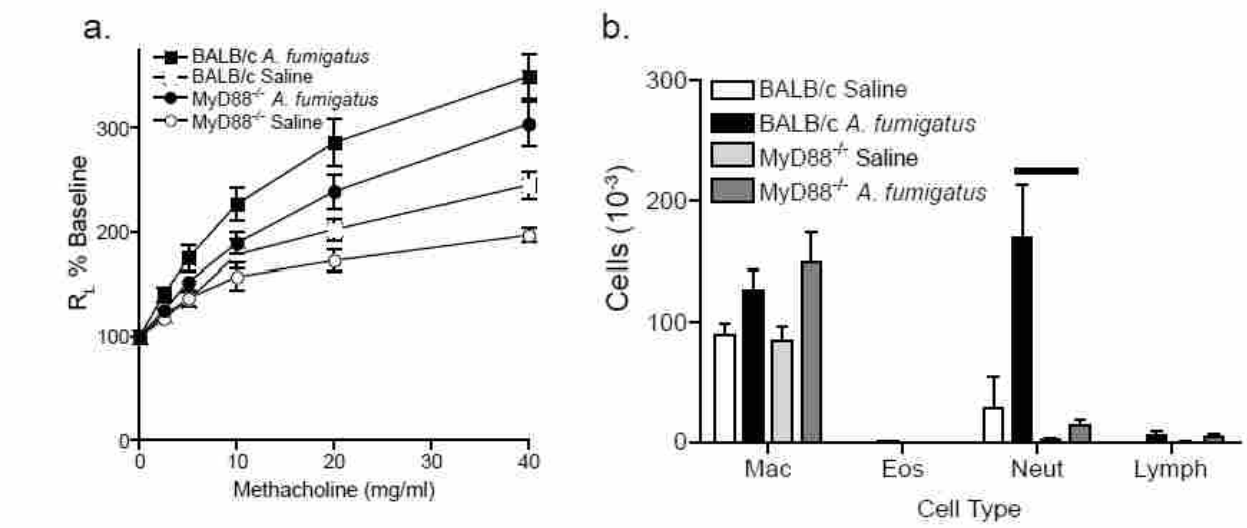

Figure 2.1 *A. fumigatus* extract induces AHR in MyD88 independent fashion. After administering three intranasal dosages of *A. fumigatus* lysate, AHR was measure directly in sedated mice by invasive plethysmography. R_L is the lung resistance in response to methacholine challenge

2.2 Preliminary studies with crude Aspergillus extracts

To test this hypothesis, we investigated the ability of crude *A. fumigatus* extract to induce airway hyperreactivity (AHR) in a mouse model (in collaboration with Dr. Dale Umetsu at Harvard Medical School). We found that WT BALB/c mice treated intranasally with 100 μg of *A. fumigatus* extract for three consecutive days develop severe AHR within 24 *h* of sensitization. It can be clearly seen from figure 2.1a that AHR induction is MyD88 independent, which means that *A. fumigatus* directly activates *i*NKT cells.

In these studies, the immunological response is characterized by an increase in the number of macrophages and neutrophils but not eosinophils in the airways (figure 2.1b). The rapidity of immunological response and quick induction of AHR indicates that this is an innate immune

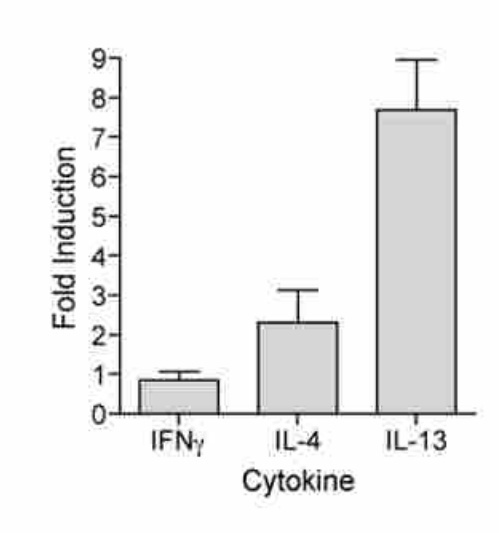

Figure 2.2 Cytokine release profile of *A. fumigatus* treated vs saline treated mice. This experiment demonstrates that *A. fumigatus* extract activates *i*NKT cells in a dose dependent manner.

response. As asthma is known to be a Th2 driven phenomenon, we decided to further investigate the Th2 cytokine release in response to *A. fumigatus* lysate and look for Th2 specific cytokines. To achieve this, post *A. fumigatus* sensitization, total lung RNA was purified and the expression of IL-4, 1L-13, 1L-25, and TSLP was quantified by QPCR. Figure 2.2 shows that the levels of mRNA for IL-4 and IL-13 but not IFN-γ were increased.

Taken together, these results suggest that *A. fumigatus* induces AHR by inducing Th2 cytokine production . To conclusively determine the involvement of *i*NKT cells, CD1d-/- BALB/c mice, which lack all CD1d restricted cells including *i*NKT cells, were treated with *A. fumigatus* lysate and assessed for the development of AHR (Figure 2.3a). These mice failed to develop AHR while WT mice had increased numbers of *i*NKT cells in the BAL fluid and the lung tissue, concluding an important role of iNKT cells in this process.

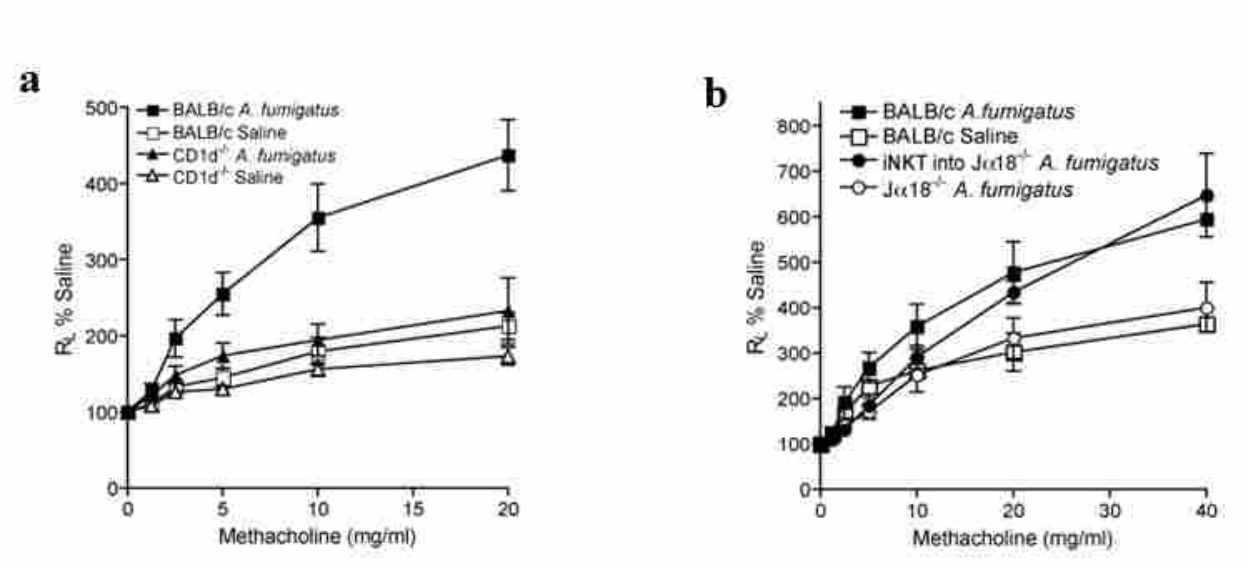

Figure 2.3 CD1d and Jα-18 knockout mice failed to develop airway hyperreactivity after receiving intranasal *A. fumigatus* extract. These experiments suggest that *i*NKT cell response to *A. fumigatus* extract is the direct one.

To further establish the importance of *i*NKT cells, Jα18-/- mice, which lack *i*NKT cells but express CD1d were intranasally administered with *A. fumigatus* extract (figure 2.3b). As expected, Jα18-/- failed to develop AHR, however, reconstitution of Jα18-/- animals with wild type iNKT cells fully restored AHR in these mice. Taken together, all these experiments conclude that iNKT cells play a crucial role in the development of AHR in response to *A. fumigatus* sensitization.

2.2.1 Direct vs Indirect Involvement of NKT cells

As described in chapter-1, *i*NKT cells are known to have both direct and indirect mechanisms of activation. With the role of iNKT cells in AHR development established, we wanted to confirm the mechanism of activation. In the direct mechanism, a lipid antigen is loaded into CD1d and presented to *i*NKT cells which initiate cytokine production. In the case of indirect pathway, anti-

gen presentation happens through Toll-like receptors (TLR) and *i*NKT cells are activated by an endogenous ligand.

TLRs use two primary adapter proteins for signaling: MyD88 and Trif.[45] To test the involvement of TLRs, crude *A. fumigatus* extract was intranasally administered to MyD88-/- mice. We found that both WT and LPS2/LPS2 C57B1/6 mice resulted in the development of AHR. These findings suggest that the indirect pathway for *i*NKT cells is not involved in the process of *A. fumigatus* sensitization and strongly argues that *A. fumigatus* extract contain glycolipid antigens which directly activate *i*NKT cells.

To identify the particular component of *A. fumigatus* that is responsible for *i*NKT cell activation, we isolated all possible glycolipid candidates from this species. Initially, our approach was to isolate each and every component of the lipidome and test it for *i*NKT cell activity. This approach proved to be very time consuming and cumbersome. Following the literature[46], the isolation strategy was changed and we decided to fractionate the lipidome into different lipid classes (fatty acids, glycerolipids, phospholipids, sphingolipids etc.) and test each class for *i*NKT cell activity. With the following objectives, we started the isolation work:

1. Identify the particular antigen in *A. fumigatus* and test it for the development of Airway hyperreactivity.

2. Elucidate the structure of the antigen using advanced spectroscopic techniques.

2.3 Experimental Procedures

Fungal isolates and growth conditions: *Aspergillus fumigatus* (ATCC 9197) was obtained from ATCC. The frozen fungus obtained from ATCC was dispersed in 10ml sterile PBS and incubated at 37^oC for 2 h. This suspension (1ml) was inoculated onto culture plates containing potato dextrose agar (PDA), which were used as a source for future inoculations. Following the general Aspergillus growth protocol[47], remaining 8 ml of PBS suspension was inoculated to 12 l (4 X 3L) of autoclaved growth medium consisting of 1% glucose, 0.2% peptone, 0.1% yeast extract, 0.1% casamino acids and q.s. water. This media was shaken in Erlenmeyer flasks at 37^oC at 200 rpm for 5 days. Mycelia were harvested by filtration through a cheese cloth and residue was washed with deionized water. Mycelia (1.5 Kg) were processed immediately for extraction.

Extraction and fractionation: Following the procedure of Folch et al[48], lipids were extracted twice by homogenizing the mycelium in chloform/methanol (2:1 v/v). A glass walled omni mixer was used for each extraction and the residue was filtered using a cheese cloth. All the extracts were pooled and dried using rotary evaporator at RT. These extracts were redissolved in 2 liters of chloroform/methanol/water (8:4:3 v/v). The extract was transferred to a separatory funnel and shaken vigorously. The lower layer containing approximately chloroform/methanol/water (86:14:1 v/v) was dried using rotary evaporator and was named the Folch phase A. The upper (aqueous) layer containing approximately chloroform/methanol/water (3:48:47 v/v) mixture was dried under nitrogen stream. The residue was redissolved in water and re-extracted with water saturated 1-butanol to recover highly polar lipids including acidic glycolipids and ganglioisides. This phase is named as Folch phase B.

High performance liquid chromatography (HPLC): To estimate the number of metabolites in this extract, we decided to perform a HPLC/MS analysis on the crude extract. Along with deciphering the complexity of metablome, this helped us plan and approach the separation in a better way. After exploring various chromatographic conditions, a C3 column (Agilent SB-C3, 1.8μ, 3.0 X 100mm) was selected. Mobile phase A constituted of water and 0.1% trifluoroacetic acid (TFA) and mobile phase B consisted of acetonitrile and 0.1%FTA. Injection volume was 5μl and a gradient flow was used to elute the column. After developing the method for the analysis of complete crude lipidome, we also developed a LC-MS method for qualitative and quantitative analysis of antigenic lipid in the crude extract. The following eluent was used for LC-MS: start with 30%A and at 5 min go to 50%B, hold 50%B for 3 min and run 100%B from 8-10 min. Column was reconditioned with 30%A from 10-12 minutes.

Thin layer chromatography (TLC): TLC was performed on aluminum base silica plates (Silica gel 60 F254, 10 X 10cm, 0.2mm thickness; Merck, Germany). Multiple solvent systems were used including varying mixtures of chloroform/methanol, chloroform/methanol/water (65:25:4, v/v/v) and chloform/methanol/1M ammonium acetate/NH_4OH (18:14:1:1:2.3, v/v/v/v). Lipids were visualized by dipping the TLC plate into one of the following solutions and subsequently developing with heat. Orcinol stain solution (100mg orcinol in 200ml of 10% H_2SO_4 in ethanol), molybdenum stain solution (1M H_2SO_4, 45mM ammonium heptamolybdate)

Aminopropyl solid phase extraction (SPE): Following the literature procedure[46], aminopropyl SPE cartridges were preconditioned with hexanes. Crude extract was dissolved in 10% $CDCl_3$/MeOH and loaded onto the SPE cartridge. In fraction 1, 2ml Chloroform methanol (23:1

V/V)was used to elute out the neutral lipids. In fraction 2, free fatty acids were eluted using 2ml diisopropyl ether-acetic acid (95:5 V/V). Glycosphingolipids were eluted in fraction 3 with 4ml of acetone-methanol(9:1.5, V/V). Neutral phospholipids were eluted using 8ml of chloroform:methanol (2:1, V/V) in fraction 4. Finally in fraction 5, acidic phospholipids are eluted using 10ml of chloroform:methanol:4M ammonium acetate (30:60:8, V/V/V).

1D and 2D NMR spectroscopy: For structure elucidation, NMR spectra of derivatized and underivatized glycolipid candidates were recorded in different solvents including CDCl3, Pyridine, d5 and DMSO, d6 (Cambridge isotope labs). Spectra were acquired using a 500MHz Innova spectrometer at room temperature.

Mass spectroscopy: Mass spectroscopy was used as an important tool in in structure elucidation using fragmentation analysis (MS/MS) as well as chromatographic analysis. Mass spectroscopy was performed in the positive ion mode using matrix assisted laser desorption ionization (MALDI) and electrospray ionization (ESI). LC-MS studies were performed on an Agilent MSD TOF with an ESI spray source. Crude and purified lipid samples were dissolved in 25:65:4 chloform/methanol/water (25:65:4 v/v). Using auto sampler, 5μl sample was introduced into the reverse phase C3 column (Agilent SB-C3, 1.8μm, 3.0 X 100mm). For fragmentation analysis, Q star pulsar with MALDI ionization source was used. Crude and purified lipid samples were mixed with recrystallized dihydroxy benzene (DHB) using chloroform and methanol (2:1) and spotted on stainless steel MALDI plate. Using N2 as a collision gas, CID spectra and purified antigen was obtained.

2.4 Results

2.4.1 Complexity of extract and problem of false hits

Aspergillus fumigatus (ATCC 9197) was cultured as described in the experimental section. Following the lipid extraction protocol by Folch et. al[48], the crude lipid extraction was performed. To estimate the approximate number of lipidomic species in the crude extract, TLC, HPLC, and shotgun mass spectroscopy analysis were performed. all these analysis suggested that the crude extract constituted a complex mixture of difficult to separate metabolites (figure2.4).

Following the relevant literature[49–51], purification process was simplified by focusing attention on the metabolites of mass range 500-1500amu and of a certain polarity range. In the process of scrutinizing crude extract for glycolipid content, a few promising leads were obtained (figure2.5). Although these compounds matched our mass, polarity and NMR criteria, they failed to stimulate *i*NKT cells.

2.4.2 Change of isolation procedures

After a few failed attempts to isolate the *i*NKT cell antigen in *A. fumigatus* extract, we decided that it would be wise to fractionate crude lipid extract into individual lipid classes, instead of going after the specific compounds . Following the literature,[52] a new isolation process (figure2.6) using an amino propyl (NH2) solid phase extraction column (SPE)was designed. Using this technique, crude lipids were separated into five lipid classes consisting of neutral lipids, free fatty acids, glycosphingolipids, neutral and acidic phospholipids (see experimental section for details). this

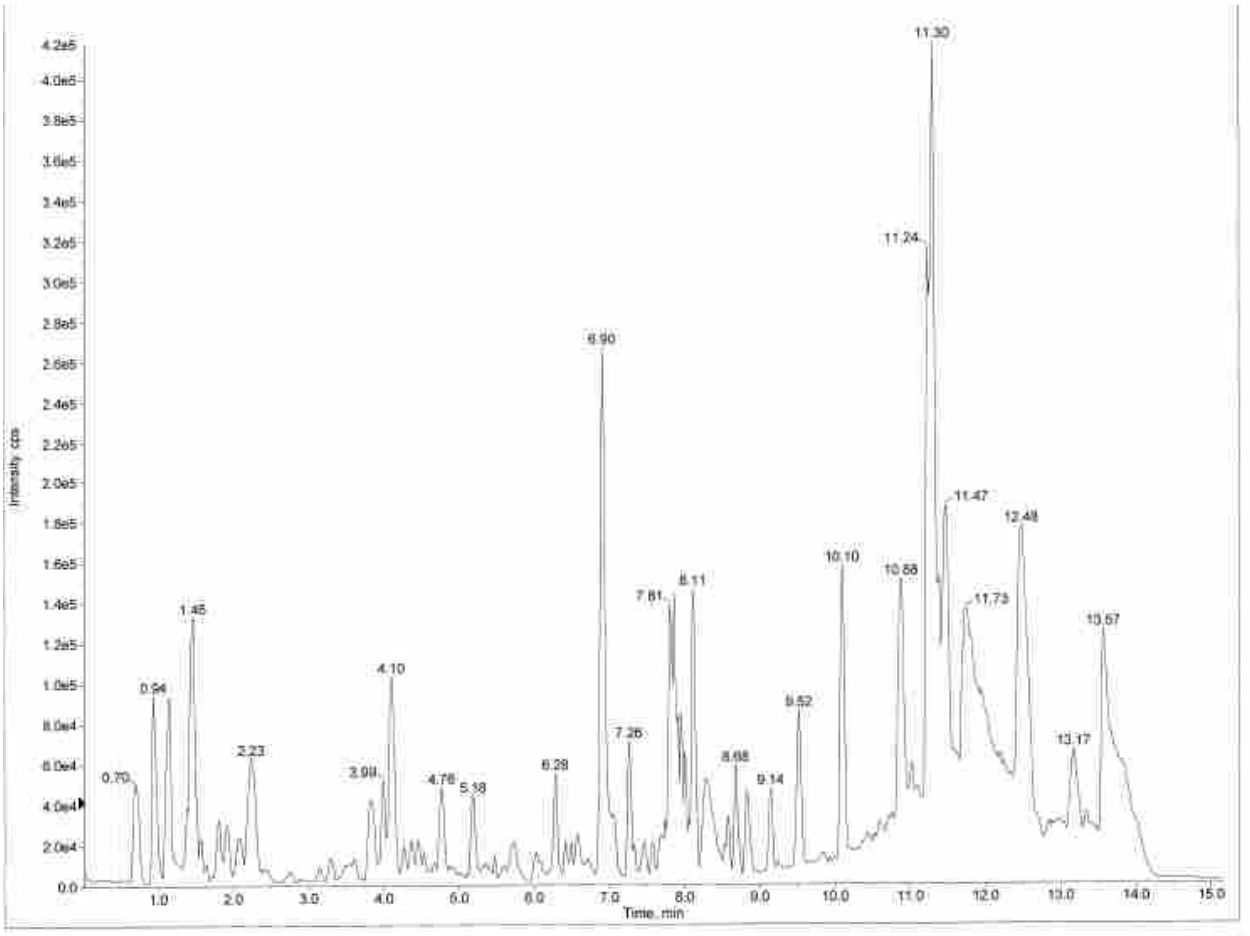

Figure 2.4 HPLC of Folch organic phase of *Aspergillus fumigatus* extract, showing the complexity of the lipidome

proved to be a better approach from both discovery and immunological testing point of views. Additionally, a bioassay guided approach was followed during all the extraction procedure.

2.4.3 Isolation of key antigenic lipid

Following the aminopropyl SPE isolation, individual lipid classes were screened for glycolipid content using TLC and orcinol staining method. In vitro analysis of these fractions showed mod-

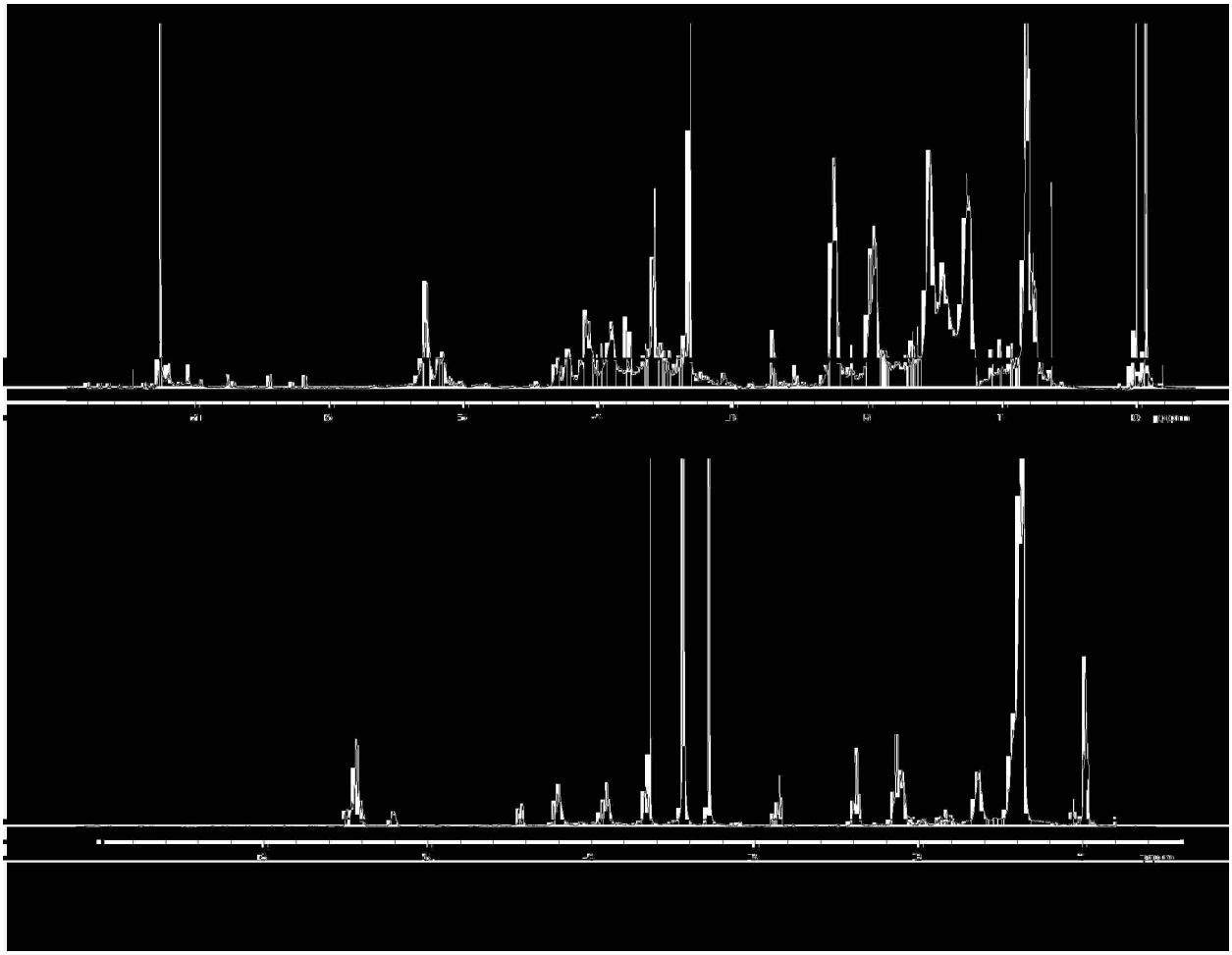

Figure 2.5 Spectrum of the two of many lipidomic components, which failed to stimulate *i*NKT cells

erate activity in fraction 3 and fraction 5. TLC of fraction 3 showed a major orcinol positive band having an Rf value consistent with monohexosyl ceramide. After multiple purifications of fraction 3, a pale yellow solid with mass 754.58 amu (M+H) was obtained. Preliminary 1HNMR analysis of this compound confirmed the presence of both carbohydrate and lipid regions. This compound was named ASP-754 and its 1H NMR is shown in figure 2.7. The 1H NMR spectrum had an intense peak at 1.25 ppm indicating the presence of one or more long chain alkyl groups and a

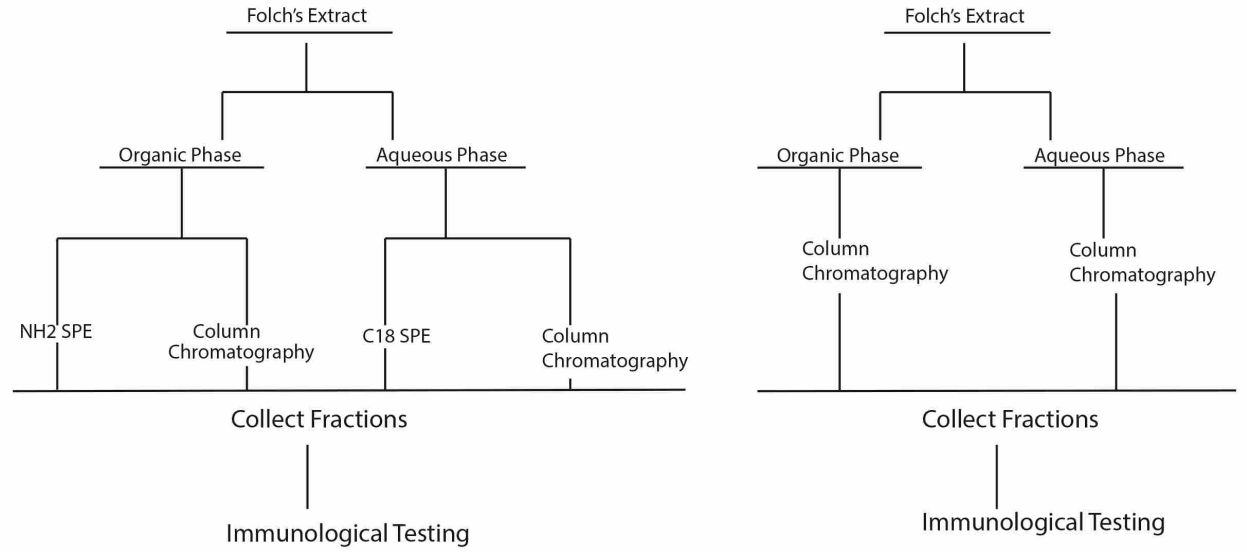

Figure 2.6 Different approaches for extraction and fractionation of *Aspergillus fumigatus*. On the right is the traditional fractionation approach and on the left is the solid phase extraction/fractionation approach

triplet at 0.88 ppm indicative of two alkyl methyl groups. Spectrum also had a doublet at 8.4 ppm (possibly NH) and multiplets at 6.0 and 6.2 ppm possibly showing the presence of double bonds in lipid chains. As the peak splitting in pyridine was not very good, spectrum was re-acquired in CDCl3 for the purpose of calculating accurate J values. Analysis of the coupling constant of peaks at 6.20 and 5.91 ppm (15.8Hz) confirmed the presence of two trans alkenyl groups in lipid chains.

2.4.4 Key information from HSQC

After recognizing the lipid (1-2ppm) and carbohydrate regions(3.9-5ppm) in 1HNMR, we decided to use HSQC to obtain 1H and 13C correlations. HSQC also provided the DEPT information which was very useful in determining the presence of primary, secondary and tertiary carbon environments. Shown above is the expanded HSQC spectrum highlighting important spectroscopic

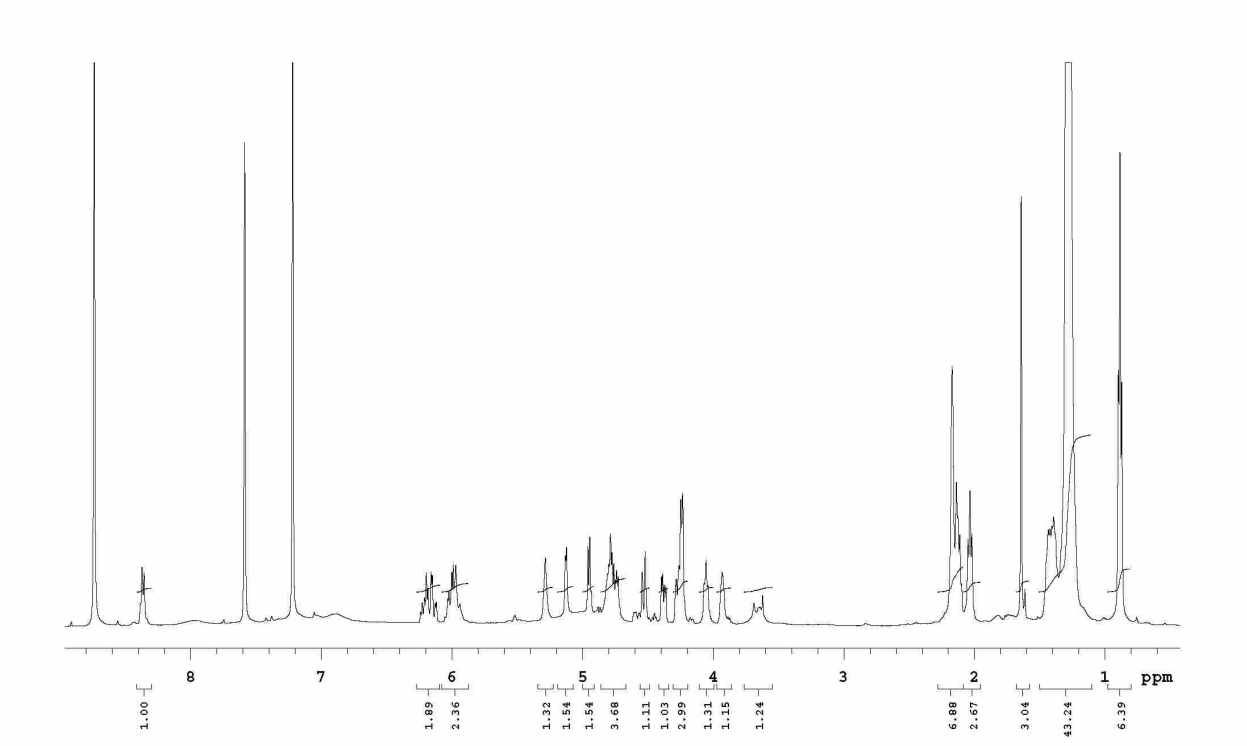

Figure 2.7 NMR spectra of ASP-754 in deuterated pyridine

correlations.

In Figure 2.8, negative (hollow) cross peaks represent secondary carbons and the positive (filled) cross peaks represent either primary or tertiary carbons. Our understanding of general chemical shifts for glycosphingolipids helped us in identifying two primary carbons as carbon-1 of sphingosine chain and carbon-6" of sugar moiety. The cross peak at 4.95 ppm and 105.5 ppm (blue square) represents the anomeric carbon (1") in the carbohydrate moiety. We were surprised to see a cross peak at 5.3 and 124.1 ppm (violet square). The downfield carbon at 124.1ppm for this peak suggests that this carbon might be a part of the alkene environment in the sphingosine or acyl chains.

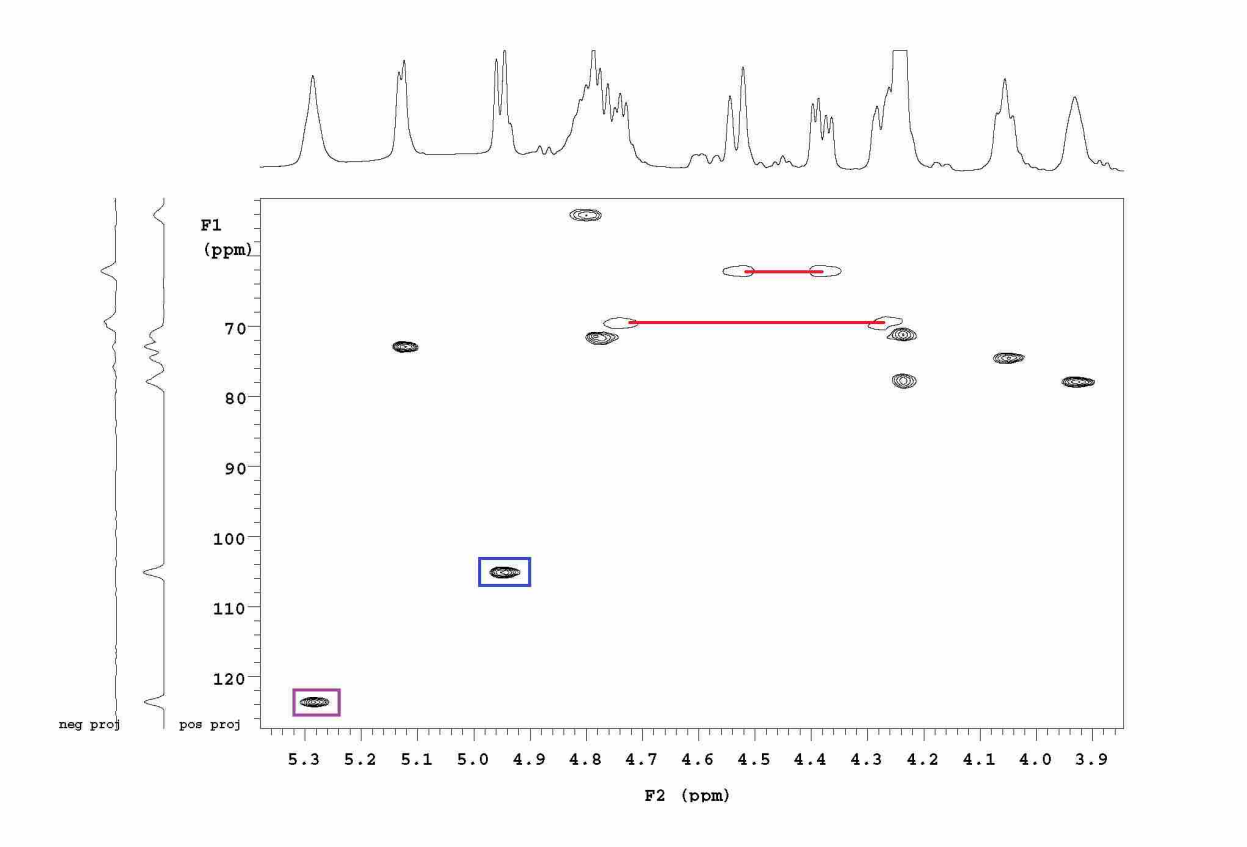

Figure 2.8 Expanded HSQC of ASP-754. On the horizontal axis (F2) information of 1H is shown and on the Vertical axis (F1) information of 13C is shown

2.4.5 Key information from COSY

To check the correlations between adjacent protons, COSY experiments were performed. Shown below is the expanded section of complete COSY spectra (figure 2.9). To begin analyzing the COSY spectrum, we started with the anomeric carbon at 4.95 ppm (from HSQC). From COSY spectra it can be clearly seen that the anomeric proton is strongly connected to 2" at 4.06 ppm and similarly we can assign all other carbohydrate peaks in this spectrum. Literature survey indicated that most of the "natural" NKT cell antigens contain either a glucose or galactose moiety attached to the ceramide via a α or β anomeric linkage . The fact that we see the protons at position 3" cou-

pling to 4” and 4” coupling to 5” combined with the literature data suggested that the carbohydrate moiety is a glucose and not galactose.

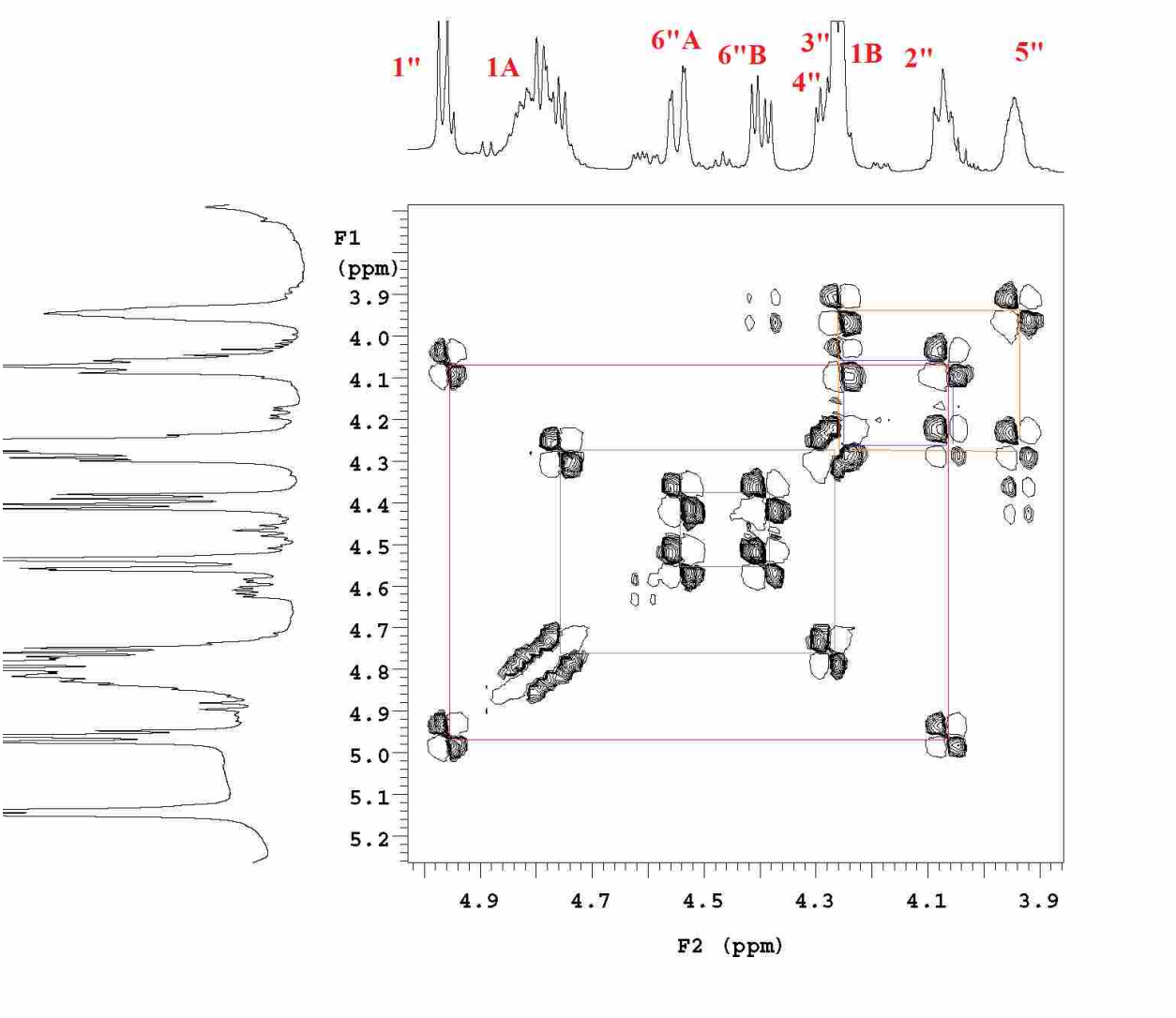

Figure 2.9 Expanded COSY spectra of ASP 754. Diagonally aligned cross peaks for all the carbohydrate protons can be seen

2.4.6 Disambiguation using HMBC

After being able to walk through the carbohydrate backbone and establish the identity of individual peaks, we used HMBC spectra to establish the identity of other key peaks in the spectrum. For example, HMBC spectrum (shown in figure 2.10) clearly showed that amide proton (NH) is strongly couple with only one carbon, which has to be 2' position in the acid chain.

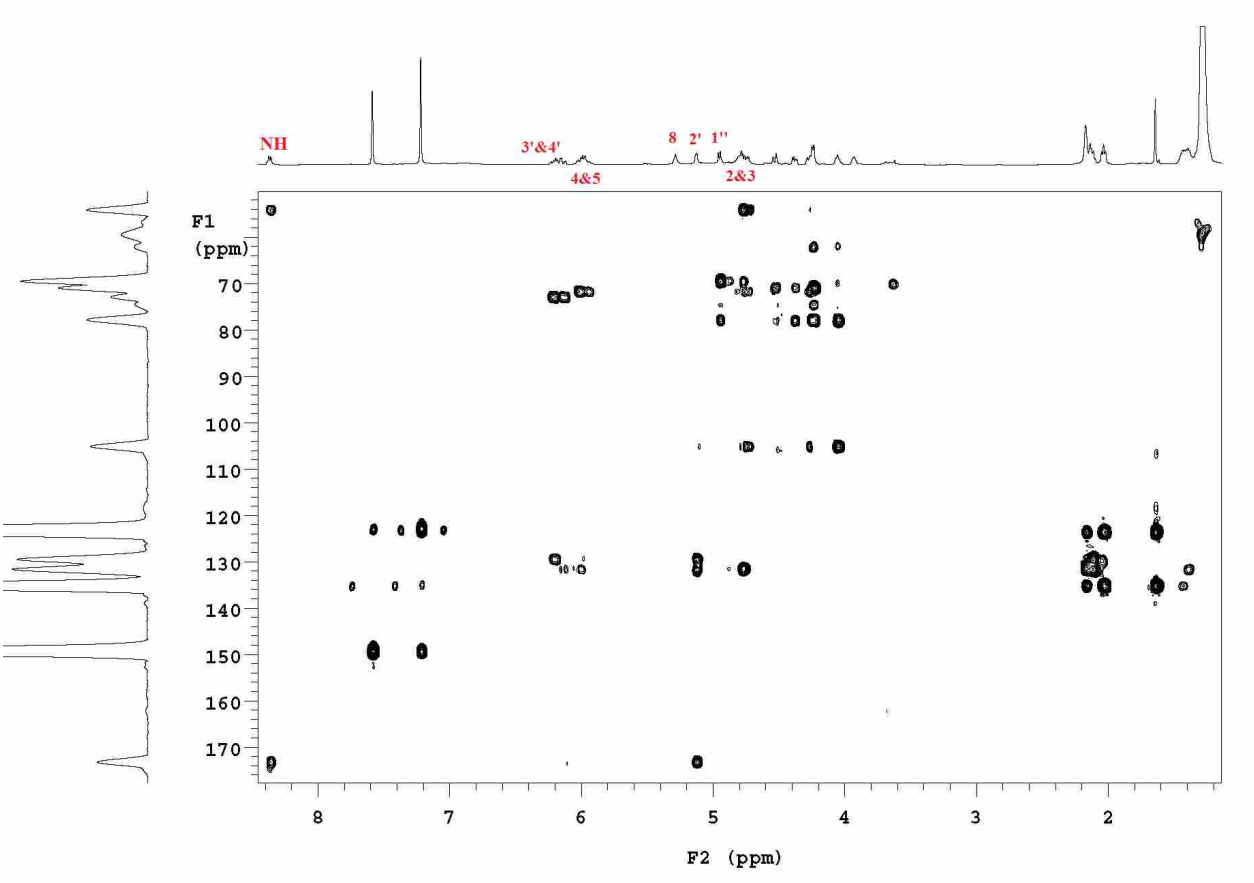

Figure 2.10 Expanded HMBC spectrum of Asp-754. The correlations helped in the assignments of peaks indicated in red

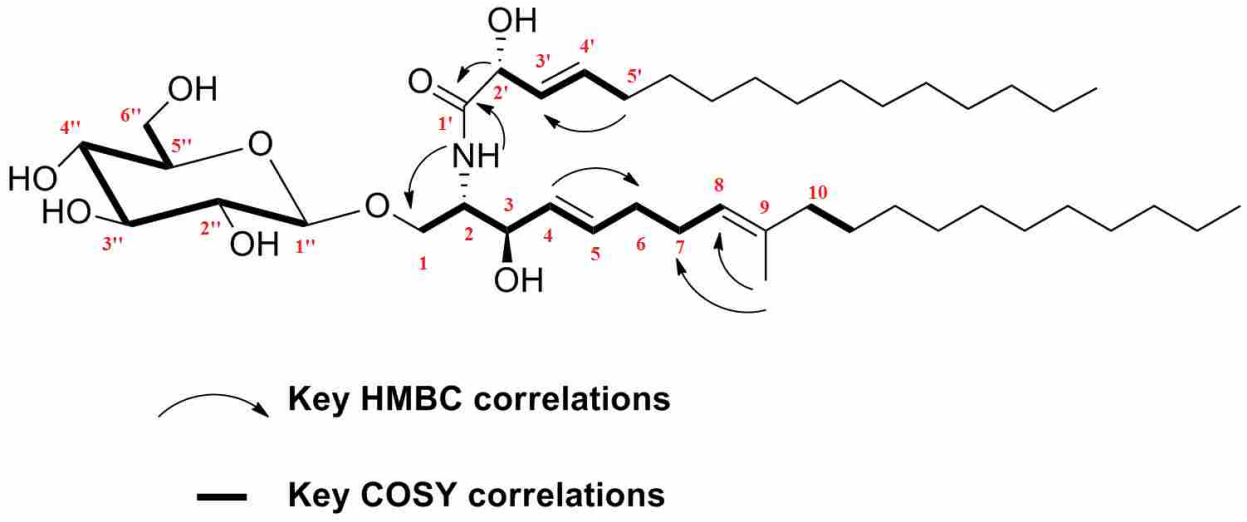

Figure 2.11 Proposed structure of Asperamide-B. The key COSY and HMBC correlations are highlighted

2.4.7 Conclusions from NMR spectrum

Taken together,the NMR and Mass spectroscopic data helped us to conclude that ASP-754 is a β-glycosylceramide having (4E,8E)-9-methyl-4,8-sphingadienine as long chain base and N-2'-hydroxy-(E)-3'-octadecenoate as an acid moiety (Fig. 2.11). Upon literature survey, we found that C-9 methylation is a common trait of fungal lipids. We were both excited and surprised to find that there were literature reports of very similar glycolipids from many fungal organisms including *Neurospora craasa*,[53] *Paracoccidioides brasiliensis*[54] and also from *Aspergillus fumigatus*[54] and *Aspergillus niger*[55]. The presence of these lipids across a wide variety of fungal species suggests that these might be important biomarkers for fungal recognition in the human body.

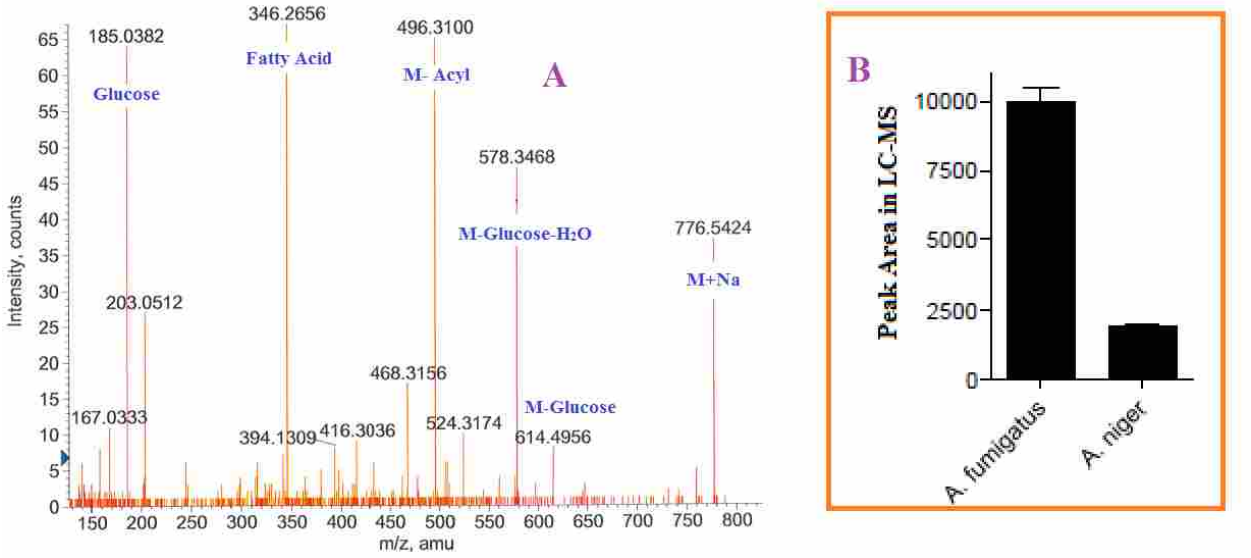

Figure 2.12 In the panel A (left panel) MS/MS spectrum for Asp-754 is shown and the key fragments are accordingly marked. In the panel B, comparative amounts of Asperamide-B in *A. fumigatus* and *A. Niger* are depicted

2.4.8 Validation of structure with MS/MS analysis

After establishing the structure of ASP-754 using NMR, we decided to support our proposition by using tandem MS/MS fragmentation analysis. In figure 2.12 A, the CID-TOF-MS of ASP-754 is shown and the proposed fragments are accordingly labeled.

We also looked at the presence of Asperamide-B in other commonly found species of the genus *Aspergillus*. LC-MS methods described in the experimental section were used for comparative analysis of Asperamide-B in these species. Figure 2.12 B represents the relative amounts of Asperamide-B in *Aspergillus fumigatus* and *Aspergillus Niger*.

2.5 Immunological testing and results

Following the structure elucidation of Asperamide-B, immunological assays were performed. As discussed briefly in introduction section, the key in-vitro and in-vivo tests were performed to measure the potential of Asperamide-B as the antigen for triggering asthma.

2.5.1 Asperamide-B activates *i*NKT cells

To check if NKT cells can be directly activated by Asperamide-B, the *i*NKT cell lines were co-cultured with Asperamide-B and wild-type or CD1d-/- bone marrow derived dendritic cells (BMDC). After 48 h, the levels of IL-4 and IFN-γ were measured using ELISA. As shown in the panel A and B of figure 2.13. The *i*NKT cells co-cultured with wild type BMDC and Asperamide-B were found to contain increased levels of IL-4 and IFN-γ compared to DMSO control. As shown in panel C and D of figure 2.13, the activation of *i*NKT cells by Asperamide-B requires CD-1d as the co-culture of BMDC with CD1d-/- mice failed to induce IL-4 or IFN-γ. Asperamide-B was also found to be directly activating *i*NKT cells as the cytokine production was independent of MyD88 and Trif pathways.

To ensure that the lipid being presented by *i*NKT cells is Asperamide-B, we directly stained *i*NKT cell lines with CD1d tetramers loaded with Asperamide-B. To achieve this, CD1d monomers were loaded with Asperamide-B as positive control. Tetramers were formed by incubating loaded monomers with streptavidin-PE and *i*NKT cells line were then stained with TCR β. These experiments unequivocally prove that Asperamide-B is presented by CD1d to the *i*NKT cells and activates them towards cytokine release.

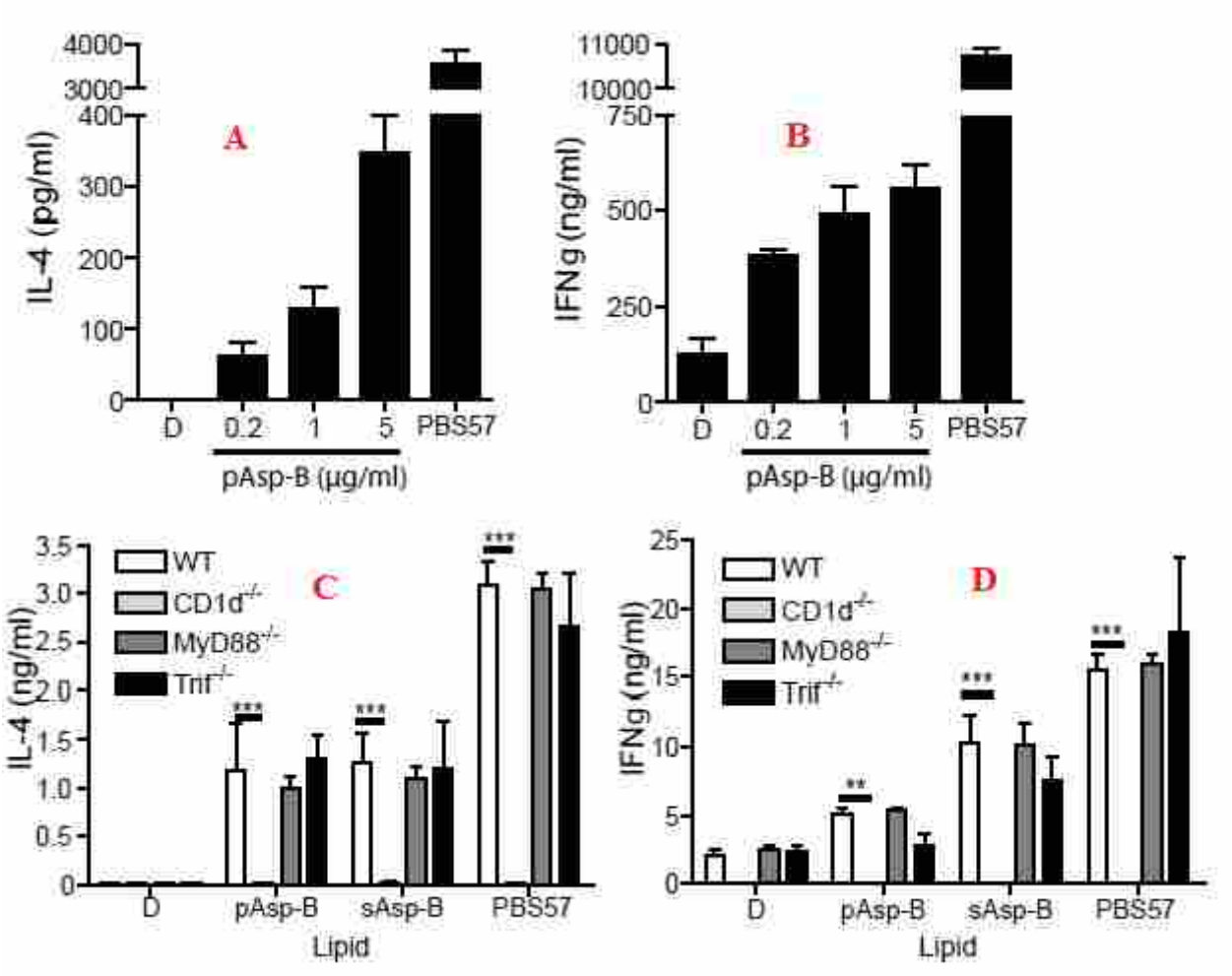

Figure 2.13 Panel A and B show the IL-4 and INFγ release in response to *i*NKT cell activation while panel C and D show the cytokine dependence on CD1-/- and MyD88-/- mice. DMSO (D), purified Asperamide-B (pAsp-B) and PBS57 is the positive control

2.5.2 Asperamide-B induces allergic asthma

After completing in-vitro studies, Asperamide-B was tested for induction of airway hyperreactivity (AHR), which is a cardinal feature of asthma. A single dose of purified Asperamide-B or a vehicle control was administered intranasally to WT or CD1d-/- mice. WT mice developed low but significant AHR compared to vehicle control, while CD1d-/- mice failed to develop AHR (figure 2.15)

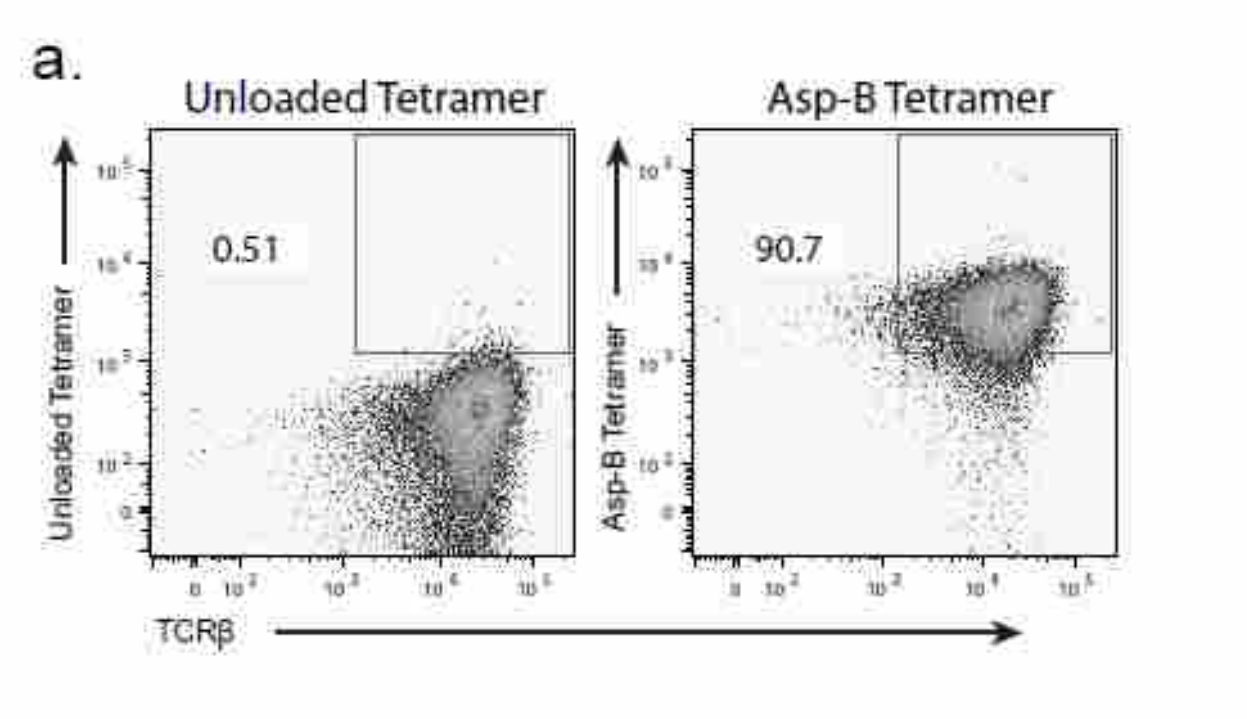

Figure 2.14 representative staining of *i*NKT cells in the liver of C57Bl/6 mice using a combination of TCR-β and Asperamide-B loaded mCD1d tetramers

Asperamide-B also induced production of IL-4 and IL-13 production, which are Th2 cytokines and have been consistently implicated in the development of allergic asthma.

2.5.3 Asperamide-B activates the release of IL-33

IL-33 is an innate cytokine that has been shown to potently cause AHR in the absence of adaptive immunity. Notably, only some of the NKT cell antigens are known to induce IL-33 production and the ability of Asperamide-B to induce IL-33 production (Figure 2.16) may be an important characteristic that distinguishes it from other glycolipids that cannot induce AHR.

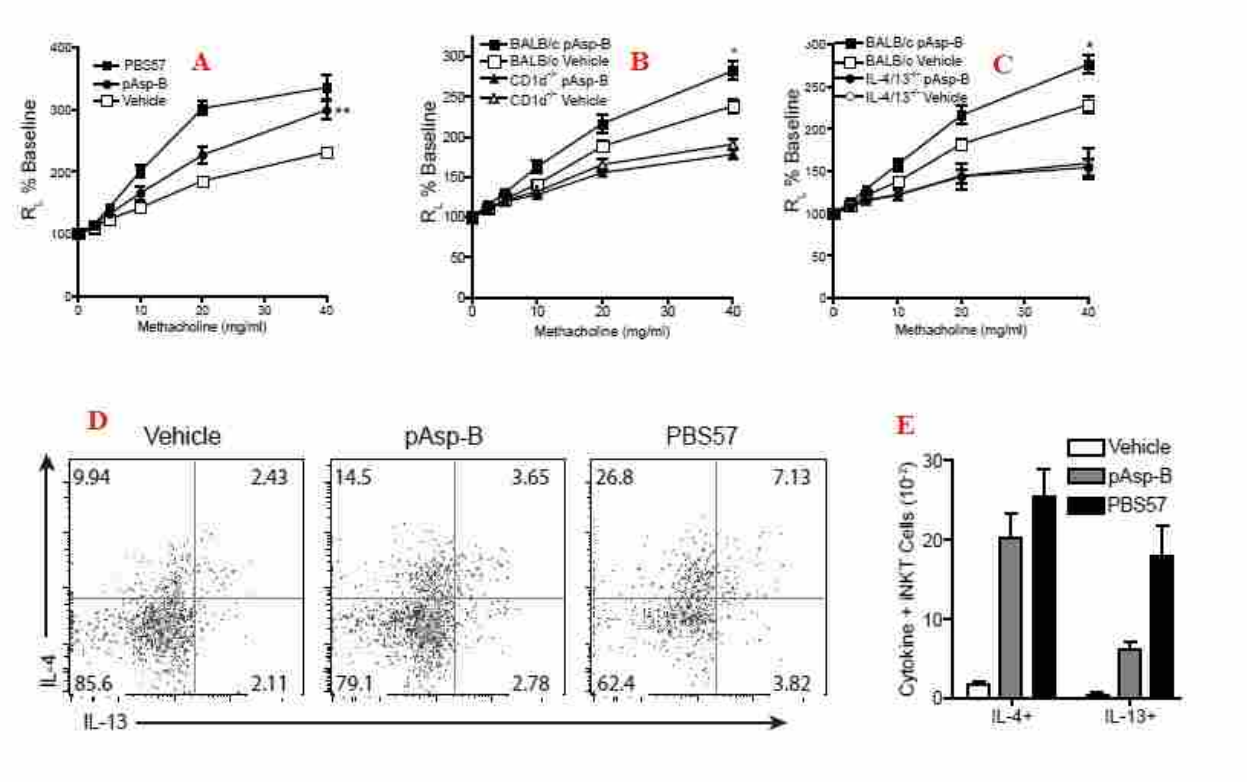

Figure 2.15 Panel A demonstrates that WT BALB/c mice develop AHR after administration of Asperamide-B. Using knockout mice, panel B and C demonstrate the requirement of CD1d and IL-4/IL-13 for the development of AHR. Panel D and E show that administration of purified Asperamide-B induces the production of IL-4 and IL-13 in *i*NKT cells

2.5.4 Discrepancy of the MyD88 requirement

Although the glycolipid identified in this chapter stimulated mouse NKT cells in vitro in a CD1d restricted, MyD88 independent manner; the in-vivo induction of AHR by Asperamide-B required MyD88. We assume that this contradiction is because the induction of AHR by Asperamide-B also requires IL-33 and its receptor ST2. It is well known that signaling through ST2 requires MyD88. In the lungs, we propose that Asperamide-B activates *i*NKT cells which then trigger antigen presenting cells to produce IL-33. After being secreted into the lungs, IL-33 activates a

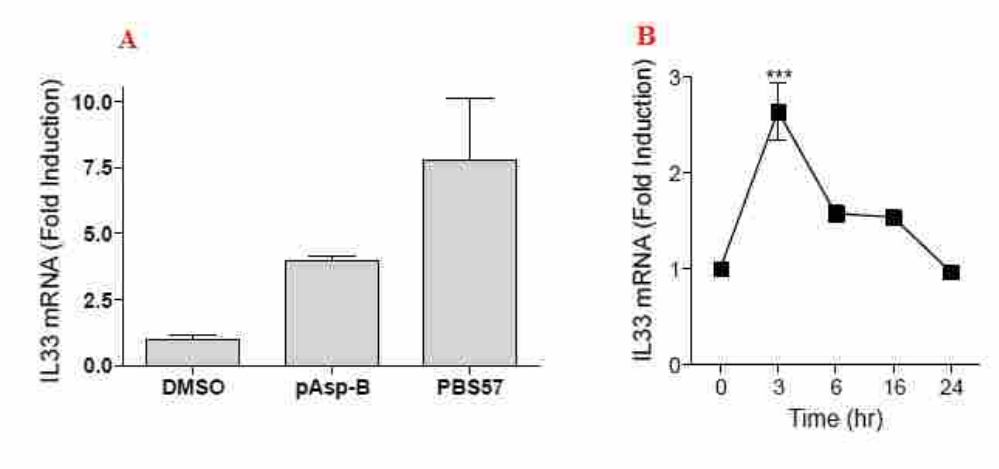

Figure 2.16 Purified Asperamide-B (pAsp-B) induces the production of IL-33

subset of IL-33 responsive NKT cells and neuocytes, both of which produce IL-13. Importantly, IL-33 mediated ST2 signalling requires MyD88, which explains the necessity of MyD88 in the in-vivo induction of AHR.

2.6 Discussion

In this chapter, we hypothesized the link between Aspergillus and asthma, performed the isolation, purification and structure elucidation of a novel fungal glycolipid, and demonstrated that this lipid is responsible for the development of AHR. To our knowledge, this is the first finding of a fungal glycolipid antigen that directly activates both mouse and human NKT cells, and therefore these studies very significantly extend the range of microorganisms recognized by NKT cells. Moreover, these studies also establish the role between *i*NKT cells and asthma. As *Aspergillus fumigatus* is ubiquitous in the environment and is frequently recovered from the respiratory tract of asthma patients, these findings are clinically important and help to explain the potency of *Aspergillus* in

causing respiratory disease and severe asthma in humans.

Although we are confident about the accuracy of the proposed structure of Asperamide-B, the final proof can only be obtained after synthesis of the proposed structure and comparison the NMR spectrum of both the isolated and synthesized material. Therefore, we decided to carry out the synthesis and structure activity relationship of Asperamide-B. Next chapter provides a detailed description of our synthetic efforts and their immunological results.

Chapter 3

Synthesis and Structure Activity Relationship of Asperamide-B

3.1 Introduction

An important aspect of *i*NKT cell research is the identification of natural exogenous antigens. For a long period of time, *i*NKT cells were only known to react primarily to gram negative, LPS negative bacteria including *Sphingomonas* spp.[56] In the past few years, researchers have demonstrated that *i*NKT cells recognize antigens from a wide variety of organisms including *Borrelia burgdorferi*,[57] *Helicobacter pylori*,[58] and *Streptococcus pneumoniae*[59]. Although the variety of antigens known to activate *i*NKT cells has grown in the past few years, no links have been found between fungal sensitization and *i*NKT cells.

In last chapter we described the identification of a fungal glycosphingolipid antigen named

asperamide-B. This antigen directly activated *i*NKT cells in CD1d dependent, MyD88 independent manner. This is the first finding of a fungal glycolipid antigen that directly activates the *i*NKT cells and this study significantly extends the range of microorganisms that are known to directly activate *i*NKT cells. These results also demonstrate an innate immune pathway that helps to explain the potency of *A. fumigatus* in stimulating mucosal sensitization and respiratory diseases.

After structural characterization and immunological testing of isolated asperamide-B, we decided to carry out the synthesis of the proposed structure and compare the spectra of the two. Conventionally, antigenic glycolipids carry an α-linkage of carbohydrate and ceramide moieties. It was very intriguing to find a glycolipid antigen with a β-glycosidic linkage. In careful analysis of the structure of asperamide-B, we noticed two distinctive structural features (A) it carries a 9-methyl, sphinga-4,8-dienine lipid chain and (B) the presence of N-2'-hydroxy-(E)-3'-hexadecanoic acid as the acyl chain. Either one of these distinctions might be responsible for the stimulatory activity of asperamide-B. Researchers have found that minor changes in either sphingosine, carbohydrate, or acyl chain of a glycolipid antigen can dramatically affect immunogenicity. Therefore, to understand the structure activity relationship, we chose to design and synthesize structural variants of asperamide-B .

3.2 Synthetic route for asperamide-B

To establish the structure of asperamide-B beyond doubt, we planned to undertake its synthesis and compare the NMR spectra of isolated and synthesized molecules. Retrosynthestic analysis of

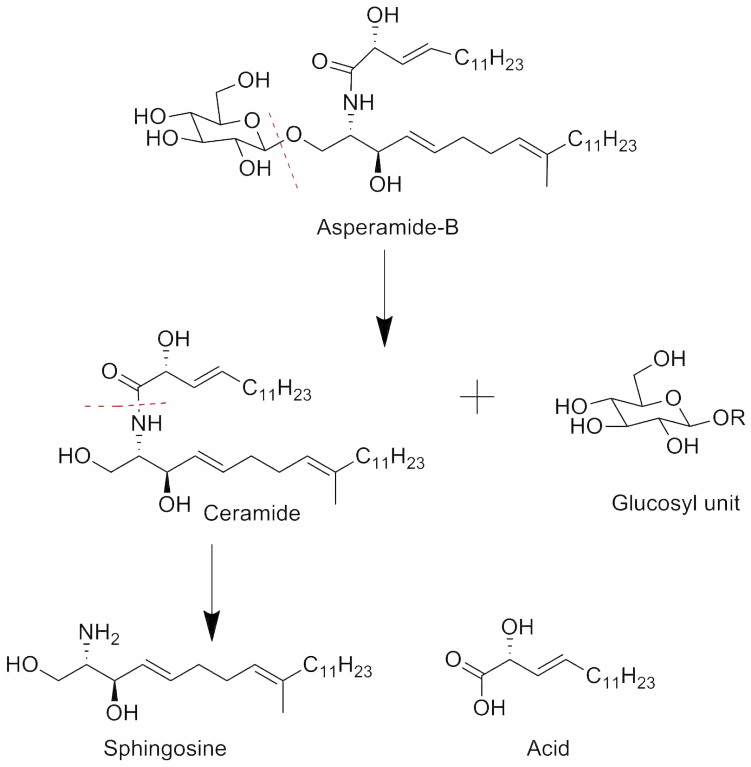

Figure 3.1 Retrosynthetic analysis of asperamide-B

asperamide-B is shown in *Figure* 3.1. Following the conventional synthetic approach, we decided to synthesize the ceramide portion which would be glycosylated to yield asperamide-B. The ceramide moiety would be obtained by coupling sphingadienine with α-hydroxy hexadecanoic acid.

3.2.1 Synthesis of 9-methyl, Sphinga-4,8-dienine

Following literature precedence,[60] the synthesis of the ceramide part was started with 1-tridecyne (Scheme 3.1). Hydrozirconation of 3.1.1 followed by paraformaldehyde quenching resulted in the allylic alcohol 3.1.2. Conversion of allylic alcohol to allylic chloride proved to be challenging. After screening through a few alternatives, Corey-Kim chlorination conditions worked well giving

modest yields. The allylic chloride 3.1.3 was reacted with lithiated 1-trimethylsilyl-1-propyne to yield 3.1.4. In the following step, the TMS group was removed by Bu_4NF to give 3.1.5. Garner's aldehyde was prepared from Boc protected serine using a reported synthetic procedure.[61] Terminal alkyne 3.1.5 was reacted with Garner's aldehyde to yield compound 3.1.6 with high stereoselectivity. Following the Birch reduction , the alkyne moiety in 3.1.6 was converted to a trans alkene and protecting groups were taken off during acidic workup (saturated NH_4Cl) to yield sphinga-4,8-dienine (3.1.7).

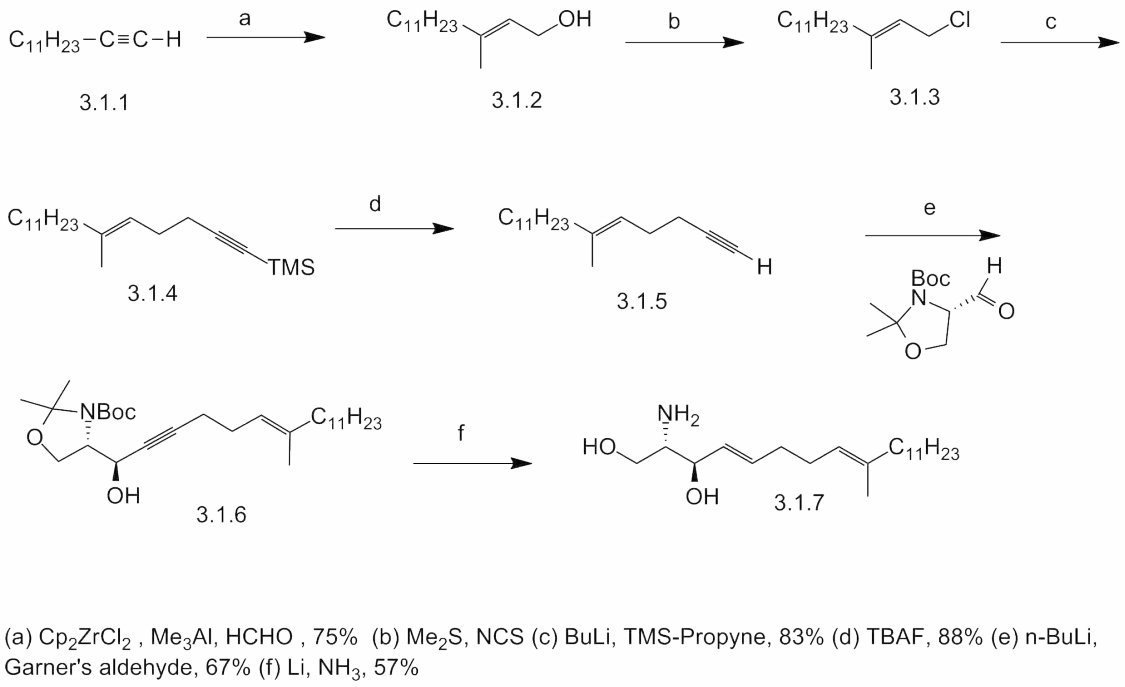

Scheme 3.1 Synthesis of sphingosine chain

3.2.2 Synthesis of N-2'-hydroxy-(E)-3'-hexadecanoic acid (route-1)

As illustrated in Scheme 3.2, synthesis of the acid part was envisioned through a Wittig reaction between commercially available (R)-(+)-2,2-dimethyl-1,3-dioxolane-4-carboxaldehyde (3.2.3) and

the phosphonium salt of 1-bromotridecane. As the Wittig reaction of non-stabilized ylides are known to afford Z-olefins, Schlosser modification of the Wittig reaction was carried out. Unfortunately, the Z-alkene was obtained as the major product. Many unsuccessful attempts were made to optimize the reaction conditions, but the major product was still the Z-alkene. After a careful literature survey,[62–64] the method outlined in Scheme 3.2 was adopted and the Wittig reaction successfully yielded desired E-alkene.

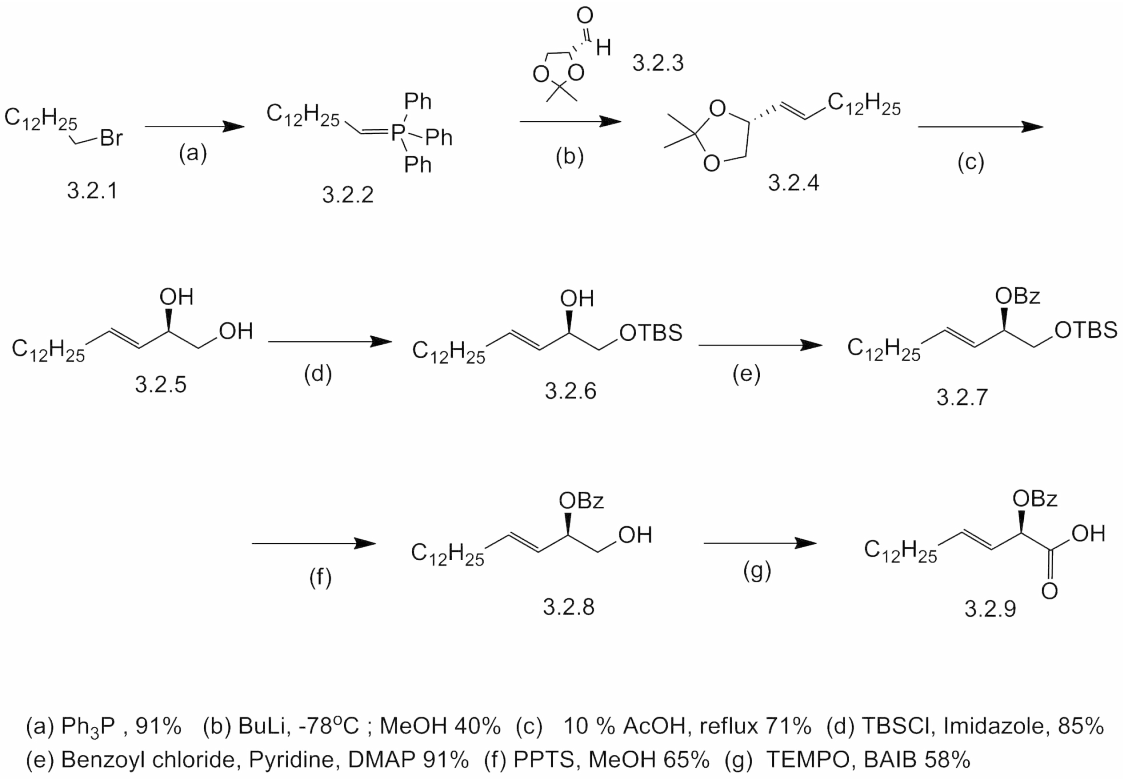

Scheme 3.2 Synthesis of N-2'-hydroxy-(E)-3'-hexadecanoic acid (route-1)

Briefly, 1-Bromotridecane was reacted with triphenyl phosphine to generate the phosphonium salt. Using one equivalent butyl lithium, Wittig reaction was performed at -78 ^{0}C. After 1 h, dry methanol was added dropwise to generate E-alkene. The possible mechanism for the reaction

is shown in *Figure* 3.2.

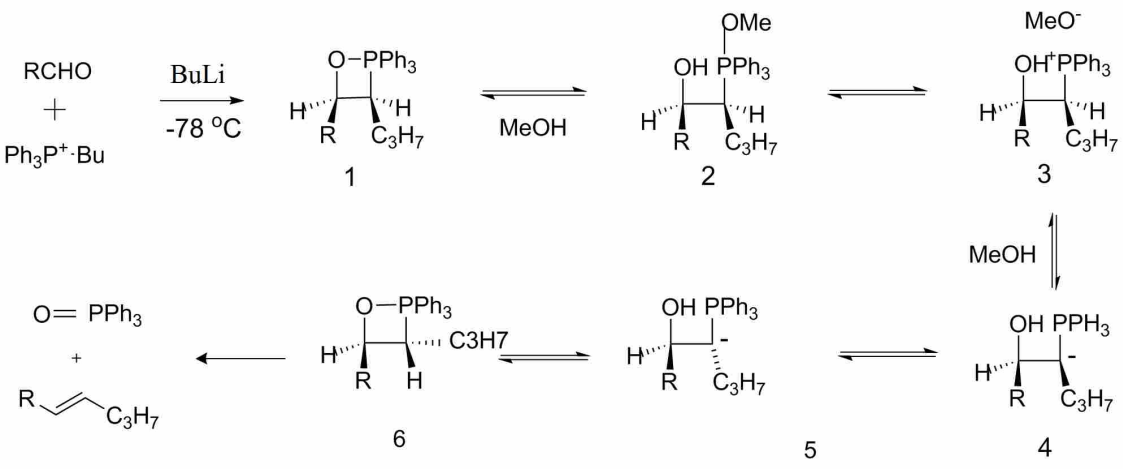

Figure 3.2 Proposed mechanism for the formation of E-alkene using aforementioned procedure

Although we obtained the desired stereochemistry using this method, the time of MeOH addition is critical to the success of this reaction and large batch to batch variations were encountered.

3.2.3 Synthesis of N-2'-hydroxy-(E)-3'-hexadecanoic acid (route-2)

Because of the reproducibility issues in the aforementioned synthetic route, we decided to pursue an alternate route for the synthesis of the desired acid. After careful literature review,[65] the synthetic approach of Prevost et al., was followed. In the first step of this synthesis, an in-situ Grignard reagent is generated using Grignard exchange between 1-tetradecyne and ethyl magnesium bromide. This Grignard reagent is consequently reacted with diethyl oxalate to afford α-keto-β, γ acetylenic ester 3.3.2. Performing the stereoselective reduction of the ester using S-alpine borane led to the generation of crucial α-hydroxy moiety in the molecule. After careful protection and deprotection, alcohol 3.3.6 was oxidized using Tempo and BAIB to yield the desired compound.

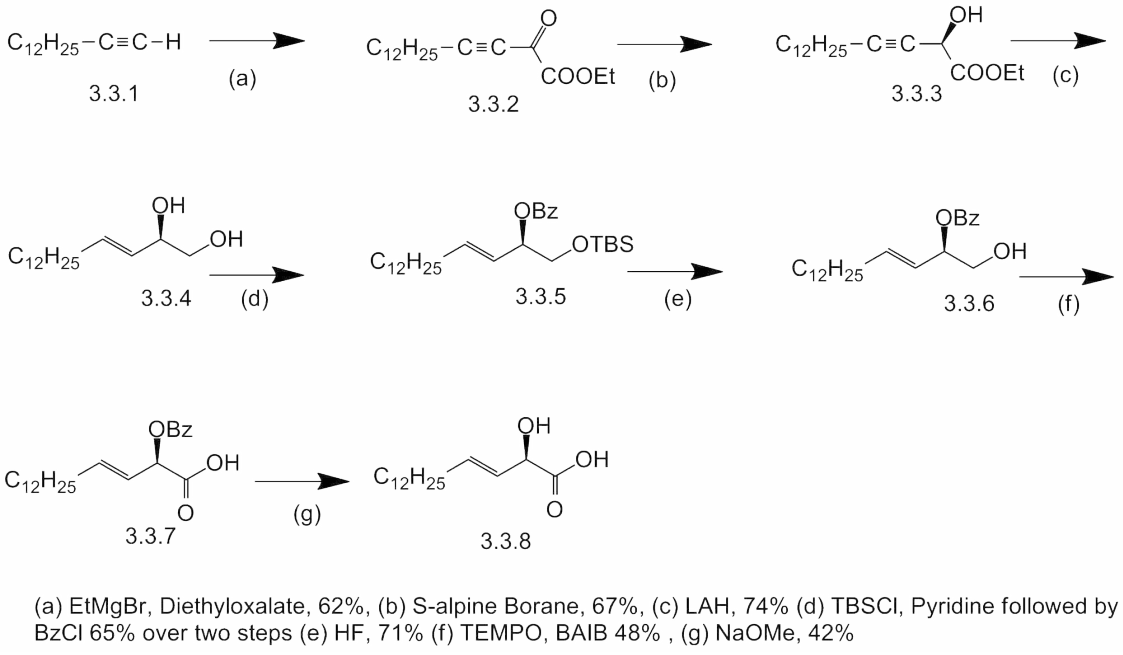

Scheme 3.3 Synthesis of N-2'-hydroxy-(E)-3'-hexadecanoic acid (route-2)

3.2.4 Preparation of ceramide and the sugar coupling

In accordance with the proposed retrosynthetic analysis, after successful synthesis of both sphingadienine and acid pieces, we focused on the synthesis of ceramide. Sphingadienine 3.1.7 and acid 3.2.9 were coupled using EDCI and HOBT to afford ceramide 3.4.1. After functional group manipulations, glycosylation using glucosyl trichloroacetimidate donor 3.4.3 and ceramide acceptor 3.4.2 was carried out. Unfortunately, this reaction failed to yield asperamide-B and after many unsuccessful attempts, we decided to change the synthetic strategy.

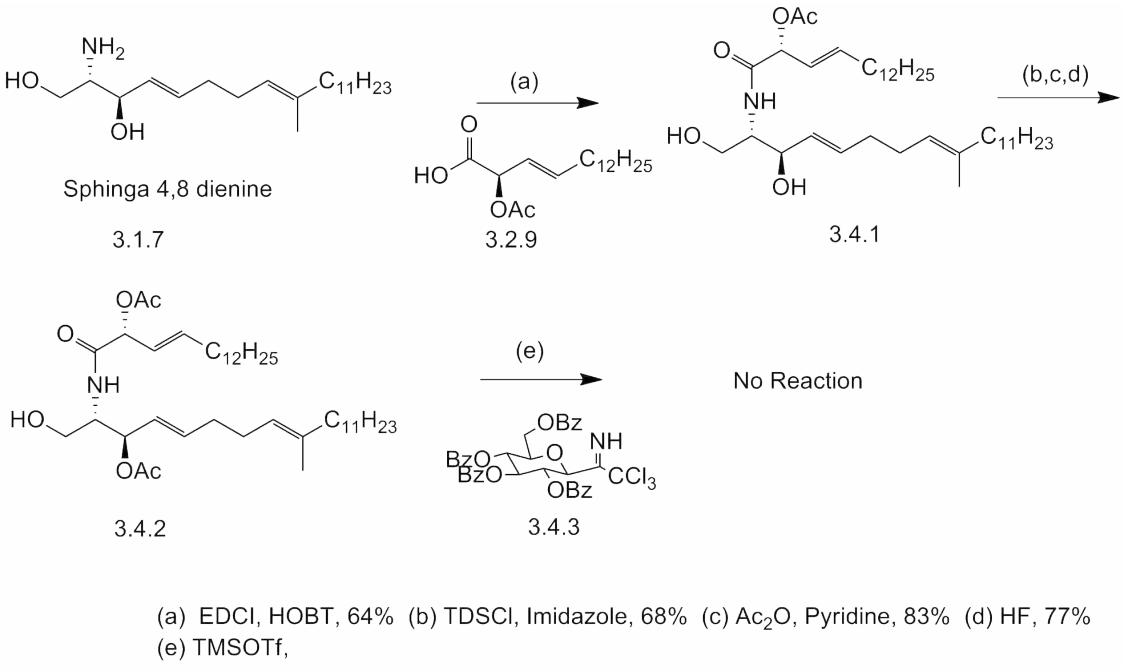

Scheme 3.4 Unsuccessful synthesis of ceramide

3.2.5 Successful synthesis of asperamide-B

We suspect, in the previous glycosylation step, the poor reactivity of ceramide was the reason for the failed Schmidt coupling. Therefore, we decided to use sphingadienine as an acceptor. In Scheme 3.5, this stepwise process is demonstrated. Briefly, azido transfer to the sphinga-4,8-dienine resulted in product 3.5.1, which upon protecting group manipulations afforded ready to couple azido sphingadienine 3.5.2. Using trimethylsilyl trifluoromethanesulfonate (TMSOTf) as a promoter, the glucosyl moeity was installed onto sphingadienine to yield 3.5.4 in good yields. For the reduction of azide moiety in 3.5.5, Staudinger conditions using triphenylphosphine and tributylphosphine resulted in very low yields. Alternatively, the reduction with Zn and acetic acid worked well giving modest yields. Protecting groups from lyso-glucosylceramide 3.5.4 were

removed using sodium methoxide to yield 3.5.5. In the final step, amide bond formation between lyso-glucosylceramide 3.5.6 and acid 3.3.8 was achieved using EDCI and HOBT to yield asperamide-B.

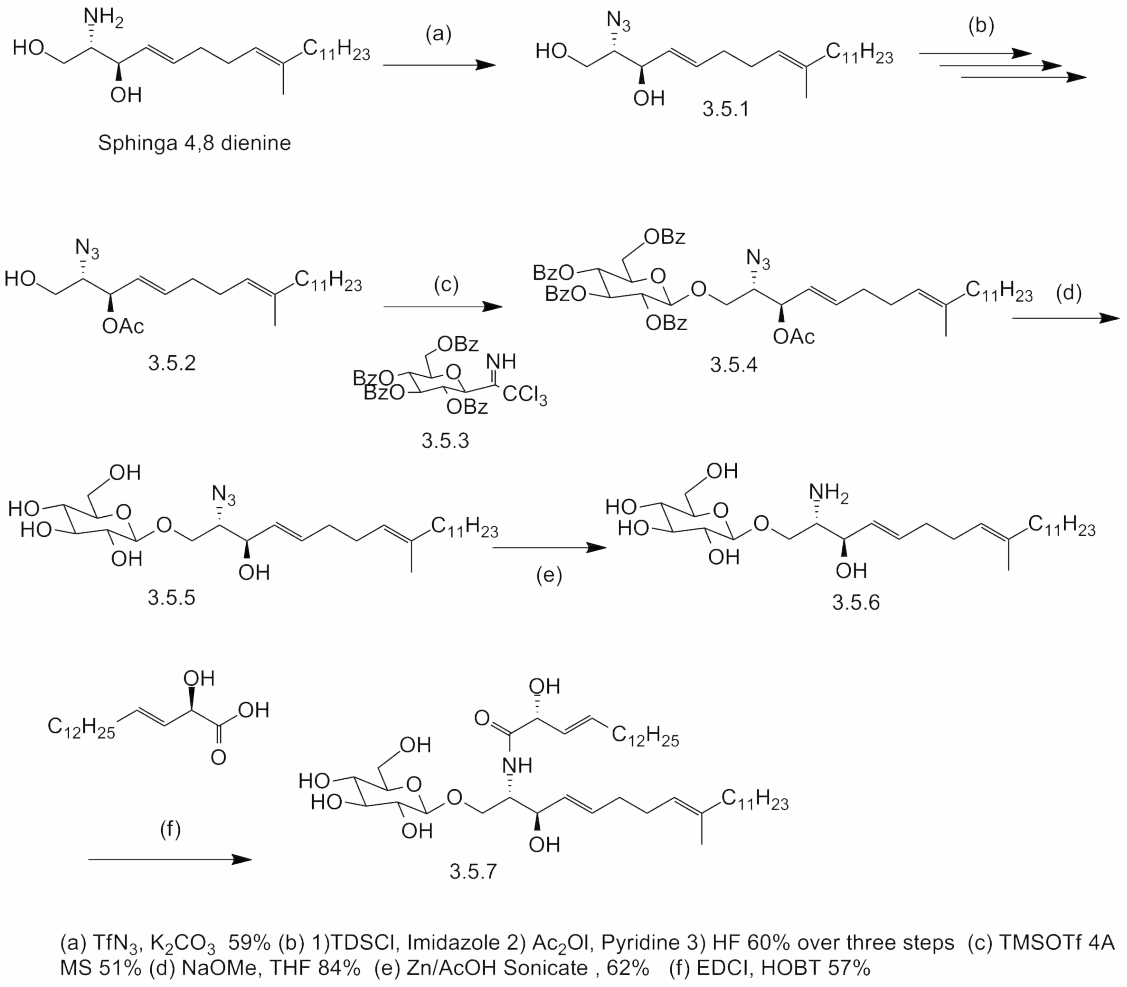

Scheme 3.5 Synthesis of acid moeity (route-2)

3.3 Synthesis of asperamide-B analogues

As discussed in section 3.1, to understand the role of unconventional sphingadienine and α-hydroxy acyl chains, structural variants of asperamide-B were synthesized. In variant-1, the 9-methyl, sphinga-4,8-dienine chain was replaced by a sphinga-4-enine ($C_{20:1}$) chain and in variant-2, the acyl chain was replaced with palmitic acid. Figure 3.4 illustrates the idea behind the choice of these variants.

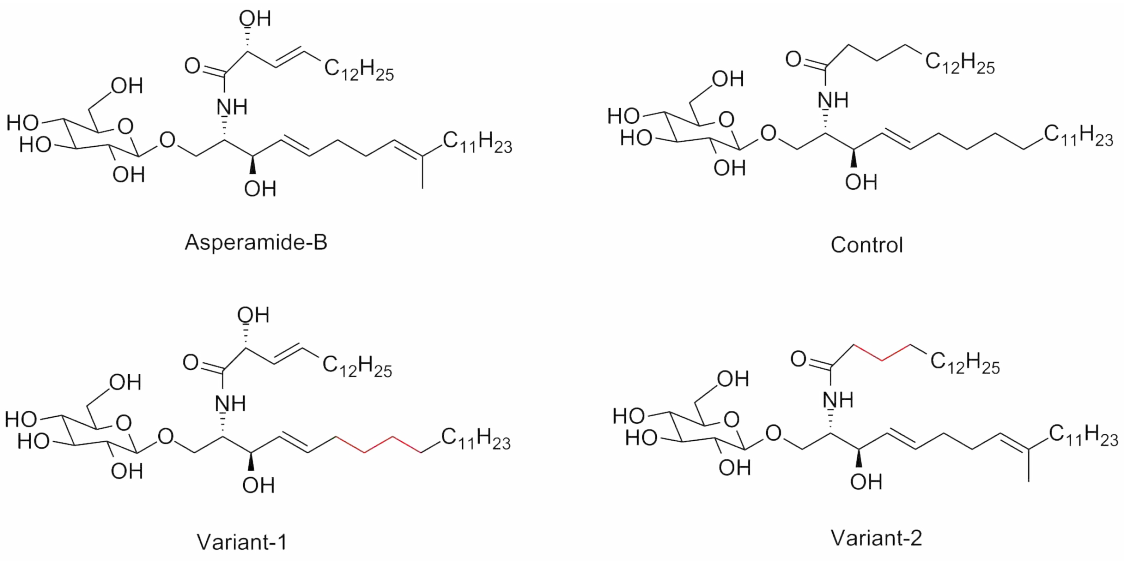

Figure 3.3 Structural variants of asperamide-B

Synthetic scheme for variant-1 with the modified sphingosine chain is shown in Scheme 3.6. Briefly, sphingosine 3.6.1 was prepared by using standard procedures. Schmidt coupling of 3.6.1 and glucosyl trichloroacetimidate afforded 3.6.2. Protecting groups from intermediate 3.6.2 were removed using sodium methoxide and the azido group was reduced to corresponding amine using zinc/HCl to yield intermediate 3.6.4. This lyso-glucosyl-ceramide 3.6.4 was coupled with N-2'-hydroxy-(E)-3'-hexadecanoic acid to finally yield the asperamide variant-1.

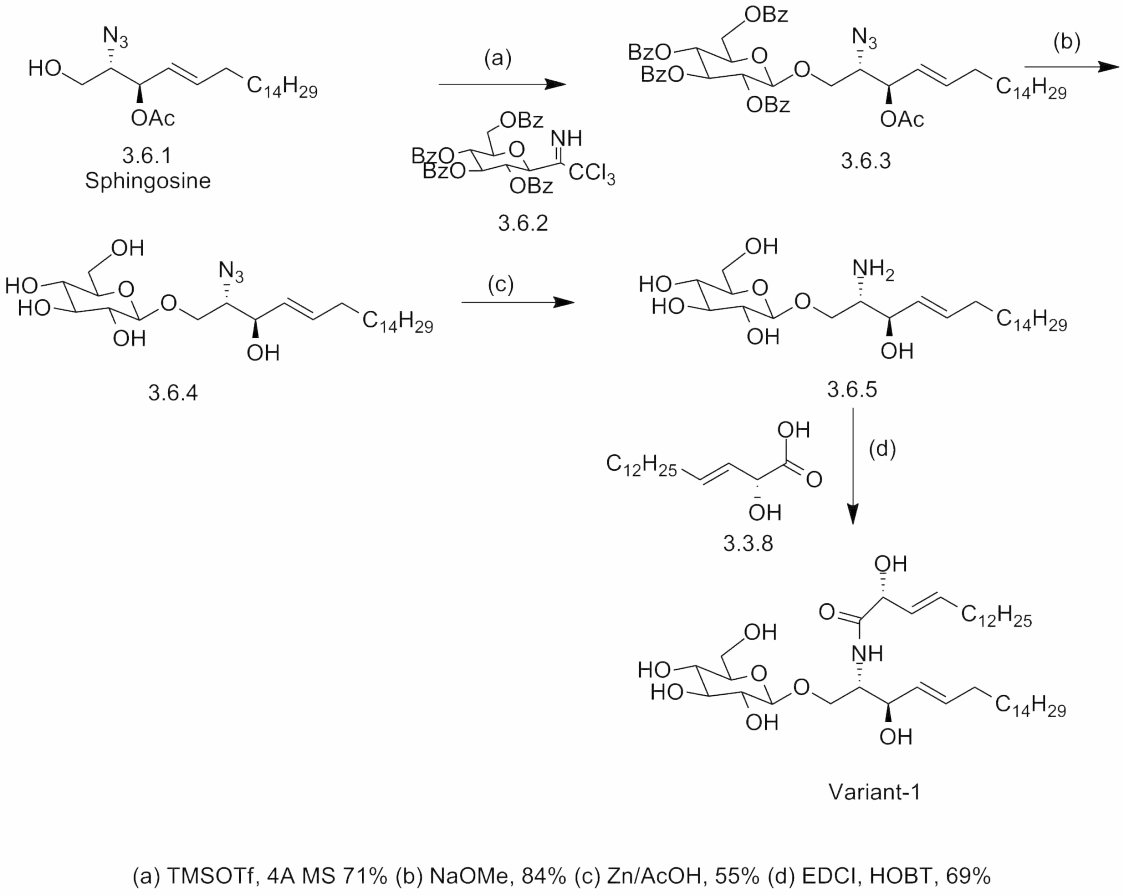

Scheme 3.6 Synthetic route for structural variant-1 of asperamide-B

In order to understand the role of acyl chain on the immunostimulatory properties of asperamide-B, we replaced the N-2'-hydroxy-(E)-3'-hexadecenoic acid with palmitic acid and the molecule was named asperamide-B variant-2. To achieve this, lysoglucosylceramide 3.5.6 was coupled with palmitic acid using EDCI and HOBT.

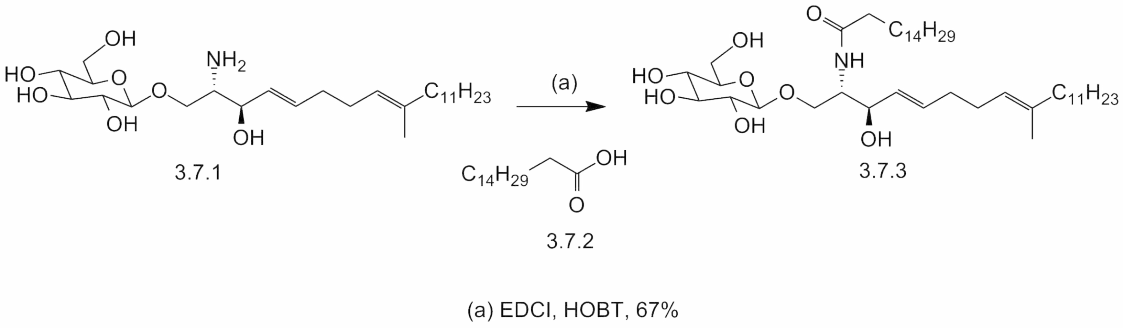

Scheme 3.7 Synthetic route for structural variant-2 of asperamide-B

3.4 Results and Discussion

After isolation and characterization of asperamide-B, we started its synthesis and structure activity studies. While the immunological results obtained from the isolated asperamide-B were exciting, there is always a dangers of the contamination from endotoxins like lipopolysaccharide (LPS), which could result in a false positive. Synthesized asperamide-B is more amenable to cell free antigen presentation using plate bound CD1d. Synthesized lipid also loaded better into CD1d tetramers which were used to stain NKT cells.

Upon completion of the synthesis, NMR spectra of the isolated and synthesized asperamide-B were compared. Except for the presence of a water peak (3.65 ppm) in isolated asperamide-B, other details of the NMR spectrum spectra were identical (figure 3.4). Being a glycosphingolipid asperamide-B is amphoteric in nature, which makes it challenging to chromatograph and remove impurities. Keeping this in mind, we acylated both the isolated and synthetic asperamide-B and compared their 1HNMR and carbon spectra (see appendix). We were very excited to observe that NMR spectrum of the acylated lipids were a perfect match. Taken together, these NMR studies

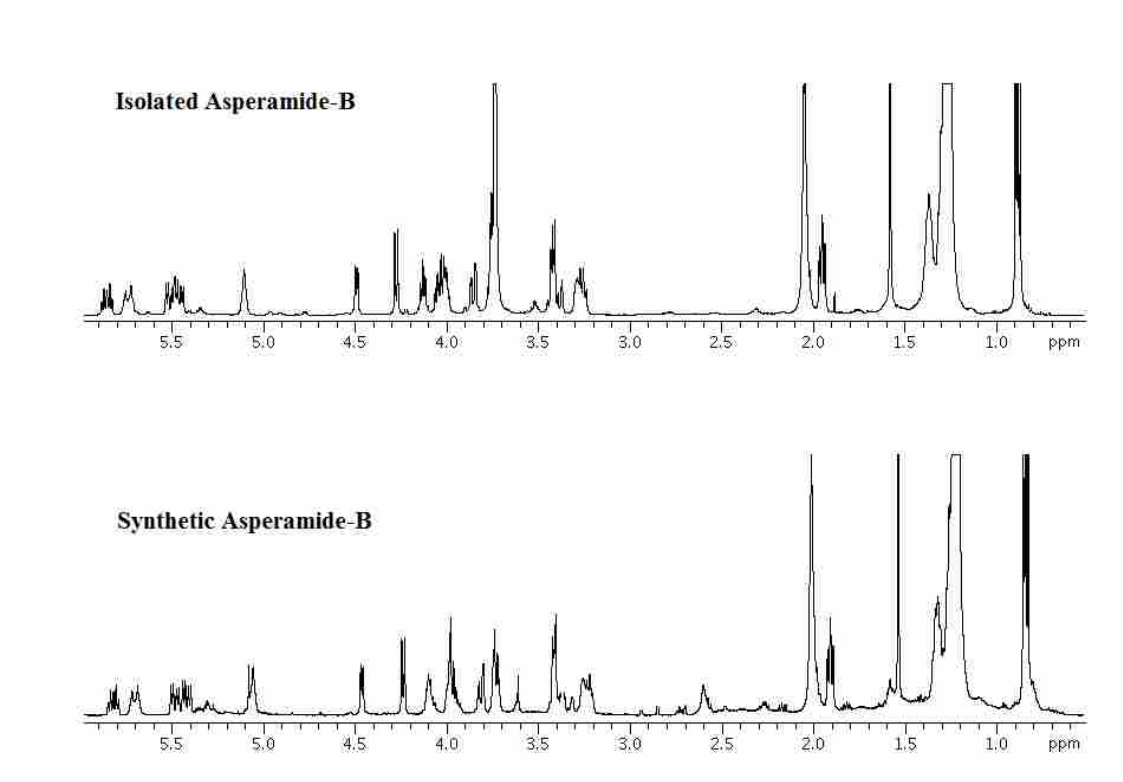

Figure 3.4 ^{1}HNMR of isolated and synthetic asperamide-B is shown. Solvent used: $CDCl_3$

confirms that the proposed structure of asperamide-B was indeed correct.

To ensure that synthetic asperamide-B has the same potency as the isolated material, both antigens were evaluated for murine CD1d-dependent IL-4 and IFN-γ secretion at varying concentrations. In figure 3.5, the cytokine production among synthetic (sAsp-B) and purified (pAsp-B) asperamide-B is shown. We were again very happy to notice that both synthetic and isolated material have similar immunological profiles(panel A-D, figure 3.5).

As discussed previously (section 2.2.1), NKT cells can be activated by antigens in either direct or indirect fashion. To understand if both the synthetic and isolated asperamide-B directly activate NKT cells, Triff and MyD88 knockout mice were used. To ensure that activation of NKT

cells by this lipid is CD1d dependent, NKT cell lines were cocultured with asperamide-B and WT or CD1d-/- bone marrow derived dendritic cells (BMDCc). In panel E and F of *Figure* 1.5, CD1d, Triff, and MyD88 dependence of both synthetic and isolated asperamide-B is illustrated. Taken together, these data strongly suggest that both the synthetic and isolated asperamide-B have the same molecular structure, as they induce similar immunological responses.

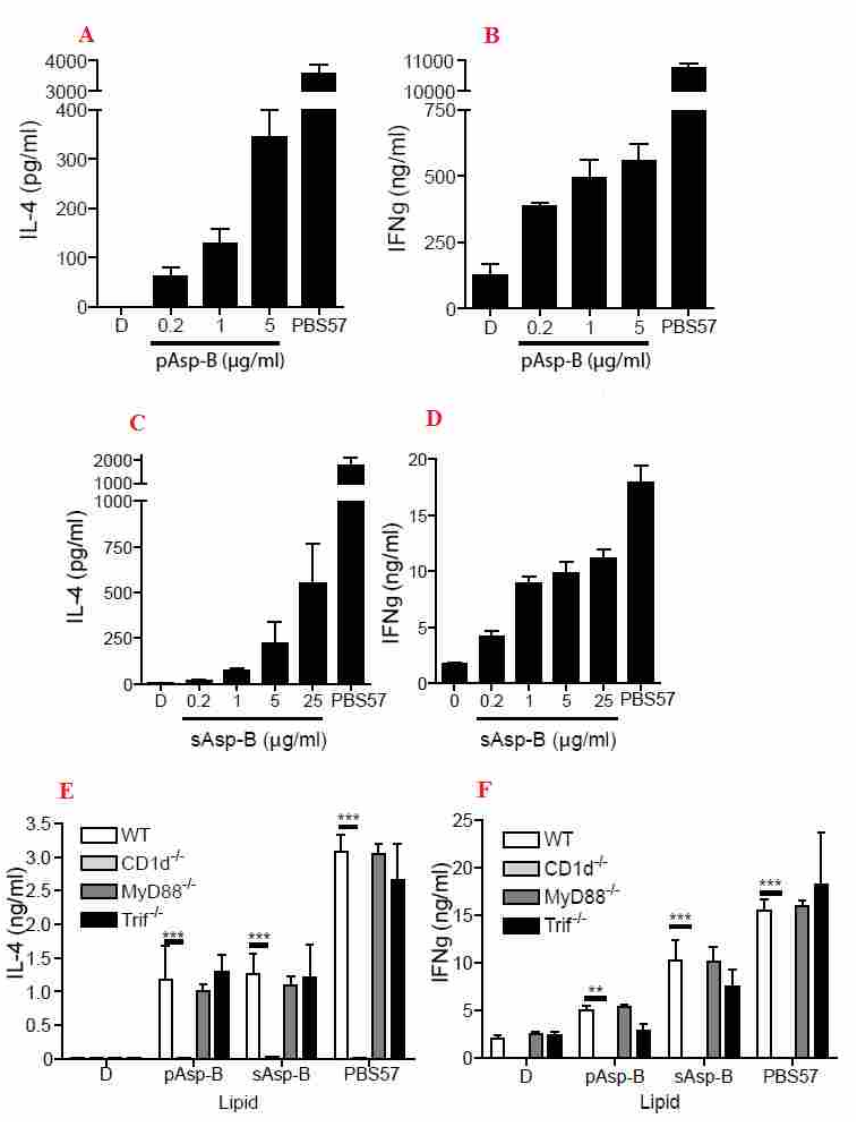

Figure 3.5 NKT cells and bone marrow dendrtitic cells (BMDCs) were incubated with DMSO(D), purified asperamide B (pAsp-B), synthetic asperamide B (sAsp-B), or PBS57 (α-GalCer analogue). After 48 h, the cytokines (IL-4 and IFN-γ) were measured by ELISA. NKT cells derived from WT, CD1d-/-, MyD88-/-, or Trif-/- BMDCs were also incubated with DMSO, purified asperamide B, synthetic asperamide B, or PBS57. There were significant differences between cultures containing WT and CD1d-/- BMDCs incubated with pAsp-B, sAsp-B, or PBS57 (panel E and F, figure 3.5). There were no significant differences between cultures containing WT and MyD88-/- or WT and Trif-/- BMDCs for any lipid tested

To compare the role of sphingadienine and α-hydroxy acyl chain in NKT cell activation, structural variants of asperamide-B were designed and tested for IL-4 and IFN-γ production. Preliminary testing on the activity of these compounds shows that 9-methyl, sphinga-4,8-dienine plays a key role in the NKT cell stimulation, as variant-2 (figure3.6) has almost similar cytokine profile as asperamide-B itself. These results also argue that α-hydroxy acyl chain is of little importance in the recognition of these molecules by NKT cells.

Various research groups have studied the roles of sphingosine chain in glycolipid recognition by NKT cells.[66] Sphingosine chains are not only known to impact the NKT cell activation, but can also influence the cytokine release profiles (Th1 vs Th2). With this information, we propose that despite asperamide-B being a β-linked glycolipid, 9-methyl, sphinga-4,8-dienine chain improves the binding of asperamide-B to NKT cell TCR which makes it a weak stimulator.

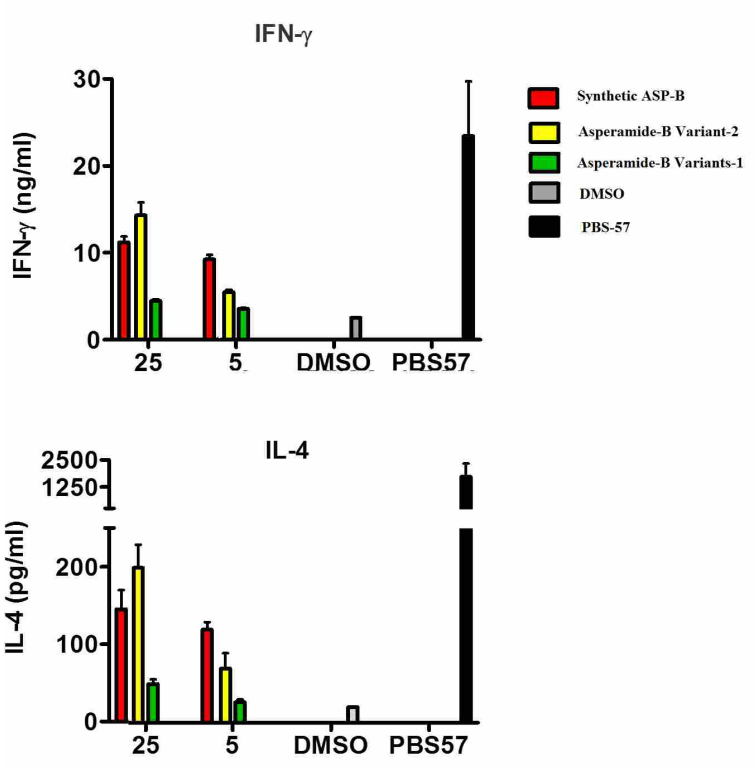

Figure 3.6 In vitro culture of iNKT cells and BMDCs incubated with DMSO, purified asperamide-B variant-1, asperamide B variant-2, or PBS57 (α-GalCer analogue). Supernatant was harversted after 48 h and cytokines were measured by ELISA for IL-4 and IFN-γ

In this chapter, we have identified and synthesized a novel glycosphingolipid antigen that directly activates NKT cells. This antigen, asperamide-B, rapidly induces airway hyperreactivity in BALB/c mouse model. This is a major finding in the field of NKT cell research and provides some valuable insights in understanding the triggers of asthma. These results also extend the range of microorganisms recognized by *i*NKT cells and help explain their high degree of conservation across many mammalian species.

Additionally, these findings present NKT cells as an attractive therapeutic target in human asthma. Lipid antigens like asperamide-B, which could induce NKT cells to secrete Th2 cytokines,

may be present in many other form of ubiquitous microorganism. If that's the case, preventing the amplification of Th2 response by NKT cells might be a good strategy against asthma and antigens with strong Th1 bias (α-GalCer) may serve as a therapeutic agent.

3.5 Experimental Procedures

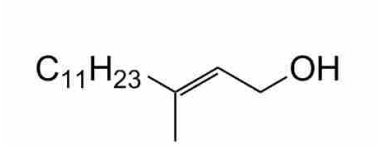

3.1.2

To a stirred suspension of Cp_2ZrCl_2 (4g, 13.9 mmol) in 70 mL of dry DCM, trimethyl aluminium (30 mL, 2 M, in hexanes) was added dropwise at -30^{o}C. The reaction was allowed to warm up to room temperature, and then re-cooled to -30^{o}C. To this resulting pale yellow solution, 1-tridecyne (5.0 mL, 27 mmol) was then added dropwise while maintaining the temperature at -30^{o}C. Reaction was allowed to warm up to room temperature and after 24 h, the reaction was again cooled down to -10^{o}C and paraformaldehyde (2 g, 60 mmol) was added in small portions over 10 minutes. After 30 minutes, the reaction was quenched with saturated ammonium chloride. The solvent was removed under vacuum and the residue was extracted using ethyl acetate. Organic extracts were combined and dried. The residue was purified using column chromatography in 5% ethyl acetate in hexanes to give 3.1.2 (3.58 g, 75%). ^{1}H NMR (500 MHz, Chloroform-d) δ 5.4 (t, J = 6.4, 1 Hz, 1H), 4.16 (d, J = 8.5 Hz, 2H), 3.68 (s, 1H), 2.07 (q, J = 8.0 Hz, 2H), 1.65 (s, 3H), 1.38 - 1.41 (m, 2H), 1.21 - 1.35 (br, 16H), 0.88 (m, 3H). ^{13}C NMR (125 MHz, Chloroform-d) δ 140.2, 124.3, 59.6, 40.1,

31.91, 29.70, 29.64, 29.37, 29.19, 28.65, 22.91, 16.80, 14.25. HRMS (ESI) calcd for $C_{15}H_{30}O$ [M+H]+: 227.2330, found: 227.2417

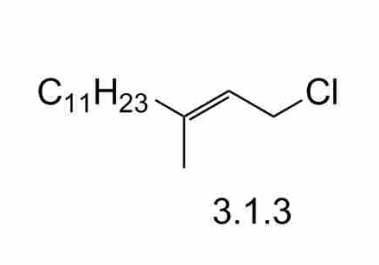

3.1.3

In a round bottom (RB) flask, N-chlorosuccinamide (4.42 gm, 33.1 mmol) was dissolved in 100 ml anhydrous DCM. This solution was cooled in an ice bath and dimethyl sulfide (2.58 ml, 35.36 mmol) was added dropwide. This suspension was cooled to -30^o and the allylic alcohol 3.1.2 (2.5 g, 11.05 mmol) was added dropwise. The reaction was stirred for additional 1 h and monitored by TLC for the disappearance of 3.1.2. Upon completion, reaction was quenched by adding water and filtered through a silica plug. Organics were pooled, dried over Na_2SO_4 and solvent was removed under vacuum. The residue was taken to the next step without purification.

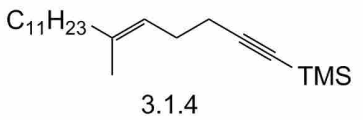

3.1.4

In a 250 ml RB flask, n-BuLi (2.8 mL, 2.5 M) was added dropwise at -78 ^{o}C to 50 ml dry THF. After 20 minutes, 1-TMS-1-propyne (0.8 g, 7.3mmol)was added to this solution. This solution was stirred at -40 ^{o}C for 30 mins and then cooled to -78 ^{o}C. To this solution, 1.5 g (6.15 mmol) of 3.1.3 was added dropwise and the reaction was allowed to warm up to -10 ^{o}C. After 1 h, saturated NH_4Cl was added to quench the reaction. The reaction mixture was extracted twice

with ethyl acetate and dried over Na_2SO_4. Combined organic extracts were dried under vacuum and purified using column chromatography with 1% ethyl acetate in hexanes to give 3.1.4 (2.1 g, 83%). ^{1}H NMR (Chloroform-d, 500 MHz) δ 5.18 (br, 1 H), 2.20 (br, 4 H), 1.96 (t, J = 8 Hz, 2 H), 1.60 (s, 3 H), 1.21-1.42 (m, 18 H), 0.88 (t, J = 6.7 Hz, 3 H), 0.143 (s, 9 H); ^{13}C NMR (Chloroform-d, 125 MHz) δ 132.42, 117.38, 79.86, 63.29, 34.89, 27.17, 24.91, 24.86, 24.66, 24.59, 23.14, 22.40, 18.03, 14.22, 0.34; HRMS (ESI) calcd for $C_{20}H_{40}$ Si [M+H]+: 321.2927, found: 321.2958.

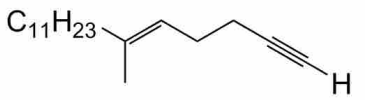

3.1.5

To an ice cooled solution of 3.1.4 (1.6g, 4.9 mmol) in 30ml of THF, a 1M solution of Bu_4NF in THF (5.3ml, 5mmol) and acetic acid (0.84 ml, 13.9 mmol) was added and the reaction was stirred for 1 h. The reaction was monitored for the disappearance of 3.1.4 by TLC and upon completion reaction was quenched with water and extracted twice with hexanes. Organic extracts were pooled and dried under vacuum. The residue was purified using column chromatography with 1% ethyl acetate in hexanes to give 3.1.5 (1.1 g, 88%) . ^{1}H NMR (Chloroform-d, 500 MHz) δ 5.16 (t, J = 7 Hz, 1 H), 2.20 (m, 4 H), 1.980 (t, J = 8 Hz, 2 H), 1.93 (t, J = 1 Hz, 1 H), 1.60 (s, 3 H), 1.20-1.40 (m, 18 H), 0.88 (t, J = 6.5 Hz, 3 H); ^{13}C NMR (Chloroform-d, 125 MHz) δ 136.98 , 122.24 , 107.48 , 84.20 , 76.73 , 39.66 , 31.92 , 30.72-29.06 (m), 27.91 , 27.32 , 22.69 , 20.37 , 16.04 , 14.12 . As this compound has no groups to ionize in mass spec (very greasy) and there are solubility issues in the mass spec eluent media, mass of this compound could not be determined.

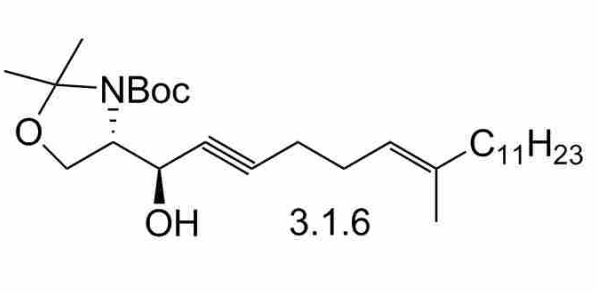

3.1.6

In a 100 ml flame dried RB flask, n-BuLi (2.1 mL, 2.5 M) was slowly added to 30 ml dry THF at -78 ^{o}C. To this solution, after 30 min, 3.1.5(1.1 g, 4.33 mmol) was added dropwise. The solution was allowed to warm and stirred at -40 ^{o}C for 30 minutes, then re-cooled to -78 ^{o}C and Garner's aldehyde (1.0g, 4.43 mmol) was added dropwise. The reaction was allowed to warm upto -30 ^{o}C and after ensuring the completion by TLC, saturated NH_4Cl was added to quench the reaction. The reaction mixture was extracted with ethyl acetate and dried over Na_2SO_4. Organic extracts were pooled and dried under vacuum. The residue was purified using column chromatography with 10% ethyl acetate in hexanesto give 3.1.5 (1.6 g, 67%). ^{1}H NMR (Chloroform-d, 500 MHz) δ 5.11 (m, J = 6.8, 5.2, 2.2 Hz, 1H), 4.71 (d, J = 8.3 Hz, 1H), 4.50 (d, J = 9.1 Hz, 1H), 4.17 - 4.10 (m, 1H), 4.07 (t, J = 8.3 Hz, 1H), 3.94 - 3.85 (m, 1H), 2.19 (s, 3H), 1.94 (t, J = 7.6 Hz, 2H), 1.58 (s, 6H), 1.50 (s, 9H), 1.36 (br, 3H), 1.25 (s, 19H), 0.87 (t, J = 6.9 Hz, 3H); ^{13}C NMR (Chloroform-d, 125 MHz) δ 154.03, 136.96, 122.06, 94.90, 86.44, 81.20, 77.83, 65.13, 64.15, 62.73, 39.65, 31.91, 29.68, 29.63, 29.56, 29.34, 29.32, 28.37, 27.93, 27.30, 25.73, 25.40, 22.68, 19.28, 15.98, 14.11. HRMS (ESI) calcd for $C_{29}H_{52}$ NO_4 [M+H]+: 478.3818, found: 478.3904.

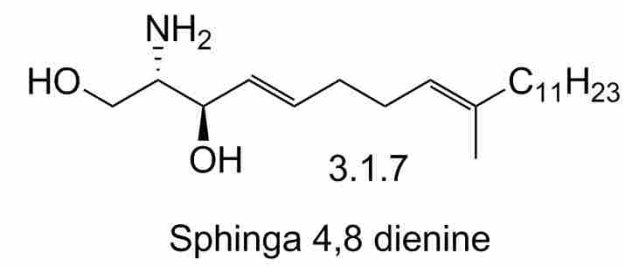

Sphinga 4,8 dienine

In a 100 ml flame dried RB flask 18 mL of $EtNH_2$, Li (250 mg, 41 mmol) was added at -78 ^oC. This solution was stirred for 30 minutes and 3.1.6 (1.0 g, 2.1 mmol) in 15 mL of dry THF was added. The reaction was stirred for 2 hrs at -78 ^oC and checked intermittently using mass spectrometer for the disappearance of 3.1.6. After reaction completion, 10 ml of saturated NH_4Cl was added to quench the reaction. The reaction mixture was extracted with ethyl acetate and dried over Na_2SO_4. Combined organic extracts were dried under vacuum and purified using column chromatography with 5% methanol in dichloromethane to give 3.1.7 (570 mg, 57%). ^1H (Chloroform-d, 500 MHz) δ 5.76 (m, 1H), 5.45 (dd, J = 15.4, 6.6 Hz, 1H), 5.07 (m, 1H), 4.28 - 4.11 (br, 4H), 3.70 (m, 2H), 2.97 (q, J = 4.9 Hz, 1H), 2.06 (s, 3H), 1.97 - 1.89 (m, 2H), 1.56 (s, 3H), 1.35 (br, 2H), 1.24 (s, 18H), 0.87 (t, J = 6.8 Hz, 3H); ^{13}C NMR (Chloroform-d, 125 MHz) δ 136.11, 136.10, 134.06, 128.67, 123.14, 123.07, 76.75, 73.54, 67.94, 62.10, 56.39, 39.72, 39.69, 39.65, 32.61, 32.52, 31.93, 31.92, 31.91, 31.90, 29.70, 29.68, 29.67, 29.64, 29.59, 29.56, 29.39, 29.35, 29.33, 28.04, 27.99, 27.62, 25.58, 24.56, 22.68, 22.66, 22.66, 16.00, 15.98, 15.96, 15.95, 14.10. HRMS (ESI) calcd for $C_{21}H_{41}NO_2$ [M+H]+: 340.3137, found: 340.3207.

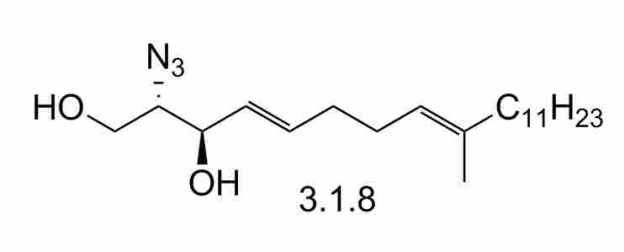

3.1.8

To an ice cold, 15 ml aqueous solution of NaN_3 (0.14 g, 2.12 mmol), 15 mL of DCM was added. Thereafter, Tf_2O (0.54 ml, 3.89 mmol) was added to this solution at 0 ^oC and the reaction was vigorously stirred for 2 hrs. Thereafter compound 3.1.7 (0.4 g, 1.8 mmol) was added to this heterogeneous reaction followed by K_2CO_3 (100 mg, 0.8 mmol) and $CuSO_4.5H_2O$ (5 mg, 0.02 mmol). Reaction progress was monitored by TLC and upon completion mixture was extracted with DCM and dried over Na_2SO_4. Organic extracts were pooled and dried under vacuum . The residue was purified using column chromatography with 20% ethyl acetate in hexanes to give 3.1.7 (350 mg, 59%). ^{1}H NMR (Chloroform-d, 500 MHz) δ 5.86 - 5.76 (m, 1H), 5.55 (dd, J = 15.4, 7.3, 1H), 5.08 (m, 1H), 4.24 (t, J = 6.4 Hz, 1H), 3.77 (t, J = 5.3 Hz, 2H), 3.50 (m, 1H), 2.14 (s, 3H), 2.05 - 1.98 (m, 3H), 1.95 (m, 2H), 1.66 (q, J = 1.3 Hz, 1H), 1.57 (d, J = 1.4 Hz, 3H), 1.25 (s, 18H), 0.87 (t, J = 6.9 Hz, 3H); ^{13}C (Chloroform-d, 125 MHz) δ 136.32, 135.56, 128.25, 122.98, 73.80, 66.72, 62.57, 39.68, 32.53, 31.91, 29.68, 29.65, 29.64, 29.56, 29.35, 29.32, 27.99, 27.30, 22.68, 15.98, 14.11; HRMS (ESI) calcd for $C_{21}H_{39}N_3O_2$ [M+H]+: 366.3042, found: 366.3050.

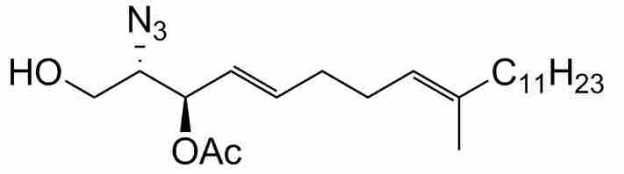

3.5.2

In a 100 ml round bottom flask, 3.5.1 (450 mg, 1.2 mmol), TDSCl (310 mg, 1.8 mmol) and 3 mL of dry pyridine were added. The solution was sonicated for 10 minutes and thereafter stirred for 3 h. Reaction was monitored with TLC for the disappearance of 3.5.1. When no starting material was left (TLC), Ac_2O (251.3 mg, 1.77 mmol) and DMAP (20 mg, 0.22 mmol) were added to this reaction. This solution was stirred for 1 h and sonicated intermittently. Upon completion, the reaction was quenched with water, extracted with ethyl acetate and dried over Na_2SO_4 . The organics were pooled and dried under vacuum. The residue was dissolved in 10 mL of 2:1 ACN:DCM. 5 mL of aqueous HF was added and the solution was stirred for 20 minutes. The residue from this reaction was dissolved in 2:1 ACN:DCM and 2 ml of HF was added. The reaction was monitored by TLC and mass spectrometry. Upon completion, the reaction was quenched with $NaHCO_3$ and extracted with ethyl acetate. Organic portion were pooled and dried over Na_2SO_4. Combined organic extracts were dried under vacuum and purified using column chromatography with 12% ethyl acetate in hexanes to give 3.5.2 (300 mg) 60% yield for three steps. ^{1}HNMR (Chloroform-d, 500 MHz) δ 5.81 (dt, J = 15.3, 5.9 Hz, 1H), 5.52 (dd, J = 15.4, 7.4 Hz, 1H), 5.09 (br, 1H), 4.27 (dd, J = 11.8, 3.6 Hz, 1H), 4.15 (m, 2H), 3.67 (m, 2H),2.32 (s, 3H), 2.10 (m, 4H), 2.01 (s, 3H), 1.58 (br, 4H), 1.25 (s, 16H), 0.88 (t, J = 6.8 Hz, 3H).; ^{13}C NMR (Chloroform-d, 125 MHz) δ 171.32 , 136.8

, 132.94 , 123.1 , 122.72 , 74.73 , 66.05 , 61.45 , 40.14 , 32.86 , 31.69 , 29.57 , 29.48 , 28.08 , 22.79 , 21.21 , 16.16 , 14.10 .HRMS (ESI) calcd for $C_{23}H_{41}N_3O_3$ [M+H]+: 408.3267, found: 408.3316.

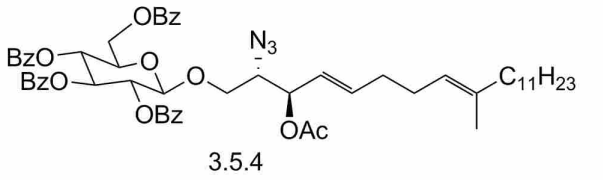

3.5.4

To a solution of glucosyl trichloroacetamidate (100 mg, 0.18 mmol) dissolved in 2 mL of dry DCM, product from the last step, 3.5.2 (95 mg, 0.19 mmol) and 20 mg of activated 4A molecular sieve were added. The mixture was cooled to 0^oC and stirred for 30 minutes. Thereafter, 10μl of TMSOTf was added to this suspension. The reaction was monitored by TLC and upon completion was quenched by adding 70 μl of Et_3N. Molecular sieves were filtered using a silica plug and the solvent was removed under vacuum. Organics were combined and dried under vacuum. The residue was purified using column chromatography with 15% ethyl acetate in hexanes to yield 3.5.4 (105 mg, 51%) ^{1}H NMR (Chloroform-d 500 MHz,) δ 8.02 (dd, J = 8.2, 1.4 Hz, 2H), 7.99 - 7.94 (m, 2H), 7.90 (dd, J = 8.2, 1.5 Hz, 2H), 7.85 - 7.79 (m, 2H), 7.53(m, 3H), 7.46 - 7.32 (m, 8H), 7.28 (t, J = 7.8 Hz, 2H), 5.90 (t, J = 9.6 Hz, 1H), 5.69 (t, J = 9.7 Hz, 1H), 5.66 - 5.50 (m, 2H), 5.35 (dt, J = 15.3, 7.8 Hz, 1H), 5.27 (dd, J = 8.2, 4.2 Hz, 1H), 4.87 (dd, J = 7.8, 1.4 Hz, 1H), 4.64 (dd, J = 12.2, 3.2 Hz, 1H), 4.51 (dd, J = 12.2, 5.1 Hz, 1H), 4.20 - 4.12 (m, 1H), 3.89 (m, 1H), 3.82 - 3.73 (m, 1H), 3.59 (dd, J = 10.3, 5.4 Hz, 1H), 2.00 (s, 1H), 1.97 - 1.87 (m, 6H), 1.64 (dd, J = 4.8, 1.4 Hz, 1H), 1.54 (br, 1H), 1.36 - 1.21 (m, 20H), 0.88 (t, J = 6.9 Hz, 3H). ^{13}C NMR (Chloroform-d 125 MHz) δ 169.68 , 169.21 , 166.84 , 165.80 , 165.38 , 134.52 , 133.34 , 132.73 , 131.10 130.36

, 129.86 , 128.76 , 127.63 , 123.72 , 100.72 , 77.62 , 72.19 , 71.40 , 69.84 , 67.33 , 63.47 , 63.01 , 40.14 , 32.86 , 31.69 , 29.49, 29.39 28.08 , 22.79 , 21.21 , 16.16 , 14.10.HRMS (ESI) calcd for $C_{57}H_{67}N_3O_{12}$ [M+H]+: 986.4911, found: 986.5008.

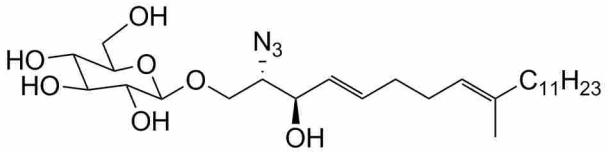

3.5.5

105 mg of the product from the previous reaction (3.5.4) was dissolved in 1:1 dry THF:Methanol. To this, 5 ml of freshly prepared 1 M sodium methoxide was added and the reaction was stirred for 3 h at the room temperature. Reaction was monitored for completion via mass spectrometry and TLC. Upon reaction completion, the solvent was removed with vacuum and residue was purified using column chromatography with 8% methanol in dichloromethane to yield 3.5.4 (43 mg, 85%) ^{1}H NMR (500 MHz, Chloroform-d) δ 5.78 (dt, J = 18.5, 6.2 Hz, 1H), 5.53 - 5.43 (m, 1H), 5.08 (dd, J = 7.9, 5.4 Hz, 1H), 4.28 (d, J = 7.8 Hz, 1H), 4.18 (t, J = 7.6 Hz, 1H), 4.04 - 3.96 (m, 1H), 3.83 (dd, J = 12.0, 3.0 Hz, 1H), 3.78 - 3.68 (m, 2H), 3.42 (m, 2H), 3.35 (m, 2H), 3.28 (br, 2H), 2.64 (s, 3H), 2.10 - 1.86 (m, 4H), 1.64 (m, 2H), 1.45 (br, 2H), 1.35 - 1.14 (m, 18H), 0.83 (t, J = 6.9 Hz, 3H). HRMS (ESI) calcd for $C_{27}H_{49}N_3O_7$ [M+H]+: 528.3910, found: 528.4011 and [M+Na] 550.3472.

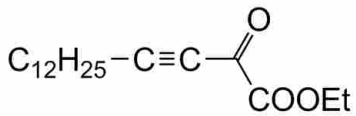

3.3.2

To a solution of 1-tetradecyne 3.3.1(2g, 10.3mmol) in 30ml dry THF, ethyl magnesium bromide (10.5ml, 10.3mmol, 1M in THF)was added. This reaction was refluxed for 6 hours at 70^{o}C, then cooled to -30^{o}C. Thereafter, diethyl oxalate (1.4ml 10.3mmol) was added dropwise over 15mins at -30^{o}C and then reaction was stirred for 2 h at this temperature. Reaction was quenched using saturated NH_4Cl, and extracted twice with ethyl acetate. Extracts were pooled, dried and purified using column chromatography with 4% ethyl acetate in hexanes. ^{1}H NMR (500MHz, Chloroform-d) δ 4.37 (q, J = 6.9 Hz, 2H), 2.42 (t, J = 7 Hz, 2H), 1.91 (s, 3H), 1.63 (m, 4H), 1.30 - 1.19 (m, 21H), 0.89 - 0.83 (t, J=7Hz, 3H). 13C NMR (125 MHz, $CDCl_3$) δ 172.47, 156.12, 93.44, 80.05, 61.13, 31.69, 29.57, 29.41, 29.32, 29.30, 29.08, 28.70, 28.34, 22.79, 19.38, 14.26, 14.10. HRMS (ESI) calcd for $C_{18}H_34N\,O_3$ [M+NH4]+: 312.2539, found: 312.2561.

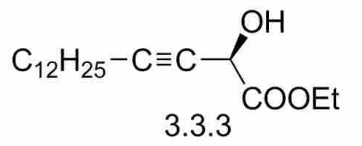

3.3.3

A solution of S-alpine borane (0.5M in THF, 12ml, 6.2mmol) was taken in a RB flask and solvent was removed under vacuum. To this RB, a solution of 3.3.2 in DCM was added dropwise at 0^{o}C and solvent was removed again using vacuum. Reaction was stirred for 12 h and then sonicated for 1 h. At this point, silica gel and ethyl acetate were added and the reaction was stirred for 1h, then filtered. The solvent was removed under vacuum and residue was purified by chromatography with 5% ethyl acetate in hexanes. The reaction not very clean and after consecutive attempts, semi-pure material was pushed to the next step. Reaction product was confirmed by recording high resolution mass spec. ^{1}H NMR (500 MHz, Chloroform-d) δ 4.80 (dt, J = 4.9, 2.4 Hz, 1H),

4.31 (q, J = 7.2 Hz, 2H), 2.94 (d, J = 7.3 Hz, 1H), 2.21 (m, 3H), 1.49 (m, 3H), 1.39 - 1.19 (m, 22H), 0.88 (t, J = 6.9 Hz, 3H). HRMS (ESI) calcd for $C_{18}H_{36}NO_3$ [M+H]+: 314.2713, found: 314.2699

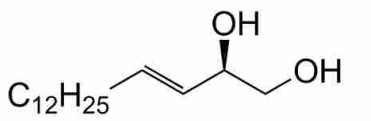

3.3.4

In a flame dried 100 ml RB flask, 30 ml dry THF and $LiAlH_4$ (400mg, 10.5mol) were added. To this suspension, a solution of 3.4.3 (500 mg, 1.7 mmol) in dry THF at 0^oC was added dropwise . Mixture was allowed to warm upto room temperature and then refluxed for 3 h. The reaction mixture was cooled down to 0^oC and quenched with saturated solution of potassium sodium tartarate. After extracting the aqueous phase with diethyl ether, solvent was removed using vacuum and residue was purified using column chromatography with 10% ethyl acetate in hexanes. ^{1} NMR (500 MHz, Chloroform-d) δ 5.86 - 5.68 (m, 1H), 4.20 (td, J = 7.0, 3.4 Hz, 1H), 3.69 - 3.57 (m, 4H), 3.49 (m, 4H), 2.10 - 1.95 (m, 2H), 1.41 - 1.16 (m, 20H), 0.88 (t, J = 6.9 Hz, 3H). ^{13}C NMR (125 MHz, Chloroform-d) δ 134.58, 128.20, 73.20, 66.59, 67.38, 30.58, 29.03, 22.62, 25.61, 29.21, 31.84, 14.11. HRMS (ESI) calcd for $C_{16}H_32NO_2$ [M+H]+: 257.2402, found: 257.2511.

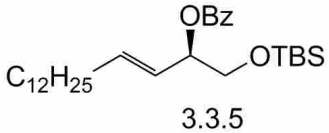

3.3.5

The product of last reaction (3.3.4, 200 mg, 0.78 mmol) was taken in a RB flask and 2ml of pyridine was added. Thereafter, TDSCl (180 mg, 1.05 mmol) was added and the reaction was

monitored by TLC and mass spectroscopy. Upon reaction completion, benzoyl chloride was added and reaction was stirred overnight. Next morning, the reaction was quenched by adding water and extracted with ethyl acetate. Extracts were pooled, dried and chromatographed with 7% ethyl acetate in hexanes to yield compound 3.3.5. ^{1} HNMR (500 MHz, Chloroform-d) δ 8.03 (m, 2H), 7.64 (m, 1H), 7.42 (m, 2H) 5.88 (dt, J = 14.9, 6.7 Hz, 1H), 5.61 - 5.46 (m, 1H), 3.80 (dd, J = 5.5, 2.2 Hz, 1H), 2.05 (q, J = 7.5 Hz, 2H), 1.37 (br, 2H), 1.33 - 1.19 (m, 21H), 0.91(s, 6H),0.86(s, 3H) 0.02 (t, 6H). ^{13}C NMR (125 MHz,Chloroform-d) δ 169.18, 155.78, 142.23, 141.52, 136.04, 129.60, 128.82, 115.36, 82.61, 70.29, 37.73, 37.27, 37.22, 35.03, 35.00, 34.93, 34.79, 34.71, 34.49, 34.15, 31.08, 28.05, 23.55, 19.48, 5.35

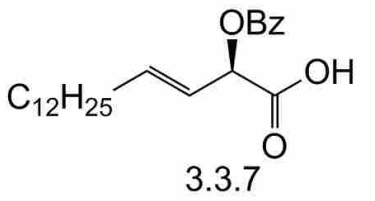

3.3.7

In a 50 ml RB flask, 10ml 2:1 ACN : DCM was used to dissolve bis(acetoxy)iodobenzene (50 mg). This solution was stirred for 10 minutes with intermittent sonication. A solution of 3.3.6(25 mg) was added to this in 2 ml DCM. Thereafter, 2,2,6,6-Tetramethyl-1-piperidinyloxy (TEMPO) was added to this solution (7 mg). This reaction was stirred overnight and checked for the disappearance of 3.3.6 by TLC and mass spectrometry. Upon reaction completion, solvents were removed under vacuum and product was extracted with DCM. Organics were pooled and dried and the residue was purified by chromatography with 20% ethyl acetate in hexanes to yield compound 3.3.7(15 mg). ^{1} NMR (500 MHz, Chloroform-d) δ 11.81(br, 1H), 8.13 (m, 2H), 7.44 (m, 1H), 7.31 (m, 2H), 5.97 (m, 1H), 5.76 (m, 1H), 2.29 - 2.15 (m, 2H), 1.44 - 1.16 (m, 21H), 0.87

(t, J = 6 Hz, 3H). HRMS (ESI) calcd for $C_{23}H_{34}NO_4$ [M+H]+: 375.2518, found: 375.2480.

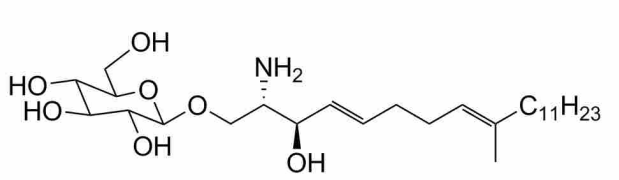

3.5.6

In a 50 ml RB flask, compound 3.5.5 (30 mg, 0.061 mmol) was dissolved in 6 mL of 1:1 THF:MeOH. To this solution, 100 mg of granular zinc and 0.5 mL of glacial acetic acid were added. This solution was sonicated for 20 minutes and reaction was monitored using mass spectroscopy. Upon reaction completion, the zinc was filtered and organics were transferred to a separate flask and the solvent was removed using vacuum. The compound was dissolved in 4 mL of 1:1 THF:MeOH and neutralized with 5% NaOH (until pH 10) and stirred for one hour. The solvent was dried under vacuum and this material was used directly in the next step.

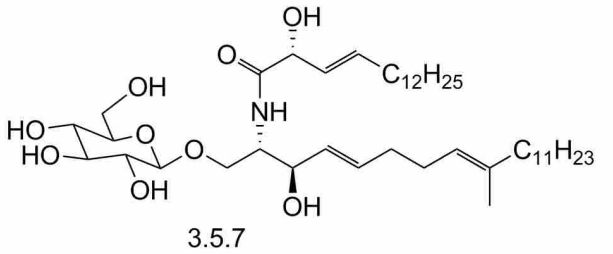

3.5.7

In a 25 ml RB flask, EDCI (12 mg, 0.081 mmol), hydroxybenzotriazol (HOBt)(12 mg,0.09 mmol), and acid 3.3.8 (18 mg, 0.069 mmol) were dissolved using 5 ml THF. To facilitate the dissolution of all the reaction components, this mixture was sonicated for 10 minutes. This solution was stirred for one hour at room temperature. Thereafter, compound 3.5.6 (41 mg, 0.09 mmol) was dissolved in anhydrous THF (3 mL) and added to this solution and stirred overnight at room

temperature. Next morning, the solvent was removed under vacuum and the residue was dissolved in water, washed with DCM and dried over Na_2SO_4. Organics were pooled and dried and the residue was purified by column chromatography with 10% methanol in dichloromathane to afford compound 3.5.7. Although mass and NMR of this compound looked clean, the NMR showed a few impurities and therefore, the compound was re-chromatographed with 10% methanol in DCM to afford satisfactory NMR data. ^{1}H NMR (500 MHz, Methanol-d4) δ 5.72 (dt, J = 15.8, 6.0 Hz, 1H), 5.53 - 5.40 (m, 2H), 5.17 - 5.11 (m, 1H), 4.43 (d, J = 6.0 Hz, 1H), 4.27 (dd, J = 7.8, 2.0 Hz, 1H), 4.12 (m, 2H), 3.85 (d, J = 1.6 Hz, 1H), 3.73 - 3.62 (m, 2H), 3.35 (m, 1H), 3.28 - 3.26 (m, 2H), 3.22 (m, 1H), 2.09 (s, 3H), 1.97 (t, J = 7.6 Hz, 2H), 1.60 (d, J = 1.5 Hz, 3H), 1.43 - 1.20 (m, 39H), 0.90 (t, J = 6.8 Hz, 6H). ^{13}C NMR (125 MHz, MeOD) δ 175.48, 136.79, 134.56, 131.06, 129.07, 124.85, 104.76, 78.02, 77.94, 75.03, 74.14, 72.92, 71.61, 69.69, 62.71, 54.67, 40.84, 33.85, 33.48, 33.14, 30.88, 30.87, 30.85, 30.83, 30.76, 30.73, 30.55, 30.54, 30.49, 30.45, 30.28, 29.18, 28.80, 23.81, 16.18, 14.51. HRMS (ESI) calcd for $C_{43}H_{79}NO_9$ [M+H]+: 754.5813, found: 754.5806.

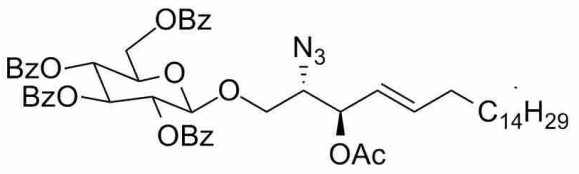

3.6.3

To a solution of glucosyl trichloroacetamidate (82 mg, 0.144 mmol) dissolved in 3 mL of dry DCM, product from the last step, 3.6.1 (77 mg, 0.15 mmol) and 27 mg of activated 4A molecular sieve were added. The mixture was cooled to 0^oC and stirred for 30 minutes. Thereafter, 10μl of TMSOTf was added to this suspension. The reaction was monitored by TLC and upon completion

was quenched by adding 100 μl of Et_3N. Molecular sieves were filtered using a silica plug and the solvent was removed under vacuum. Organics were combined and dried under vacuum. The residue was purified using column chromatography with 10% ethyl acetate in hexanes to yield 3.6.3 (109 mg, 54%) ^{1}H NMR (500 MHz, Chloroform-d) δ 8.02 (d, J = 7.6 Hz, 1H), 7.97 (d, J = 7.6 Hz, 1H), 7.90 (d, J = 7.9 Hz, 1H), 7.82 (d, J = 7.8 Hz, 1H), 7.58 - 7.46 (m, 2H), 7.45 - 7.32 (m, 4H), 7.29 (d, J = 7.7 Hz, 1H), 5.90 (t, J = 9.6 Hz, 1H), 5.69 (t, J = 9.7 Hz, 1H), 5.64 - 5.51 (m, 2H), 5.33 (dd, J = 15.2, 8.2 Hz, 1H), 5.26 (dd, J = 8.2, 4.2 Hz, 1H), 4.86 (d, J = 7.7 Hz, 1H), 4.64 (dd, J = 12.2, 3.2 Hz, 1H), 4.51 (dd, J = 12.2, 5.1 Hz, 1H), 4.16 (dd, J = 9.2, 5.1, 3.2 Hz, 1H), 3.89 (dd, J = 10.2, 6.8 Hz, 2H), 3.78 (q, J = 6.3, 5.8 Hz, 1H), 3.58 (dd, J = 10.2, 5.6 Hz, 1H), 2.00 (s, 3H), 1.90 (m, 1H), 1.34 - 1.14 (m, 15H), 0.88 (t, J = 6.8 Hz, 3H). 13C NMR (125 MHz, Chloroform-d) δ 169.33, 166.08, 165.77, 164.87, 138.70, 133.43, 133.24, 133.21, 133.15, 129.83, 129.81, 129.74, 129.70, 129.20, 128.73, 128.38, 128.33, 128.28, 122.61, 109.99, 100.91, 76.73, 74.15, 72.75, 72.38, 71.64, 69.56, 68.11, 63.03, 32.24, 31.91, 29.70, 29.68, 29.66, 29.64, 29.61, 29.39, 29.35, 29.14, 28.62, 22.68, 21.00, 14.11. HRMS (ESI) calcd for $C_{56}H_{67}N_3O_{12}$ [M+H]+: 974.4800, found: 974.4914.

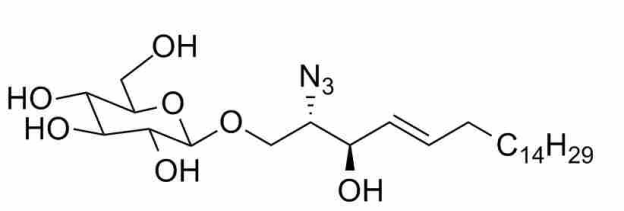

3.6.4

In a 25 ml RB flask, product from the previous reaction 3.5.4(52 mg, 0.051 mmol) was dissolved in 1:1 dry THF:Methanol. To this, 5 ml of freshly prepared 1 M sodium methoxide was

added and the reaction was stirred for 1 h at the room temperature. Reaction was monitored for completion via mass spectrometry and TLC. Upon reaction completion, the solvent was removed with vacuum and residue was purified using column chromatography with 5% methanol in DCM to yield 3.5.4 (18 mg, 79%). ^{1}H NMR (500 MHz, Methanol-d4) 7.93 (s, 1H), 7.55 (q, J = 9.3, 8.4 Hz, 2H), 5.84 (m, 1H), 5.49 (s, 1H), 4.83 (s, 8H), 4.34 (dd, J = 8.4, 6.4 Hz, 1H), 4.28 (d, J = 7.1 Hz, 1H), 3.80 - 3.61 (m, 3H), 3.60 (m, 1H), 3.56 - 3.46 (m, 2H), 3.46 - 3.39 (m, 2H), 3.30 (p, J = 1.7 Hz, 5H), 2.15 - 2.07 (m, 2H), 1.41 (q, J = 6.5 Hz, 2H), 1.38 - 1.26 (m, 19H), 0.88 (t, J = 6.8 Hz, 3H).

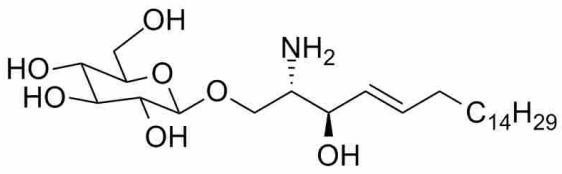

3.6.5

In a 25 ml RB flask, compound 3.6.4(22 mg, 0.056 mmol) was dissolved in 4 mL of 1:1 THF:MeOH. 150 mg of granular zinc and 0.5 ml glacial acetic acid were added to this flask. This mixture was sonicated for 30 minutes and reaction was monitored by mass spec. Upon completion, the solvent was transferred to a separate RB flask and the solvent was removed using vacuum. Next, the compound was dissolved in 4 mL of 1:1 THF:MeOH, basified with 5 % NaOH and stirred for one hour. Upon reaction completion, the solvent was dried off and the residue was used in the next step without purification. HRMS (ESI) calcd for $C_{26}H_{55}N_2O_7$ [M+NH4]+: 507.4009, found: 507.4110.

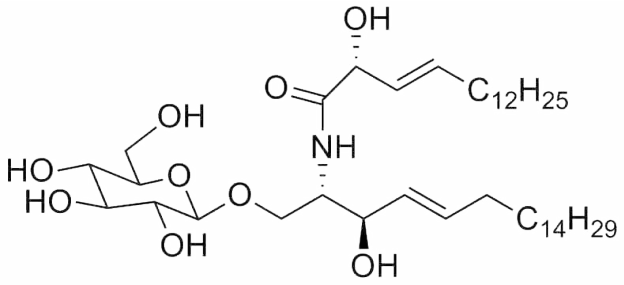

3.6.6

In a 25 ml RB flask, EDCI (6 mg, 0.032 mmol), hydroxybenzotriazol (HOBt)(4.5 mg,0.035 mmol), and acid 3.3.8 (10 mg, 0.039 mmol) were combined in anhydrous THF (5 mL). To dissolve all the reaction components, this mixture was sonicated for 10 minutes and thereafter, stirred for one hour at room temperature. Compound 3.6.5(9 mg, 0.037 mmol) was dissolved in anhydrous THF (3 mL) and added to this reaction mixture. The reaction was stirred overnight at room temperature. Next day, the solvent was removed under vacuum and the residue was dissolved in water, washed with DCM and dried over Na_2SO_4. Organics were pooled and dried and the residue was purified by column chromatography with 8% methanol in DCM to yield 3.6.6. ^{1}H NMR (500 MHz, Chloroform-d) δ 5.51 (t, J = 6.8 Hz, 1H), 5.47 - 5.31 (m, 2H), 4.20 (d, J = 7.7 Hz, 1H), 4.04 (m, 2H), 3.94 (br, 1H), 3.83 (m, 1H), 3.69 (d, J = 5.0 Hz, 1H), 3.41 (m, 2H), 3.25 - 3.16 (br, 2H), 2.85 (d, J = 6.9 Hz, 2H), 1.94 (q, J = 5.8, 4.6 Hz, 4H), 1.19 (s, 48H), 0.81 (t, J = 6.8 Hz, 6H).^{13}C NMR δ (125 MHz, Chloroform-d) 171.8, 134.49, 135.64, 122.50, 128.69, 103.95, 72.28, 68.71, 53.14, 61.51, 61.58, 68.60, 76.32, 70.06, 75.94, 73.38, 54.83, 40.09, 31.08, 29.01, 22.61, 29.40, 29.56, 27.52, 24.36, 25.96, 30.79, 33.82, 31.70, 21.39, 29.52, 13.89. HRMS (ESI) calcd for $C_{42}H_{79}NO_9$ [M+H]+: 742.5608, found: 742.5714.

Chapter 4

Analytical Method Development for Quantitative Determination of Ceragenins in Complex Biological Matrices

4.1 Need for novel antimicrobial technologies:

After the commercialization of penicillin in 1932, the remarkable success of antimicrobial drugs has created a misconception that infectious diseases have been conquered. However, as per World Health Organization (WHO), infectious diseases remain the second largest cause of deaths worldwide. The advent of antibiotics and their widespread use also brought the problem of antimicrobial resistance with it. The emergence of multidrug-resistant bacteria is posing a great challenge towards the scientific community, but unfortunately there are very few alternatives. Another failed

area for antibiotics is biofilm related infection. Biofilms are clusters of bacteria that are found in infections involving medical devices such as catheters and prosthetics[67]. Although biofilm related infections result in about 100,000 deaths in the United States, there exist no clinically useful treatments to date. Among the few possible solutions to these problems are the antimicrobial peptides(AMPs). AMPs are the evolutionarily conserved components of the innate immune system and posses broad spectrum antibiotic properties, which makes them the ideal candidates for therapeutic use.[68] However, clinical development of AMPs involves several problems including the cost and enzymatic degradation[69].

In the quest for developing novel antimicrobial therapies, our lab has focused on the development on non-peptide mimics of AMPs which have similar or improved bioactivity but don't carry the disadvantages of AMPs. These compounds are called ceragenins (CSAs) and have shown great potential in various clinical applications. AMPs such as cathelicidin (LL-37) and magainin are known to be facial amphiphiles i.e, they have a hydrophobic face and a cationic, hydrophilic face (Figure 5.3). AMPs use the cationic face to associate with the negatively charged components in the bacterial membrane. This attachment is followed by membrane depolarization and cell death[70].

Our lab is developing various applications of CSAs for numerous clinically relevant scenarios. Many of these applications involve controlled release of CSAs from different polymeric coatings and biomedical devices including contact lenses, endotracheal tubes and catheters. As we moved ahead into clinical applications of CSAs as an alternative antimicrobial therapy, we needed to evaluate the following:

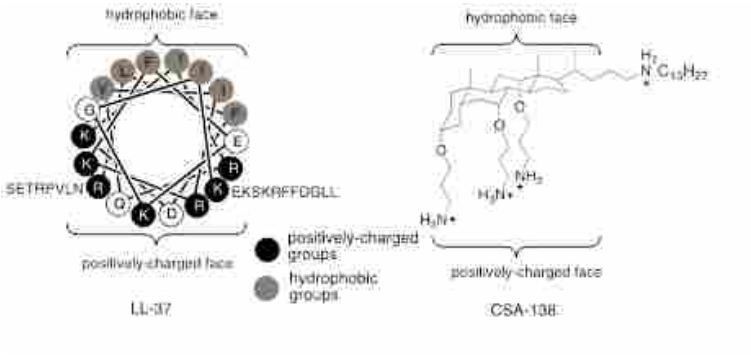

Figure 4.1 Helix-wheel representation of the human AMP LL-37 and CSA-138 showing the facially amphiphilic morphology common to both molecules

1 Mechanism of action

2 Pharmacokinetic, pharmacodynamic and toxicological studies

3 Proof of concept applications for existing microbiological problems

Keeping in mind the structural features of AMPs, CSAs were designed to mimic the facially amphiphilic character of AMPs and therefore we expect similarities in their mechanism of actions[71]. To study the mechanistic similarities between AMPs and CSAs, we decided to study their impact on bacterial lipid membranes, which is a well documented method of choice.[72,73]

To assess the pharmacokinetics data and to ensure safety and efficacy, we needed robust analytical methods for quantitative determination of CSAs. To ensure the selectivity, reproducibility and accuracy of these methods, FDA guidelines for bio-analytical method development and validation were followed. These guidelines provide various parameters for this purpose including the determination of linearity of response, storage stability, recovery, and the calibration curve.With these aforementioned tasks in mind, we started the clinical investigations of CSAs.

4.2 Experimental Procedures

4.2.1 Investigation into the mechanism of action

Serial passage experiments

Learning from literature,[72] we decided to study the similarities in the mechanism of resistance development against CSAs and AMPs. To achieve this, serial passaging was initiated by harvesting bacterial cells growing at the highest concentration of the antimicrobial (just below the minimum inhibitory concentration) and inoculating into fresh triptic soy broth. This inoculum was subjected to another minimum inhibitory concentration (MIC)assay. After an 18-24 h incubation period, cells growing in the highest concentration of the antimicrobial from the previous passage were once again harvested and assayed for the MIC. The process was repeated for 30 passages. Antimicrobial concentrations were adjusted during the process to compensate for rising MIC values

Lipid A isolation and characterization

An established method was used to isolate lipopolysaccharide (LPS) and truncate it to lipid A.[74] Briefly, lyophilized bacterial cells (20 mg) were suspended in TRI reagent (500 μl) (Sigma Aldrich). Cells were vortexed and incubated at 37^{o}C for 20 min. Chloroform (200 μl) was added and the resulting mixture was vigorously vortexed. Cells were centrifuged at 5000 g for 10 min to separate the aqueous and organic phases. The aqueous phase was transferred to a new tube and the organic phase was re-extracted with water (3 X 300 μl) to completely remove LPS from the organic phase. All the aqueous extracts were pooled and lyophilized. LPS was further purified by

adding cold, aqueous $MgCl_2$ (1 mL of 0.375 M solution). The resulting mixture was centrifuged at 10,000 g for 10 min to obtain semi-pure LPS as a white precipitate. To remove phospholipids, the semi-pure LPS was washed with a mixture of chloroform and methanol [200 μl of a cold 2: 1 (v/v) mixture] and centrifuged at 10,000 g for 5 min. The precipitate was dissolved in an aqueous buffer containing SDS [1 ml of a 1% solution in 10 mM sodium acetate buffer (pH 4.5)]. The resulting mixture was heated at 100 ^{o}C for 1 h. This mixture was lyophilized, washed twice with cold HCl in ethanol (0.02 N) to remove SDS and then with 95% cold ethanol, followed by drying under vacuum. The resulting material was dissolved in dichloromethane/methanol (1 : 1, v/v) and analysed via mass spectrometry (electrospray, time-of-flight analysis)

4.2.2 Analytical method development for pharmacological studies

General procedures Samples for LC-MS analysis were prepared in water. While performing LC-MS quantitation, isotopically labelled version of the analyte is regarded as the best internal standard. Evidently, an isotopically labeled internal standard has a similar extraction recovery, ionization response, and chromatographic retention time as the analyte itself. Using this information, isotopically labelled CSA-13 (two hydrogens replaced with two deuteriums) was used an the internal standard. Samples consisting of biological matrices including blood, serum, and broth were extracted using the following procedure:

500 μL sample was placed in 2 ml eppendorf tube. To this, 500 μl of aqueous deuterated CSA-13 (CSA13 D2) was added and the solution was vortexed. To this resulting solution, 50 μl of 10% sodium hydroxide was added to make the solution basic and convert CSA salt into the free

base form. The resulting solution was intermittently vortexed for 5 mins. After ensuring that the solution was basic, 1 ml organic solvent (dichloromethane or ethyl acetate) was added and vortexed for 2 min. The eppendorf tubes were centrifuged for 5 min to separate the organic and aqueous layers. The organic layer was transferred to 1 ml glass vials and dried under a nitrogen stream. The residue was redissolved in 30:70 mixture of acetonitrile:water (v/v) and queued for LC-MS analysis.

Optimization of chromatographic methods

Following a literature precedent[75] and looking at the retention characteristics of CSAs, a C18 column was used for chromatographic analysis. Multiple mobile phase modifiers (TFA, formic acid, acetic acid) and their combinations at various concentrations were screened. Using acetonitrile and water as mobile phase, many isocratic and gradient elution profiles were also screened.

Calibration Curve

The relationship between instrument response and the known concentration of the analyte is depicted in the calibration curve. Following the FDA guidelines, different calibration curves for different biological matrix were prepared. Concentrations of standards used in this analysis were chosen on the basis of concentration range expected in our studies. Analyses consisted of a blank sample (matrix sample processed without internal standard), a zero sample (matrix sample processed with internal standard) and five non-zero samples covering the expected range, including lowest limit of quantification (LLQ). Briefly, two sets of CSA solutions (a) five samples with 5μg/ml CSA-13 D2 and varying concentration of CSA-13 (0.5, 1, 3, 5, and 10μg/ml), and (b) six samples with 50 μg/ml CSA-13 D2 and varying concentration of CSA-13 (10, 20, 30,

50, 100μg/ml) were prepared. Samples were processed using general procedure, and calibration curves were obtained by calculating the abundances of CSA against internal standard (CSA-13 D2).

Storage stability

Following the FDA guidelines, stability of CSAs in different biological matrices were evaluated. For this, three aliquots of CSA solutions in varying matrices were analyzed using freeze-thaw cycles, at RT and 45 ^{o}. Additionally, the accelerated stability of CSA-44 at various pH levels was also determined. Using various buffer combinations, aqueous buffers for pH 6, 5.5, 5, and 4.5 were prepared. Solutions of CSA-44 along with internal standard (cholic acid) were prepared at aforementioned pH values. These solutions were maintained at 45 ^{o}C for 12 weeks while analyzing them every week for degradation products.

Recovery

Because of their facial amphiphilicity, CSAs have strong association with many matrices including various culture media and blood and these interactions make recovery of CSAs very challenging. FDA defines recovery as the detector response obtained from a known amount of analyte added to and extracted from a complex biological matrix, compared to the detector response obtained for the true concentration of pure standard. Recovery primarily depends upon the extraction efficiency of the particular sample preparation method. Methods including liquid-liquid extraction with organic solvents (dichloromethane and ethyl acetate) and solid phase extraction (SPE) using C18 and aminopropyl cartridges were screened. Briefly, a working sample was prepared by adding a known concentration of CSA solution to the known volume of the particular

matrix. the sample was equilibrated for 24 h. The sample was made basic by addition of appropriate volume of 10% sodium hydroxide and thereafter CSA was extracted using liquid - liquid separation. Internal standard in this particular case was added after the extraction of CSA from the matrix, and samples were processed for LC-MS analysis.

4.2.3 Elution profile of controlled release contact lenses

In the process of designing controlled release applications of CSAs for prevention of bacterial colonization on hydrogel contact lenses, elution of CSAs from these lenses was studied. CSAs were incorporated into the contact lenses at 1% dosage (relative to the mass of lens material). Lenses containing different CSA variants were placed in 2 ml of 10 % TSB in PBS and challenged with *S. aureus*. Samples were incubated for 24 h with gentle agitation. After 24 h, lenses were removed, gently rinsed with PBS, then placed in fresh media and reinoculated. This process was repeated every 24 h, until there was microbial growth in the culture media. The release of CSAs from lenses was quantified by soaking lenses in PBS (1.5 ml), exchanged for fresh PBS every 24 h. Aliquots were removed every 24 h, processed as described in general procedures, and analyzed for CSA concentration using LC/MS.

4.2.4 Active release antimicrobial coating to prevent osteomyelitis

Active release coatings for biomedical devices provide a promising method for preventing biofilm related infections. Our collaborators have designed controlled release coatings using medical grade PDMS (Polydimethoxysiloxane), which could potentially replace currently used fracture fixation

plates.[76] For this study, 2 cm X 2 cm stainless steel (SS) plates were dip coated using varying ratios of PDMS:naptha (0.5:1, 1:1, and 2:1) as well as varying concentrations of CSA-13 (2% to 20% W/W). Using a carefully machined flow cell system to imitate blood flow in the human body, TSB broth at 5 ml/min was used to elute CSA from these coatings. The aforementioned general procedures were used for sample preparation and analyzed for CSA concentration using LC/MS. The abundance ratio of CSA-13 and CSA-13 D2 were used to calculate the concentration of CSA-13 in the broth.

4.3 Results and discussion

4.3.1 Mechanistic similarities between AMPs and CSAs

As AMPs are evolutionarily conserved components of the immune system and are found among all forms of life, bacteria have developed several methods for engendering resistance against them. The primary method of resistance is via structural modifications in bacterial membrane components, such as lipopolysaccharide (LPS). To affirm the hypothesis that AMPs and ceragenins have the same mechanism of action, we expected CSA resistant bacteria to have the same cellular membrane modifications as in AMP resistant organisms. Experimentally, the bacterial resistance towards CSAs can be induced by serially exposing them to antibacterial agents[77]. Two gram negative bacteria, *Pseudomonas aerigunosa* and *Acinetobacter baumannii*, were cultured under these conditions and their lipid A structures were compared.

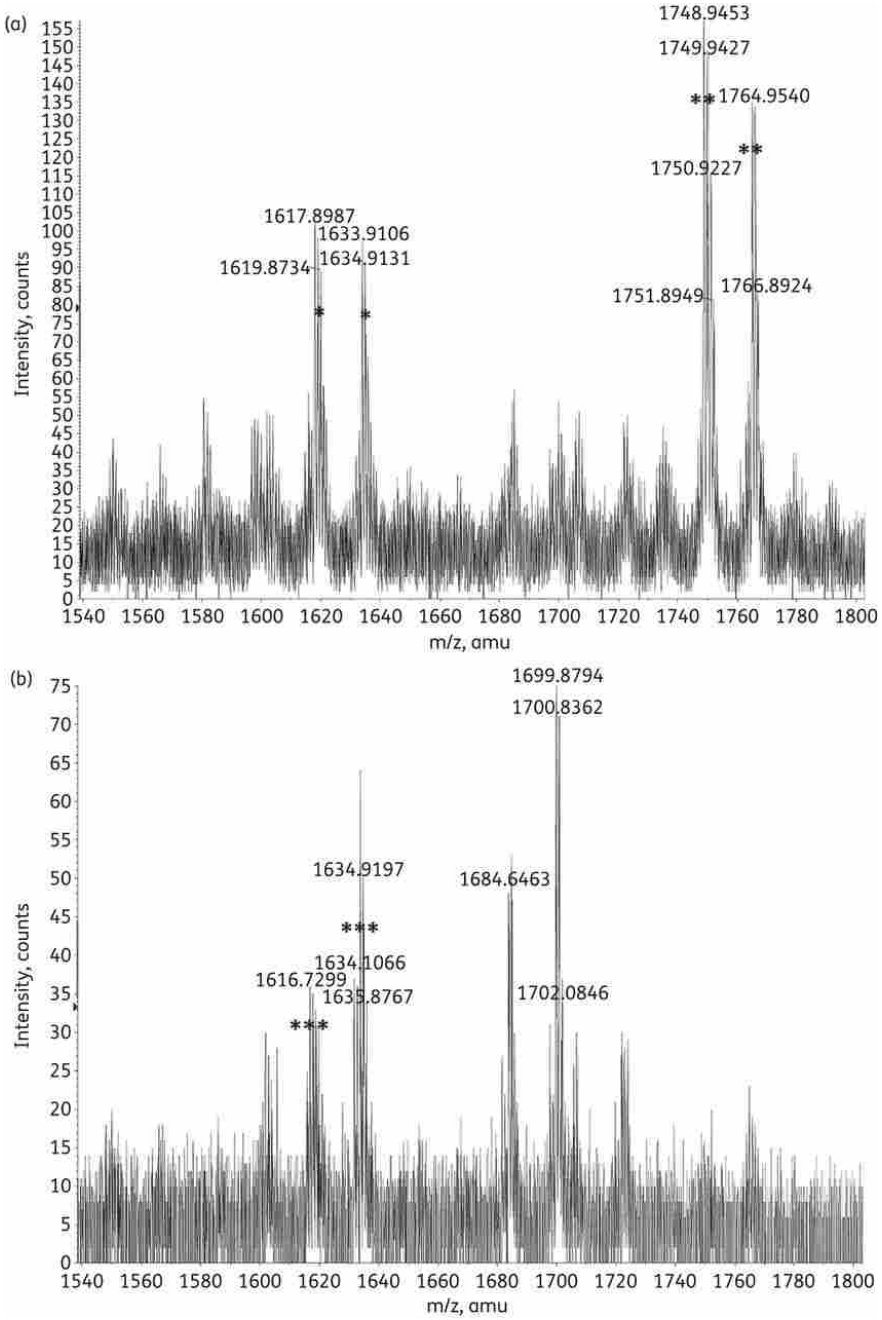

Figure 4.2 Mass spectra of lipid A from *P. aeruginosa*. LPS was isolated by extraction and partially hydrolysed to give lipid A.(a) Lipid A from CSA-13-resistant *P. aeruginosa*: *diphosphoryl lipid A, **4-aminoarabinose-appended lipid A. (b) Lipid A from CSA-13-susceptible P. aeruginosa: ***diphosphoryl lipid A.

Consistent with the literature reports, both CSA and AMP resistant organisms were found to

carry aminoarabinose modification of lipid-A . We believe that these modifications help bacterium in reducing the anionic charge on the cellular membrane and thereby helping in immune evasion. These results reaffirm the hypothesis that CSAs have the same mode of action as AMPs.

4.3.2 Analytical method development

In spite of the new technologies in pharmaceutical research, drug discovery and development remains a very time consuming and challenging process. Analytical techniques play a major role in enabling target identification, synthesis of potential drug candidates, toxicity and metabolism studies. Keeping this in mind, we started the analytical method development for quantitative and qualitative determination of CSAs in complex biological matrices.

Chromatography optimization

Having a good chromatographic method is vital in the LC-MS method development, therefore, it was our primary focus. Using a syringe pump, the detection limit for mass spectrometer (Agilent MSD TOF) was measured at 500 ng/ml. Following literature precedence,[75] we first tried the isocratic elution (30% acetronitrile:water with 0.1% formic acid). After optimizing this isocratic method our detection limit was 500 ng/ml, However, our analytes were not well retained under these conditions and asymmetrical peaks were obtained. The observed asymmetrical results (peak tailing) indicated more than one retention mechanism is acting in the separation process (presence of both C18 and "uncapped" silanol groups). The chromatogram for isocratic method is shown in Figure 4.3.

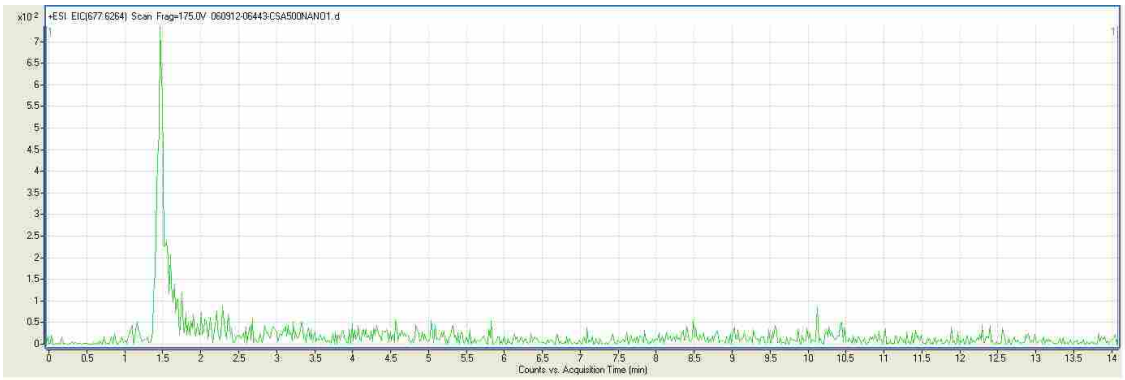

Figure 4.3 Selected ion (m/z 677.67) chromatogram of CSA. Conditions: 10 cm X 0.3 mm column packed with 1.8 μ C18 particles. Elution started by 100 % mobile phase A for 0-4 min; followed by column rinsing 100 % B (4-9 min) and reconditioning the column after 9 min with 100 % A [A = acetonitrile:water:formic acid (35:65:0.025 v/v/v); B = acetonitrile:water:formic acid (90:10:0.025 v/v/v)].

As peak tailing is often associated with the isocratic elutions, we switched to gradient elution and changed the mobile phase modifier from formic acid to mixture of formic acid and TFA. According to literature reports,[78] TFA can improve peak shape in chromatography, but also contributed to signal suppression in mass spectrometer. Keeping this in mind, various combinations of formic acid/TFA concentrations were screened and the gradient shown in gradient eluent table (figure 3.4) was found yield best results. This gradient resolved the issue of asymmetrical peaks and improved the detection limit from 500 ng/ml to 250 ng/ml.

Gradient eluent composition table

% A	%B	Time (min)	Flow (ml/min)
30	70	0	0.35
50	50	3	0.35
100	0	6	0.35
100	0	8	0.35
30	70	9	0.35
30	70	10	0.35

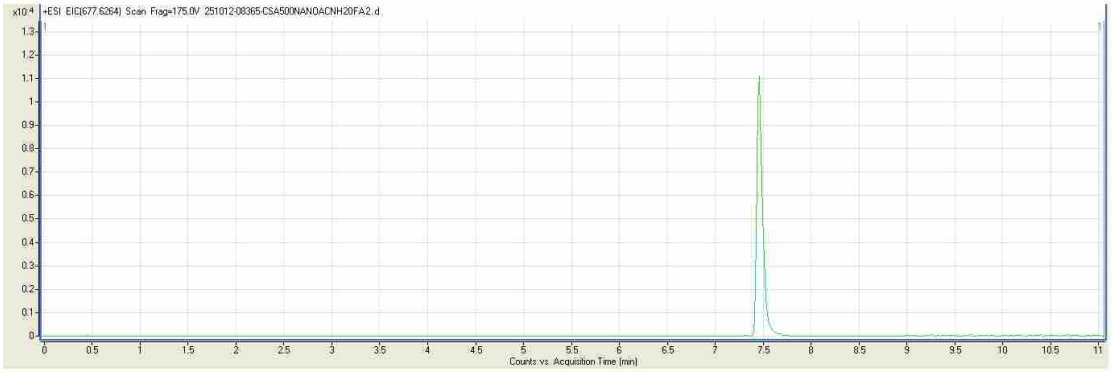

Figure 4.4 Selected ion (m/z 677.6) chromatogram of CSA-13 elution using aforementioned gradient flow. [A = water:formic acid:TFA (100:0.09:0.005 v/v/v); B = acetonitrile:formic acid:TFA (100:0.09:0.005 v/v/v)].

4.3.3 Linearity of response

The linearity of analytical procedure is its ability to provide results that are directly proportional to the concentration of the analyte. Although we are using isotopically labelled internal standard which have the same chemical and physical characteristics as the analyte itself, FDA mandates the linearity range to be established. With aforementioned experimental procedure, linearity of response for CSA-13 was measured. The calibration curves for two ranges are shown below

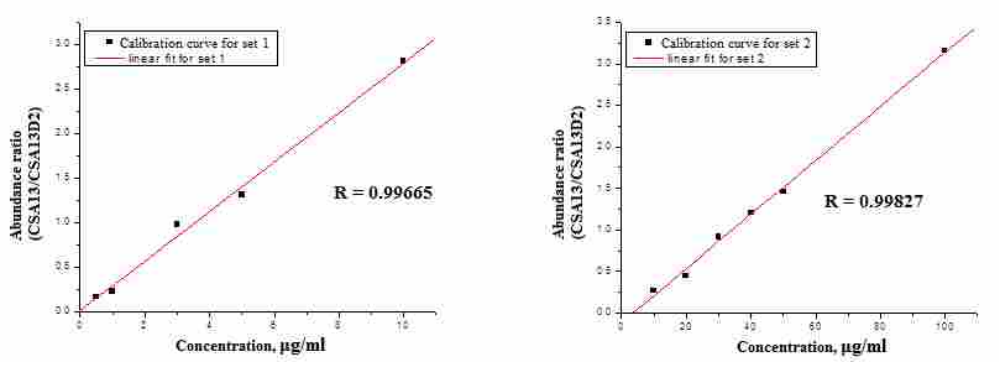

Figure 4.5 Calibration curve for CSA-13

4.3.4 Contact lens elution

During the process of designing proof of concept applications for CSAs, the idea of incorporating them into contact lenses was conceived. Although multiple types of drugs, including antimicrobial agents have been incorporated into lenses, drug resistance and lack of sustained antimicrobial activity still remains a challenge[79,80]. As the mimics of AMPs, CSAs are active bacteriocidal agents and do not readily engender resistance by bacteria. These characteristics make CSAs ideal candidates for controlled release antimicrobial applications. CSA-13, a lead antimicrobial ceragenin, served as the starting point in controlled release contact lens development. Our analytical results indicated that CSA-13 (C_8 side chain length)was eluting out very quickly (within 3-5 days) rending it unpractical for use. Learning from these results, we incrementally varied (figure 3.6) the hydrophobic character of the CSAs by increasing the lipid chain length (C_{10}, C_{12}, C_{13}, AND C_{14})

All these different CSAs were incorporated into contact lenses and the CSA released over 15 days was quantified using aforementioned analytical methods. The detection limit for quantification of these ceragenins was 1 μg/ml. When the amount of the ceragenin fell below the detection

limit, analysis was halted. As expected, the length of the lipid chain at C_{24} impacted the elution of the ceragenin from lenses. CSA-131, with a C_{12} chain, eluted more rapidly than CSA-134 and CSA-138, with C_{14} and C_{13} lipid chain lengths, respectively (figure 3.6). Microbiological and analytical data from these experiments suggest that the amount of CSA-138 that elutes into the surrounding broth was sufficient to eliminate up to 1 X 10^6 CFU of *S. aureus*.

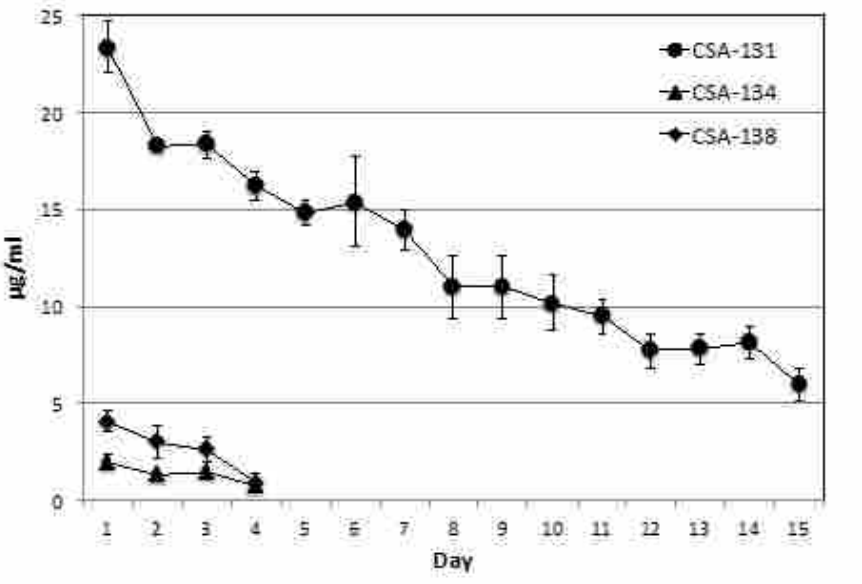

Figure 4.6 Elution of ceragenins from lenses containing 1% (w/w) of the indicated ceragenin. Lenses were soaked in PBS (1.5 ml) for 24 h and ceragenin concentrations were determined via LC/MS. Solutions in which lenses were soaked were replaced with fresh PBS every 24 h

4.3.5 Active release coatings to prevent implant related infections

Bone fractures need protection from infections during the healing process and fracture fixation plates can sometimes increase the possibility of acute bone infections which causes osteomyelitis. Literature reports suggest that in the majority of fractures, bacteria predominantly resides in biofilm

phenotype[81]. Active release coatings provide a promising approach to prevent and eliminate implant related biofilm infections[82].To optimize the *in-vivo* efficacy of control release coatings, we conducted several *in-vitro* studies with varying concentration of CSA-13 and different types of biocompatible polymeric matrices.Short and long term elution results from these *in-vitro* experiments are indicated in Figure 4.7. Short term elution data (Figure 4.7a) indicated that although there was a reduction in the overall μg/mL of CSA-13 from 4 hours to 24 hours in the chamber broth and in the bottle broth, there was no significant difference in the overall release of CSA-13, which was indicative of zero-order release. This was likely due to the fact that CSA-13 was saturated in the solution during that time.

Long term elution data indicated that the release of CSA-13 declined in a first-order fashion over the first five days. After five days, the detection limit of the particular LC/MS technique used in this study was surpassed as the broth samples contained less than 0.5μg/mL of CSA-13 , therefore, only 5 days of data is presented.

Broth Sample	µg/mL	Overall % Release
4 Hour Chamber	66.56 ± 32.4	8.8 ± 4.1
4 Hour Bottle	16.66 ± 12.48	
8 Hour Chamber	57.37 ± 36.89	8.5 ± 3.7
8 Hour Bottle	19.35 ± 12.62	
24 Hour Chamber	23.68 ± 18.86	8.1 ± 3.9
24 Hour Bottle	9.38 ± 5.25	

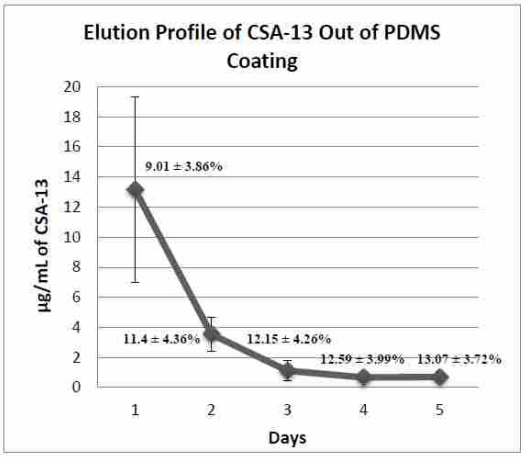

Figure 4.7 Elution profile of CSA-13 out of the PDMS coatings over a five day period is shown. The overall % release of CSA-13 at each day is also noted. Table (a) shows the LC/MS data and overall % release calculated from each of the broth samples collected at 4, 8, and 24 h.

Based on our in-vitro elution results, 18% W/W concentration with 1:1 PDMS:naptha ratio was selected and open wound surgeries in an animal model were carried out. In these studies, Type-III B Gustilo open fracture were modeled in sheep. In control animals, an un-coated fracture fixation plate was used, while an other group was treated with a CSA-13 coated fracture fixation plate. In the surgical follow up, control group animals were found to be severely infected and died within 9 weeks while the treatment group animals had a 100 % survival rate.

In this chapter we discussed the need of novel antimicrobial therapies and how CSAs can solve many existing problems in this field. We also discussed the development of analytical methods and their usefulness in developing clinical applications for CSAs. Our lab is continually developing more applications of CSAs in relevant areas and these analytical methods have played a vital role in this process.

Chapter 5

Synthesis of BODIPY Appended Cyclooctyne for Glycolipid Trafficking

5.1 Introduction

As discussed in the previous chapters, NKT cells play an important role in regulating the immune system and recognize glycolipid antigens that are bound to CD1, the non-classical MHC-like antigen presenting molecule. NKT cells can be classified into two categories - type I and type II. Type I NKT cells, also called semi-invariant NKT cells, carry a T cell receptor (TCR) with an invariant Vα24-Jα18 TCRα chain (Vα-Jα18 in mice) paired with a restricted subset of TCR Vβ chains and recognize the non-self glycolipid antigen α-galactosylceramide (α-GalCer).[1] Alternatively, type II NKT cells express a different and more diverse TCR and do not recognize α-GalCer.[83]

Immunological cells like dendritic cells (DCs) constantly survey and sample the blood stream

to look for foreign entities. Once these pathogenic organisms (non-self) are identified, antigen acquisition and uptake process is initiated. These antigen presenting cells have evolved a complex antigen processing machinery to break down the pathogen's cellular components and deliver them to intracellular endocytic compartments where antigen presenting molecules like CD1 can bind them. For example, MHC class I molecules selectively bind antigens in the endoplasmic reticulum whereas MHC class II molecules bind antigens from lysosomes. Porcelli et al.[84] have recently shown that α-GC, a potent NKT cell agonist that induces strong IFN-γ secretion, loads into CD1d in an endocytic compartment and is selectively trafficked to lipid rafts. Meanwhile the Th2-biased agonists load directly into CD1d proteins present on the cellular surface.

5.1.1 Cellular trafficking of glycolipids

With this information, it is clear that kinetics and the site of cellular loading are of critical importance in NKT cell activation and influence the Th1/Th2 bias of cytokine release by NKT cells. Conventionally, to study glycolipid trafficking, researchers have used C6" appended fluorescent probes (on sugar moiety).[85] The rationale for specifically choosing C6" position is that it does not significantly alter the cytokine release profile of NKT cells. While this rationale might be true for the immunogenicity of the antigen, fluorophores being large in nature (200-400 amu) almost certainly impact the trafficking of these molecules.

To solve this problem, we decided to use the azide-alkyne Huisgen cycloaddition (often refereed to as click chemistry) for studying trafficking patterns of glycolipid antigens. The click reaction, identified by Sharpless et al, is a bio-orthogonal reaction which means that it is very se-

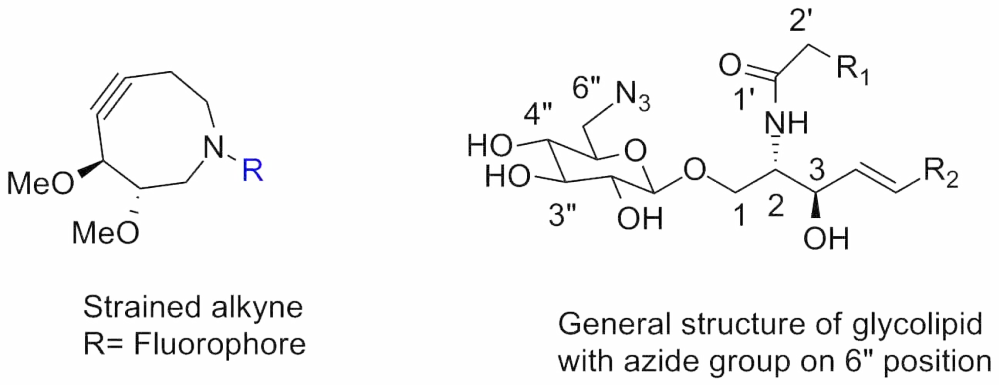

Figure 5.1 General structure of strained alkyne and 6" azido-glycolipid

lective even in a complex biological systems.[86] The original Huisgen reaction involved the thermal treatment of both alkyne and azide but the discovery of Cu(I) catalyzed 1,3 dipolar cycloaddition made the reaction possible at room temperature and provided substantial rate enhancements.[87] Recently Bertozzi et al, devised another variant of azide alkyne cycloaddition reaction to visualize membrane associated glycans in developing zebrafish.[88] As copper is cytotoxic, rendering the use of Cu(I) catalyzed cycloaddition infeasible, utilizing the ring strain of cyclooctyne, authors devised strain promoted azide-alkyne cycloaddition to be used for in vivo imaging. As the azide is small and stable in biological systems, it is used as a "chemical reporter" and can be easily placed on the substrate. The chemical structure of strained alkyne and that of a general 6" azido glycolipid is shown in figure 5.1.

5.2 Synthesis of strained alkyne

Following the work of Bertozzi et. al, we decided to synthesize the strained cyclooctyne system and attach it to a BODIPY fluorophore.[88] Details of the synthetic route are provided in scheme 5.1.

Briefly, glucose was protected with benzylidine to yield 5.1.2, which upon methylation resulted in 5.1.3. Upon bromination and deprotection of benzylidine, methyl 6-bromoglucopyranoside 5.1.4 was obtained. Reductive amination with zinc and allylbromide resulted in acyclic diene 5.1.5. After protecting the free amine with di-tert-butyl dicarbonate (Boc), ring closure was achieved by using second generation Grubb's catalyst. Oxidation of allylic alcohol 5.1.7 resulted in ketone 5.1.8. After successful hydrogenation of 5.1.8, removal of the Boc protecting group proved to be a mistake, as the amine attacks the carbonyl to generate a bicyclic product 5.1.10, which is unusable. We had to start the synthesis over again and decided to remove the Boc towards the end of the synthetic procedure.

5.2.1 Overcoming the problem of accidental cyclization

Learning from the last attempt to synthesize the cyclooctyne, we decided to transform the ketone in 5.1.9 to selenadiazole before undertaking Boc removal. The ketone (5.1.9) was first transformed into a semicarbazone, which upon reaction with selenium dioxide resulted in selenadiazole (5.2.1). After removing the Boc protection, selenadiazole was attached to BODIPY via a simple amide coupling to yield 5.2.3 and thereafter it was readily fragmented to the desired cyclooctyne 5.2.4.

5.3 Results and discussion

After sucessful synthesis of "clickable" cyclooctyne, we tested it's ability to label azido-glycolipid antigens inside NKT cells. In this in-vitro assay, NKT cells were incubated with either control or

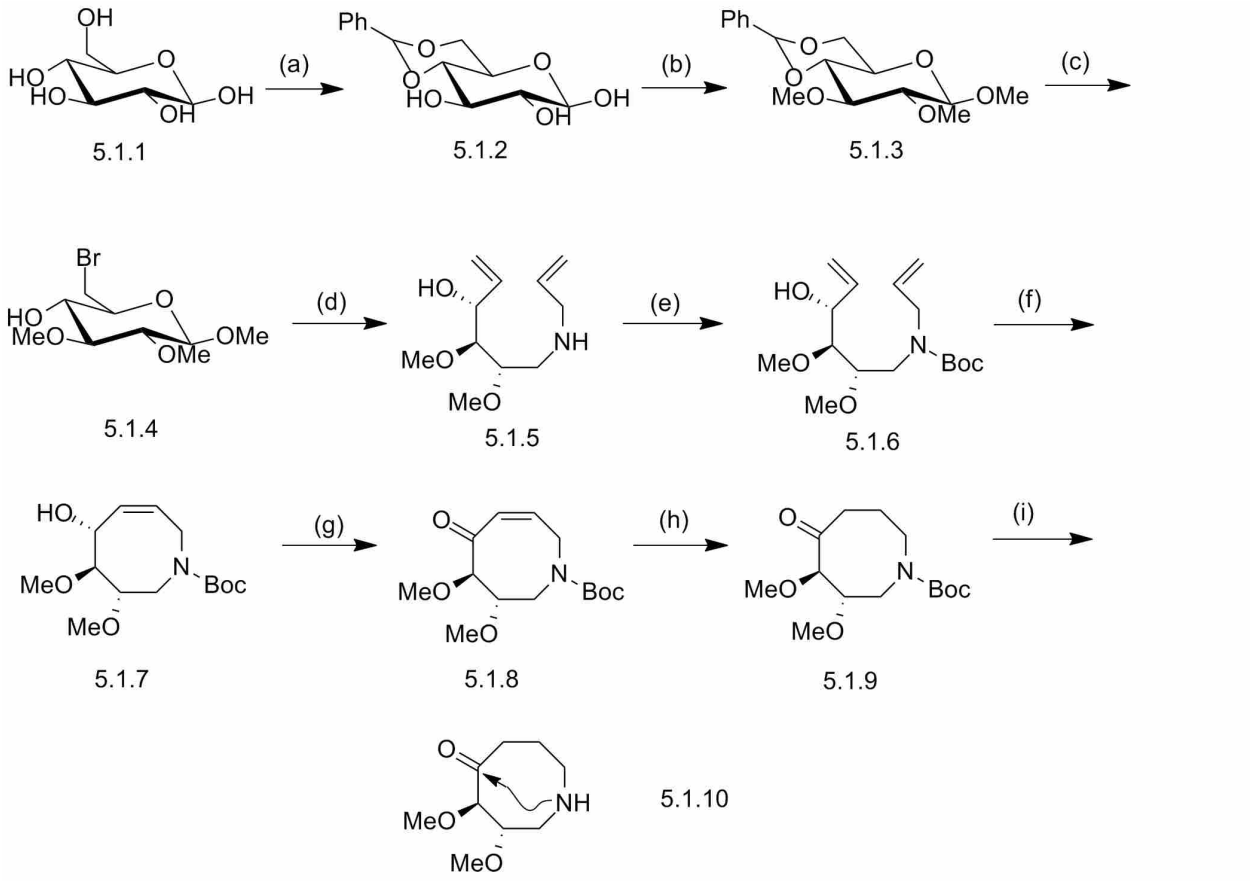

(a) Benzaldehyde dimethyl acetal , PPTS, 80% (b) MeI, KOH, 65% (c) 1) NBS, $CaCO_3$, CCl_4 2)1%NaOH 71%
(d) Zn, $NaBH_3CN$, 2) Allylamine 58% (e) $(Boc)_2O$, TEA, DMAP 77% (f) Grubb's Sec. Gen catalyst 5mol%, 62%
(g) PCC, 69% (h) H_2, PD/C, 71% (i) TFA , DCM , 64%

Scheme 5.1 Synthesis of BODIPY appended strained alkyne for glycolipid trafficking via click reactions

a 6" azido appended α-GalCer variant. Our results indicated that there was no need for fixing and permeabilization of NKT cells which suggests that cyclooctyne is highly permeable. As α-GalCer is known to accumulate in lysosomes, we indeed were able to find the fluorescence from bodipy appended cyclooctyne-6" azido α-GalCer complex in lysosomal compartments (figure 5.2).

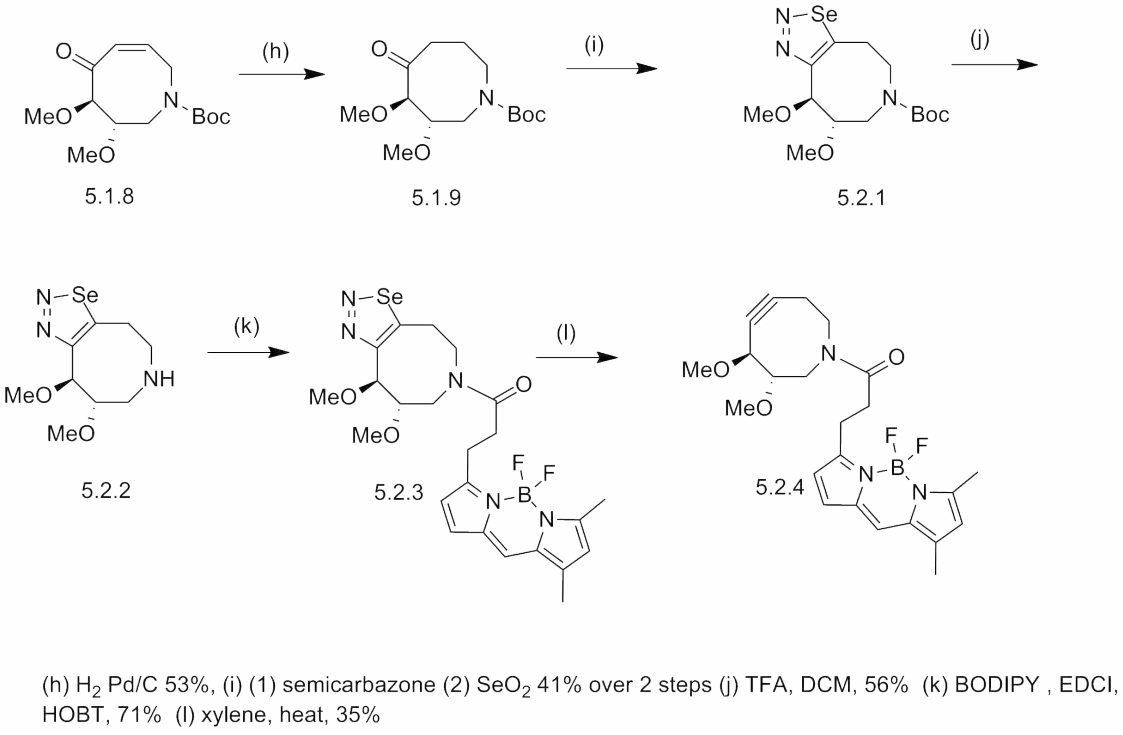

Scheme 5.2 Improved synthesis of BODIPY appended cyclooctyne

5.3.1 Trafficking of sulfatides

Sulfatide is an endogenous antigen of type-II NKT cells which carries a galactosylceramide with a sphingosine scaffold and a sulfate at the 3"-hydroxyl position. Unlike α-GalCer, sulfatide has a binding affinity to multiple CD1 moieties and has been shown to bind to CD1a, b, and c. Since the discovery of sulfatide-reactive T cells, it has been implicated in tumor immunity, experimental autoimmune encephalomyelitis (EAE), multiple sclerosis (MS), and type 1 diabetes.[89,90] Although sulfatide can bind to human CD1a, CD1b, CD1c, and CD1d ; researchers have shown that trafficking pattern of CD1b, unlike that of CD1a, impaired sulfatide presentation.[91] On its way to the cell surface, CD1a trafficks through early and recycling endosomes, whereas CD1b and CD1d are

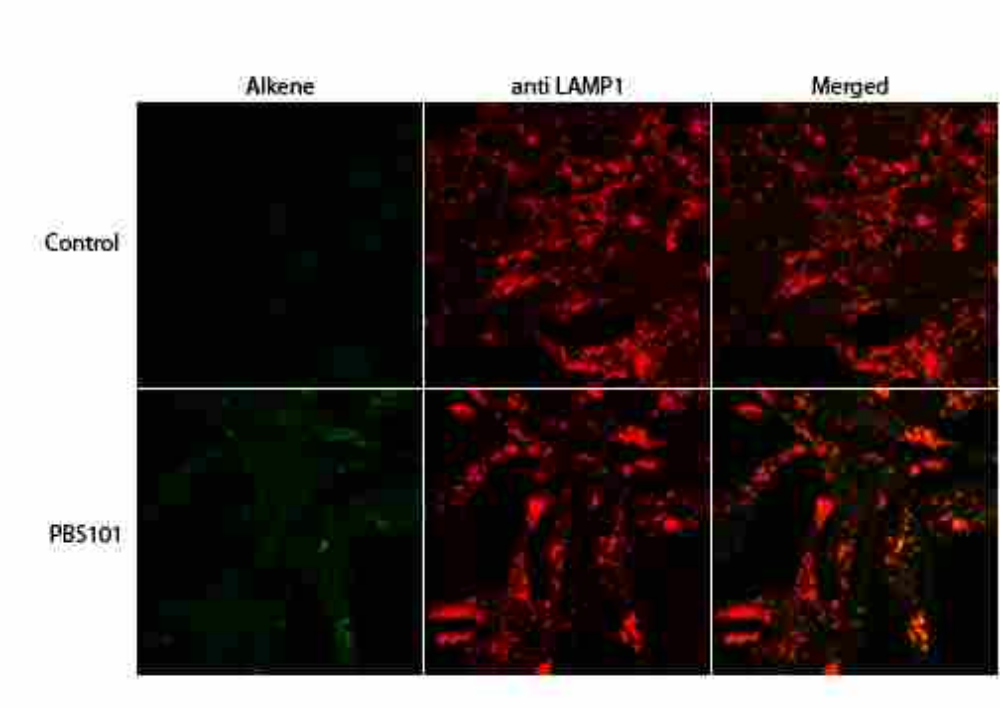

Figure 5.2 Accumulation of azido appended α-GalCer in lysosomes

localized in the late endosome and lysosome where microbial lipids accumulate during infections. Recently, there has been some debate whether sulfatides are trafficked to the lysosome but not loaded into CD1d, or if they are trafficked to the endosome and don't reach lysosomes at all.

With sulfatide being a physiologically important glycolipid antigen, we decided to monitor its trafficking. To achieve this, HeLa CD1d cells were incubated with C6" appended sulfatide. After 24 h, sulfatide was stained using anti LAMP-1 antibody and cyclooctyne. Notably, anti LAMP-1 antibody only stains sulfatide bound to CD1d, whereas, cyclooctyne shows the presence of sulfatide in unbound form. Using this technique, we were able to convincingly show that the sulfatides do get trafficked to the lysosome (Figure 5.3), and because of the low pH conditions, they might quickly dissociate from CD1d-sulfatide complex.

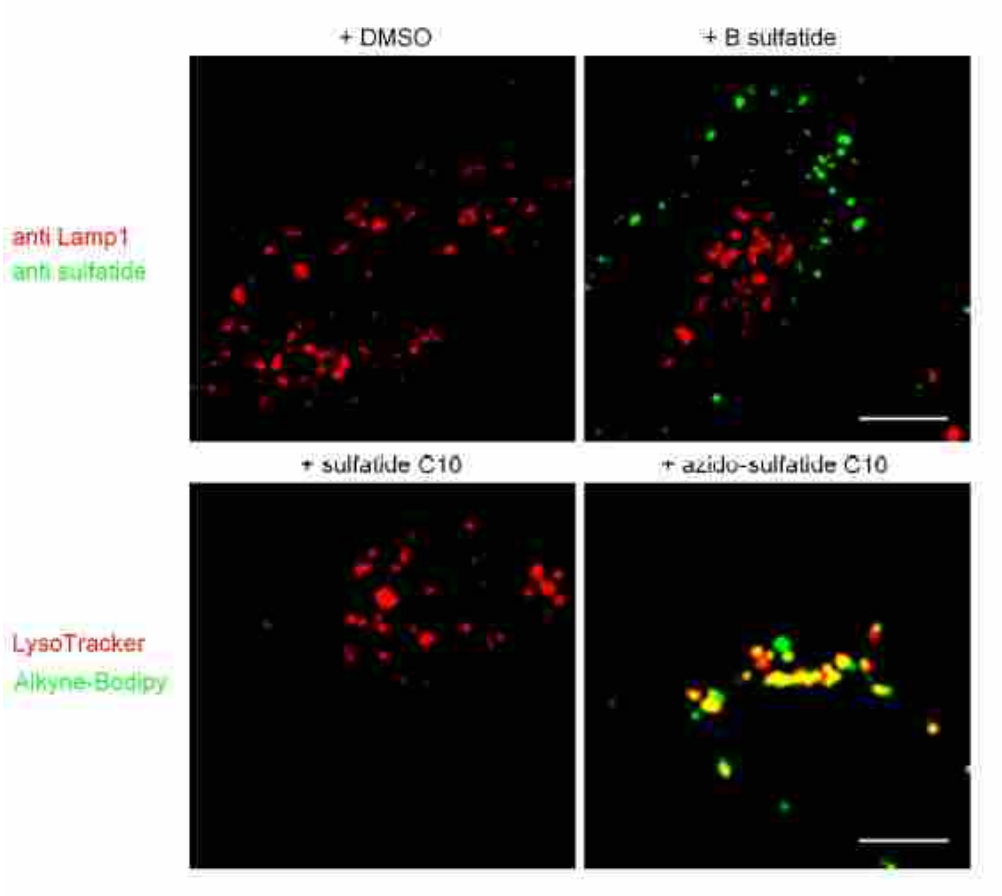

Figure 5.3 intracellular location of bovine sulfatide (5 mg/ml) incubated for 24 hours. staining was done with anti-sulfatide Ab O4 (green) and anti-Lamp1 (red). The results obtained from cyclooctyne-Bodipy are shown in the panel below

These experiments demonstrate that BODIPY appended strained cyclooctyne efficiently serves as a fluorescent tag for azido glycolipids. Because of its ability to permeate through the membrane, bio-orthogonality, and acceptable kinetics (time taken in staining) it outperforms most fluorescent tags in the market. Another advantage of this process is its ability to allow the use of the smallest possible modification (azide) on the substrate of interest. We are confident that using this technique, important discoveries in the field of glycolipid trafficking can be made.

5.4 Experimental Procedures

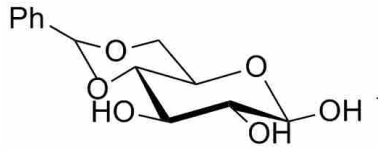

5.1.2

In a 500 ml RB flask, compound 5.1.1 (5 gm, 26.2 mmol) was dissolved in 100 ml toluene and Benzaldehyde dimethyl acetal (4.8 ml, 31.5 mmol) was added. To this solution p-toluene sulfonic acid (0.05 g, 0.26 mmol) was added and the reaction was stirred overnight. Next day, the reaction was checked for the disappearance of 5.1.1 and quenched by adding water and mixture was extracted with DCM (500 ml, 3 times). Organic layer was pooled and dried over Na_2SO_4 and thereafter evaporated to a residue. The crude product was purified by flash chromatography to yield compound 5.1.2 as pure product. ^{1}H NMR (500 MHz, Chloroform-d) δ 7.51 - 7.47 (m, 2H), 7.39 - 7.33 (m, 2H), 7.22 - 7.17 (m, 1H), 5.47 (d, J = 1.8 Hz, 1H), 4.83 (m, 1H), 4.13 (m 1H), 3.88 (dd, J = 8.8, 5.5 Hz, 1H), 3.63 (br, 1H), 3.57 (m, 1H), 3.47 (dd, J = 12.4, 7.3 Hz, 1H), 3.13 (m, 1H), 2.45 (s, 1H), 2.41 (s, 1H), 2.18 (s, 1H). ^{13}C NMR (125 MHz,Chloroform-d) 143.90, 128.76, 127.45, 126.63, 94.79, 78.55, 76.05, 71.88, 71.60, 71.42, 68.24, 23.08. HRMS (ESI) calcd for $C_{14}H_{20}O_6$ [M+H]+: 285.1233, found: 285.1310

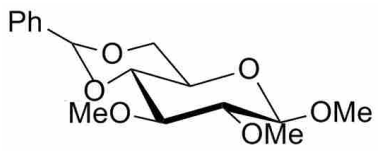

5.1.3

In a 500 ml RB flask, compound 5.1.2 (3 gm, 10.5 mmol) was dissolved in 500 ml of toluene

and NaOH (3 g, 2.8 mmol) was added. This mixture was heated to reflux for 1 h and 200 ml of toluene was added again. The reaction was cooled to room temperature and methyl iodide (21 ml, 146.4 mmol) was added slowly. The reaction mixture was heated to reflux for 6 h and reaction progress was monitored by TLC. Upon reaction completion, water was added to quench the reaction and organic layer was separated. Organics were pooled and dried over Na_2SO_4 and thereafter evaporated to a residue. The residue was purified by flash chromatography with 20% ethyl acetate in hexanes to yield compound 5.1.3. ^{1}H (500 MHz, Chloroform-d) δ 7.54 - 7.49 (m, 2H), 7.33 (m, 3H), 7.22 (m, 1H), 5.54 (d, J = 8.4 Hz, 1H), 4.87 (dd, J = 9.0, 3.7 Hz, 1H), 4.30 - 4.21 (m, 1H), 3.86 - 3.77 (m, 1H), 3.72 - 3.68 (m, 1H), 3.64 (s, 3H), 3.62 (s, 1H), 3.55 (s, 3H), 3.45 (d, J = 2.4 Hz, 3H), 3.40 (s, 1H), 3.30 (dd, J = 9.2, 3.7 Hz, 1H). HRMS (ESI) calculated for $C_{17}H_{27}O_6$ [M+H]+: 327.1802, found: 327.1844

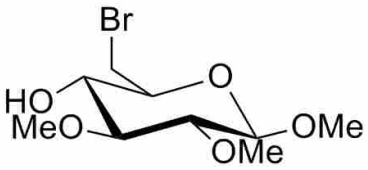

5.1.4

In a 1000 ml RB flask, compound 5.1.3 (3 g, 9.7 mmol) was dissolved in anhydrous CCl_4 (100 ml) and $CaCO_3$ (1.06 g, 10.64 mmol) was added. Under nitrogen atmosphere, this mixture was heated to reflux. The reaction was cooled to RT and then, N-bromosuccinimide (1.9 g, 10.5 mmol)) was added and the reaction was heated to 65 degrees again. Upon reaction completion, organics were dried under vacuum and residue was washed with aqueous $Na_2S_2O_3$ and $NaHCO_3$.

Extraction was done using ethyl acetate and organic layer was separated and evaporated to dryness. This residue was dissolved in aqueous 1% NaOH in MeOH (1.5 L). After 1 h, the solution was neutralized with 5M HCl and solvents were removed under vacumm. The residue was dissolved in H_2O (1.5 L) and extracted with CH_2Cl_2 (8 x 500 mL). Organics was pooled and dried over Na_2SO_4 and thereafter evaporated to a residue. The crude product was purified by flash chromatography with 5% ethyl acetate in hexanes to yield compound 5.1.4. ^{1}H NMR (500 MHz, Chloroform-d) δ 4.83 (d, J = 3.5 Hz, 1H), 3.75 - 3.64 (m, 3H), 3.63 - 3.49 (m, 3H), 3.49 - 3.31 (m, 8H), 3.21 (dd, J = 9.3, 3.6 Hz, 1H), 3.10 (d, J = 2.9 Hz, 1H). 13C NMR (125 MHz, Chloroform-d) δ 97.38, 82.63, 82.62, 81.74, 77.35, 76.84, 71.70, 69.87, 61.20, 58.44, 58.43, 55.36, 55.35, 55.34, 53.42, 33.38. HRMS (ESI) calculated for $C_9H_{18}BrO_5$ [M+H]+: 285.0332, found: 285.0299, and 302.0591

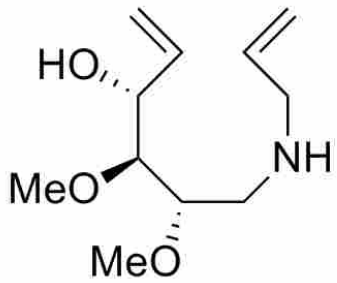

5.1.5

Compound 5.1.4 (1.9g, 6.5mmol, 1equiv) was dissolved in 500 ml of 19:1 1-propanol/water in an Erlenmeyer flask. To this solution, allylamine (16 ml, 30 eqiv), zinc (25 g, 54 equiv) and $NaBH_3CN$ (2 g, 5 equiv) were added. The reaction mixture was heated to 90^{o}C and monitored by TLC for disappearance of starting material. After the reaction was complete (approx 90min), the mixture was cooled and filtered through celite. The filterate was evaporated to dryness and redis-

solved in 800 ml of 6:4:1 MeOH/DCM/1.5M HCl and stirred vigorously for 1 h. After confirming the completion of reaction by TLC, 500ml water was added and mixture was extracted with DCM (500 ml, 3 times). Organic layer was pooled and dried over Na_2SO_4 and thereafter evaporated to a residue. The crude product was purified by flash chromatography with 50% ethyl acetate in hexanes to yield compound 4 as pure product. ^{1}H NMR (500 MHz, Chloroform-d) δ 6.03 (m, 1H), 5.87 (m, 1H), 5.40 (m, 1H), 5.30 (d, J = 0.6 Hz, 1H), 5.23 - 5.17 (m, 2H), 5.16 (td, J = 1.8, 0.5 Hz, 1H), 5.13 (m, 1H), 4.32 - 4.28 (m, 1H), 3.55 - 3.51 (m, 1H), 3.45 (d, J = 0.6 Hz, 3H), 3.42 (d, J = 0.5 Hz, 3H), 3.36 - 3.33 (m, 1H), 3.27 - 3.23 (m, 3H), 2.90 (br, 2H), 2.84 (br, 1H). HRMS (ESI) calculated for $C_{11}H_{22}NO_3$ [M+H]+: 216.1600, found: 233.1871 (M+NH4)

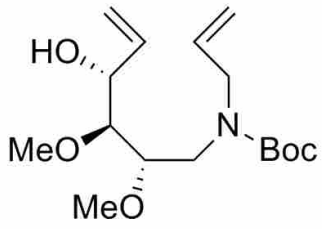

5.1.6

In a 100 ml RB flask, compound 5.1.5 (1.2g, 5.57mmol, 1 equiv) was dissolved in 200 ml acetonitrile. To this solution, triethylamine (1.6ml, 3equiv) and di-tert-butyl dicarbonate (1.4g, 1.2equiv) were added. Reaction was monitored by TLC and after completion, the reaction was dried under vaccum. Flash chromatography was performed using 3:1 ethyl acetate/hexanes to yield pure compound as a pale yellow oil. HRMS (ESI) calculated for $C_{16}H_{29}NO_5$ [M+H]+: 316.2010, found: 316.2024

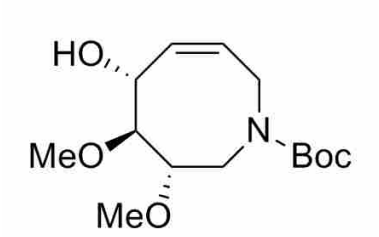

5.1.7

In a 500 ml RB flask, compound 5.1.6 (800mg, 2.3mmol, 1equiv) was dissolved in 400ml DMC and heated to reflux under N_2. After 10 min, Grubb's second generation catalyst (80mg, 0.04 equiv) was added. The reaction was monitored by TLC in 1:1 toluene/acetone for the disappearance of starting material. Upon completion (approx. 4 h) the reaction was cooled to RT and filtered through celite 3 times. Flash chromatography was performed to yield pure compound 5.1.7 as yellow oil. ^{13}C NMR (125 MHz, Chloroform-d) δ 155.37, 133.71, 125.23, 83.10, 81.83, 80.63, 77.03, 66.91, 61.59, 58.11, 53.38, 47.15, 46.61, 45.49, 28.38.

5.1.8

Compound 5.1.7 (1.8 g, 6.27 mmol) was dissolved in 150 ml of DCM and pyridinium chlorochromate , PCC (2.02 g, 9.48 mmol) was added. The reaction was heated overnight at 50^o under inert atmosphere. Next day, the reaction completion was checked by TLC and water was

added to quench the reaction and extraction was done with DCM . Organic layer was pooled and dried over Na_2SO_4 and thereafter evaporated to a residue. The crude product was purified by flash chromatography with 10% ethyl acetate in hexanes to yield 5.1.8. ^{13}C NMR (122 MHz, Chloroform-d) δ 201.80, 154.26, 133.60, 127.48, 89.63, 80.89, 79.54, 59.67, 57.90, 49.65, 48.73, 47.70, 28.11. HRMS (ESI) calculated for $C_{14}H_{23}NO_5$ [M+H]+: 286.1674, found: 286.1721.

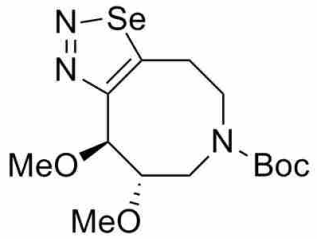

5.2.1

In a 250 ml RB flask, compound 5.1.9 (0.6 g, 2.09 mmol) was dissolved in 1:1 H_2O/EtOH containing 100 mM aniline (40 ml). To this solution, semicarbazide hydrochloride (2.33 g, 20.91 mmol) and acetic acid (0.15 ml) were added. This mixture was stirred at RT and the reaction progress was monitored by TLC. Upon reaction completion the acid was neutralized with 10% NaOH and the ethanol was removed under vacuum. The aqueous layer was extracted with Ethyl acetate. The organics was pooled and dried, to yield in crude semicarbazone that was directly converted to selenadiazole 5.2.1. To achieve this, the crude semicarbazone was dissolved in dioxane (10 mL) and a solution of 10% SeO_2 in 1:1 dioxane/H_2O (8 mL) was added dropwise over 1 h to the semicarbazone solution. The mixture was left stirring at RT. The reaction progress was monitored by mass spectrometry and upon completion, the organics were filtered through a silica plug. Filtrate was pooled ,dried an chromatographed to yield compound 5.2.1. This reaction was

not very clean and despite a few attempts to obtain the pure compound, we sere not successful and semi-pure 5.2.1 was carried over to the next reaction.

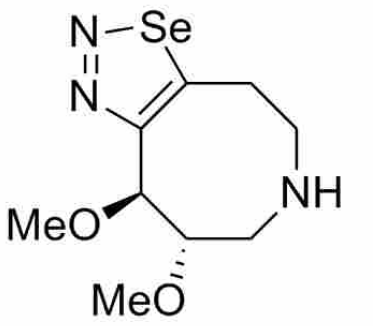

5.2.2

Compound 5.2.1 was dissolved in 50 ml of DCM. To this solution 5 ml of trifluoro acetic acid (TFA) was added. This reaction was stirred for 3 h at -10^o and the reaction progress was monitored by TLC and mass spectrometry. Upon reaction completion, saturated $NaHCO_3$ solution was added and extraction was done using DCM. Organics were pooled and dried. The residue was chromatographed with 40% ethyl acetate in hexanes to give compound 5.2.2. ^{1}H NMR (500 MHz, Chloroform-d) δ 5.39 (d, J = 6.0 Hz, 1H), 3.77 (ddd, J = 6.0, 3.9, 1.2 Hz, 1H), 3.67 - 3.58 (m, 1H), 3.50 (s, 3H), 3.33 (s, 4H), 3.31 (d, J = 3.9 Hz, 1H), 3.16 (dt, J = 13.8, 3.9 Hz, 1H), 3.13 - 3.05 (m, 1H), 2.98 (ddd, J = 14.0, 10.4, 3.9 Hz, 1H), 2.72 (d, J = 15.1 Hz, 1H),

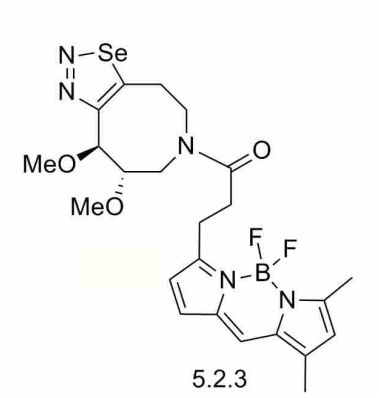

5.2.3

BODIPY FL propionic acid (5 mg, 0.18 mmol) was purchased from Invitrogen and was dissolved in 10 ml of 1:1 dry THF: methanol. To his solution, EDCI (4 mg, 0.2 mmol) and HOBT (0.27 mg, 0.2 mmol) were added and sonicated for 30 mins.. This mixture was stirred for 1 h and compound 5.2.2 (5mg, 0.18 mmol) was dissolved in 2 ml DCM and added to this reaction. Progress of the reaction was monitored by TLC and upon reaction completion solvent was removed under vacuum. HRMS (ESI) calculated for $C_{23}H_{28}BF_2N_5O_3Se$ [M+H]+: 551.1479, found: 552.1887 amu and the Fluoride ion loss adduct was also found at 532.1684 amu. Due to the small amount of material, purification was not attempted and the crude 5.2.3 was directly taken to the next step.

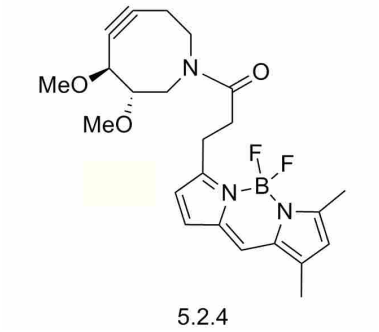

5.2.4

Crude selenadiazole 5.2.3 from the last reaction was dissolved in 2 ml of xylenes and heated to 115 ^{o}C. The Progress of the reaction was monitored by TLC. This reaction took a long time (3

days). Upon completion the reaction was cooled to RT and organics were evaporated under vacuum. The crude product was purified via flash chromatography with 5% ethyl acetate in hexanes to yield compound 5.2.4. Due to the small amount of material and the difficulty in purification, semi pure product was washed multiple times with hexanes and the NMR spectrum was recorded. ^{1}H NMR (500 MHz, Chloroform-d) δ 7.08 (d, J = 7.3 Hz, 1H), 6.89 (d, J = 4.0 Hz, 1H), 6.31 (d, J = 4.0 Hz, 1H), 6.11 (d, J = 7.0 Hz, 1H), 4.24 - 4.18 (m, 1H), 4.10 - 4.02 (m, 2H), 3.85 (td, J = 8.8, 1.2 Hz, 1H), 3.70 (s, 3H), 3.38 (s, 3H), 3.37 - 3.28 (m, 3H), 3.07 (br, 2H), 2.84 (m, 2H), 2.76 (dd, J = 13.9, 8.9 Hz, 1H), 2.71 - 2.59 (m, 2H), 2.55 (s, 3H), 2.25 (d, J = 3.0 Hz, 3H), 1.54 (s, 4H). 13C NMR (125 MHz, Chloroform-d) δ 172.08, 160.18, 157.75, 143.77, 135.07, 133.36, 128.33, 123.75, 120.35, 117.84, 96.21, 92.54, 85.17, 59.10, 57.26, 55.54, 52.19, 33.45, 24.89, 21.99, 14.92, 11.30. HRMS (ESI) calculated for $C_{22}H_{28}BF_2N_2O_3$ [M+H]+: 443.2256, found: 424.2876 amu (M+H-F, the fluoride ion loss adduct)

Bibliography

[1] Bendelac, A.; Savage, P. B.; Teyton, L. *Annu Rev Immunol* **2007**, *25*, 297–336.

[2] Godfrey, D. I.; Hammond, K. J.; Poulton, L. D.; Smyth, M. J.; Baxter, A. G. *Immunol Today* **2000**, *21*, 573–83.

[3] Bendelac, A.; Rivera, M. N.; Park, S. H.; Roark, J. H. *Annu Rev Immunol* **1997**, *15*, 535–62.

[4] Tatituri, R. V. et al. *Proc Natl Acad Sci U S A* **2013**,

[5] Rymarchyk, S. L.; Lowenstein, H.; Mayette, J.; Foster, S. R.; Damby, D. E.; Howe, I. W.; Aktan, I.; Meyer, R. E.; Poynter, M. E.; Boyson, J. E. *Immunology* **2008**, *125*, 331–43.

[6] Matsuda, J. L.; Naidenko, O. V.; Gapin, L.; Nakayama, T.; Taniguchi, M.; Wang, C. R.; Koezuka, Y.; Kronenberg, M. *J Exp Med* **2000**, *192*, 741–54.

[7] Sullivan, B. A.; Nagarajan, N. A.; Wingender, G.; Wang, J.; Scott, I.; Tsuji, M.; Franck, R. W.; Porcelli, S. A.; Zajonc, D. M.; Kronenberg, M. *J Immunol* **2010**, *184*, 141–53.

[8] Nagaleekar, V. K.; Sabio, G.; Aktan, I.; Chant, A.; Howe, I. W.; Thornton, T. M.; Benoit, P. J.; Davis, R. J.; Rincon, M.; Boyson, J. E. *J Immunol* **2011**, *186*, 4140–6.

[9] Sumida, T.; Sakamoto, A.; Murata, H.; Makino, Y.; Takahashi, H.; Yoshida, S.; Nishioka, K.; Iwamoto, I.; Taniguchi, M. *J Exp Med* **1995**, *182*, 1163–8.

[10] Wilson, S. B.; Kent, S. C.; Patton, K. T.; Orban, T.; Jackson, R. A.; Exley, M.; Porcelli, S.; Schatz, D. A.; Atkinson, M. A.; Balk, S. P.; Strominger, J. L.; Hafler, D. A. *Nature* **1998**, *391*, 177–81.

[11] Kee, S. J.; Kwon, Y. S.; Park, Y. W.; Cho, Y. N.; Lee, S. J.; Kim, T. J.; Lee, S. S.; Jang, H. C.; Shin, M. G.; Shin, J. H.; Suh, S. P.; Ryang, D. W. *Infect Immun* **2012**, *80*, 2100–8.

[12] Kronenberg, M.; Gapin, L. *Nat Rev Immunol* **2002**, *2*, 557–68.

[13] Cui, J.; Shin, T.; Kawano, T.; Sato, H.; Kondo, E.; Toura, I.; Kaneko, Y.; Koseki, H.; Kanno, M.; Taniguchi, M. *Science* **1997**, *278*, 1623–6.

[14] Mendiratta, S. K.; Martin, W. D.; Hong, S.; Boesteanu, A.; Joyce, S.; Van Kaer, L. *Immunity* **1997**, *6*, 469–77.

[15] Szalay, G.; Ladel, C. H.; Blum, C.; Brossay, L.; Kronenberg, M.; Kaufmann, S. H. *J Immunol* **1999**, *162*, 6955–8.

[16] Ishigami, M.; Nishimura, H.; Naiki, Y.; Yoshioka, K.; Kawano, T.; Tanaka, Y.; Taniguchi, M.; Kakumu, S.; Yoshikai, Y. *Hepatology* **1999**, *29*, 1799–808.

[17] Mattner, J. et al. *Nature* **2005**, *434*, 525–529.

[18] Sada-Ovalle, I.; SkÃűld, M.; Tian, T.; Besra, G. S.; Behar, S. M. *Am J Respir Crit Care Med* **2010**, *182*, 841–7.

[19] Nieuwenhuis, E. E.; Matsumoto, T.; Exley, M.; Schleipman, R. A.; Glickman, J.; Bailey, D. T.; Corazza, N.; Colgan, S. P.; Onderdonk, A. B.; Blumberg, R. S. *Nat Med* **2002**, *8*, 588–93.

[20] Thedrez, A.; de Lalla, C.; Allain, S.; Zaccagnino, L.; Sidobre, S.; Garavaglia, C.; Borsellino, G.; Dellabona, P.; Bonneville, M.; Scotet, E.; Casorati, G. *Blood* **2007**, *110*, 251–8.

[21] Sandberg, J. K.; Fast, N. M.; Palacios, E. H.; Fennelly, G.; Dobroszycki, J.; Palumbo, P.; Wiznia, A.; Grant, R. M.; Bhardwaj, N.; Rosenberg, M. G.; Nixon, D. F. *J Virol* **2002**, *76*, 7528–34.

[22] Juno, J. A.; Keynan, Y.; Fowke, K. R. *PLoS Pathog* **2012**, *8*, e1002838.

[23] Mattner, J. et al. *Nature* **2005**, *434*, 525–529.

[24] Salio, M.; Speak, A. O.; Shepherd, D.; Polzella, P.; Illarionov, P. A.; Veerapen, N.; Besra, G. S.; Platt, F. M.; Cerundolo, V. *Proc Natl Acad Sci U S A* **2007**, *104*, 20490–5.

[25] Kinjo, Y. et al. *Nat Immunol* **2006**, *7*, 978–86.

[26] Sriram, V.; Du, W.; Gervay-Hague, J.; Brutkiewicz, R. R. *Eur J Immunol* **2005**, *35*, 1692–701.

[27] Fischer, K.; Scotet, E.; Niemeyer, M.; Koebernick, H.; Zerrahn, J.; Maillet, S.; Hurwitz, R.; Kursar, M.; Bonneville, M.; Kaufmann, S. H.; Schaible, U. E. *Proc Natl Acad Sci U S A* **2004**, *101*, 10685–90.

[28] Kinjo, Y. et al. *Nat Immunol* **2011**, *12*, 966–74.

[29] Gapin, L. *Nat Rev Immunol* **2010**, *10*, 272–7.

[30] Umetsu, D. T.; Meyer, E. H.; DeKruyff, R. H. *Int Rev Immunol* **2007**, *26*, 121–40.

[31] Kim, H. Y.; DeKruyff, R. H.; Umetsu, D. T. *Nat Immunol* **2010**, *11*, 577–584.

[32] Gilroy, D. W.; Feldmann, M.; Dabbagh, K. *Int J Biochem Cell Biol* **2010**, *42*, 480–1.

[33] Matangkasombut, P.; Pichavant, M.; Dekruyff, R. H.; Umetsu, D. T. *Mucosal Immunol* **2009**, *2*, 383–92.

[34] Anderson, G. P. *Lancet* **2008**, *372*, 1107–19.

[35] Wenzel, S.; Wilbraham, D.; Fuller, R.; Getz, E. B.; Longphre, M. *Lancet* **2007**, *370*, 1422–31.

[36] Akbari, O.; Stock, P.; Meyer, E.; Kronenberg, M.; Sidobre, S.; Nakayama, T.; Taniguchi, M.; Grusby, M. J.; DeKruyff, R. H.; Umetsu, D. T. *Nat Med* **2003**, *9*, 582–8.

[37] Bullens, D. M.; Truyen, E.; Coteur, L.; Dilissen, E.; Hellings, P. W.; Dupont, L. J.; Ceuppens, J. L. *Respir Res* **2006**, *7*, 135.

[38] Kim, E. Y. et al. *Nat Med* **2008**, *14*, 633–40.

[39] Savage, P. B.; Teyton, L.; Bendelac, A. *Chem Soc Rev* **2006**, *35*, 771–779.

[40] Agarwal, R. *Curr Allergy Asthma Rep* **2011**, *11*, 403–413.

[41] Agarwal, R.; Gupta, D. *Med Mycol* **2011**, *49 Suppl 1*, S150–S157.

[42] O'connor, G. T.; Walter, M.; Mitchell, H.; Kattan, M.; Morgan, W. J.; Gruchalla, R. S.; Pongracic, J. A.; Smartt, E.; Stout, J. W.; Evans, R.; Crain, E. F.; Burge, H. A. *J Allergy Clin Immunol* **2004**, *114*, 599–606.

[43] Shelton, B. G.; Kirkland, K. H.; Flanders, W. D.; Morris, G. K. *Appl Environ Microbiol* **2002**, *68*, 1743–1753.

[44] Umetsu, D. T.; Dekruyff, R. H. *J Allergy Clin Immunol* **2010**, *125*, 975–979.

[45] Kawai, T.; Akira, S. *Cell Death Differ* **2006**, *13*, 816–825.

[46] Bodennec, J.; Pelled, D.; Futerman, A. H. *J Lipid Res* **2003**, *44*, 218–226.

[47] Toledo, M. S.; Levery, S. B.; Straus, A. H.; Takahashi, H. K. *FEBS Lett* **2001**, *493*, 50–56.

[48] FOLCH, J.; LEES, M.; SLOANE STANLEY, G. H. *J Biol Chem* **1957**, *226*, 497–509.

[49] Toledo, M. S.; Levery, S. B.; Bennion, B.; Guimaraes, L. L.; Castle, S. A.; Lindsey, R.; Momany, M.; Park, C.; Straus, A. H.; Takahashi, H. K. *J Lipid Res* **2007**, *48*, 1801–1824.

[50] Bennion, B.; Park, C.; Fuller, M.; Lindsey, R.; Momany, M.; Jennemann, R.; Levery, S. B. *J Lipid Res* **2003**, *44*, 2073–2088.

[51] Levery, S. B.; Toledo, M. S.; Doong, R. L.; Straus, A. H.; Takahashi, H. K. *Rapid Commun Mass Spectrom* **2000**, *14*, 551–563.

[52] Kim, H. Y.; Salem, N., Jr *J Lipid Res* **1990**, *31*, 2285–2289.

[53] Park, C.; Bennion, B.; François, I. E. J. A.; Ferket, K. K. A.; Cammue, B. P. A.; Thevissen, K.; Levery, S. B. *J Lipid Res* **2005**, *46*, 759–768.

[54] Toledo, M. S.; Levery, S. B.; Straus, A. H.; Suzuki, E.; Momany, M.; Glushka, J.; Moulton, J. M.; Takahashi, H. K. *Biochemistry* **1999**, *38*, 7294–7306.

[55] Zhang, Y.; Wang, S.; Li, X.-M.; Cui, C.-M.; Feng, C.; Wang, B.-G. *Lipids* **2007**, *42*, 759–764.

[56] Mattner, J. et al. *Nature* **2005**, *434*, 525–9.

[57] Kinjo, Y. et al. *Nat Immunol* **2006**, *7*, 978–86.

[58] Chang, Y.-J. et al. *J Clin Invest* **2011**, *121*, 57–69.

[59] Kinjo, Y. et al. *Nat Immunol* **2011**, *12*, 966–74.

[60] Murakami, T.; Hirono, R.; Sato, Y.; Furusawa, K. *Carbohydr Res* **2007**, *342*, 1009–1020.

[61] Philip Garner, J. M. P. *The journal of organic chemistry* **1987**, *52 (12)*, 2361–2364.

[62] Hess, L. C.; Posner, G. H. *Org Lett* **2010**, *12*, 2120–2122.

[63] Azuma, H.; Takao, R.; Niiro, H.; Shikata, K.; Tamagaki, S.; Tachibana, T.; Ogino, K. *J Org Chem* **2003**, *68*, 2790–2797.

[64] Jun Yoshida, H. S., Masako Nakagawa; Hino, T. *Journal of the Chemical Society, Perkin Transactions 1* **1992**, *3*, 343–350.

[65] Sébastien Prévost, P. P., Tahar Ayad *Advanced Synthesis & Catalysis* **2011**, *353*, 3213–3226.

[66] Pei, B.; Vela, J. L.; Zajonc, D.; Kronenberg, M. *Ann N Y Acad Sci* **2012**, *1253*, 68–79.

[67] Williams, D. L.; Haymond, B. S.; Beck, J. P.; Savage, P. B.; Chaudhary, V.; Epperson, R. T.; Kawaguchi, B.; Bloebaum, R. D. *Biomaterials* **2012**, *33*, 8641–8656.

[68] Zhang, L.; Falla, T. J. *Expert Opin Pharmacother* **2006**, *7*, 653–663.

[69] Giuliani, A.; Rinaldi, A. C. *Cell Mol Life Sci* **2011**, *68*, 2255–2266.

[70] Epand, R. F.; Pollard, J. E.; Wright, J. O.; Savage, P. B.; Epand, R. M. *Antimicrob Agents Chemother* **2010**, *54*, 3708–3713.

[71] Lai, X.-Z.; Feng, Y.; Pollard, J.; Chin, J. N.; Rybak, M. J.; Bucki, R.; Epand, R. F.; Epand, R. M.; Savage, P. B. *Acc Chem Res* **2008**, *41*, 1233–1240.

[72] Yeaman, M. R.; Yount, N. Y. *Pharmacol Rev* **2003**, *55*, 27–55.

[73] Tzeng, Y.-L.; Ambrose, K. D.; Zughaier, S.; Zhou, X.; Miller, Y. K.; Shafer, W. M.; Stephens, D. S. *J Bacteriol* **2005**, *187*, 5387–5396.

[74] Yi, E. C.; Hackett, M. *Analyst* **2000**, *125*, 651–656.

[75] Li, A. C.; Sabo, A. M.; McCormick, T.; Johnston, S. M. *J Pharm Biomed Anal* **2004**, *34*, 631–641.

[76] Williams, D. L.; Haymond, B. S.; Beck, J. P.; Savage, P. B.; Chaudhary, V.; Epperson, R. T.; Kawaguchi, B.; Bloebaum, R. D. *Biomaterials* **2012**, *33*, 8641–8656.

[77] Fosse, T.; Giraud-Morin, C.; Madinier, I. *Lett Appl Microbiol* **2003**, *36*, 25–29.

[78] Chakraborty, A. B.; Berger, S. J. *J Biomol Tech* **2005**, *16*, 327–335.

[79] Willcox, M. D. P. *Clin Exp Optom* **2011**, *94*, 161–168.

[80] Cole, N.; Hume, E. B. H.; Vijay, A. K.; Sankaridurg, P.; Kumar, N.; Willcox, M. D. P. *Invest Ophthalmol Vis Sci* **2010**, *51*, 390–395.

[81] Williams, D. L.; Haymond, B. S.; Woodbury, K. L.; Beck, J. P.; Moore, D. E.; Epperson, R. T.; Bloebaum, R. D. *J Biomed Mater Res A* **2012**, *100*, 1888–1900.

[82] Hetrick, E. M.; Schoenfisch, M. H. *Chem Soc Rev* **2006**, *35*, 780–789.

[83] Smyth, M. J.; Godfrey, D. I. *Nat Immunol* **2000**, *1*, 459–60.

[84] Im, J. S. et al. *Immunity* **2009**, *30*, 888–898.

[85] Cheng, J. M. H.; Chee, S. H.; Knight, D. A.; Acha-Orbea, H.; Hermans, I. F.; Timmer, M. S. M.; Stocker, B. L. *Carbohydr Res* **2011**, *346*, 914–926.

[86] Kolb, H. C.; Finn, M. G.; Sharpless, K. B. *Angew Chem Int Ed Engl* **2001**, *40*, 2004–2021.

[87] Rostovtsev, V. V.; Green, L. G.; Fokin, V. V.; Sharpless, K. B. *Angew Chem Int Ed Engl* **2002**, *41*, 2596–2599.

[88] Laughlin, S. T.; Baskin, J. M.; Amacher, S. L.; Bertozzi, C. R. *Science* **2008**, *320*, 664–667.

[89] Buschard, K.; Blomqvist, M.; Osterbye, T.; Fredman, P. *Diabetologia* **2005**, *48*, 1957–1962.

[90] Girardi, E.; Maricic, I.; Wang, J.; Mac, T.-T.; Iyer, P.; Kumar, V.; Zajonc, D. M. *Nat Immunol* **2012**, *13*, 851–856.

[91] Cernadas, M.; Cavallari, M.; Watts, G.; Mori, L.; De Libero, G.; Brenner, M. B. *J Immunol* **2010**, *184*, 1235–1241.

Appendix A

List of Abbreviations

AHR	Airway hyperreactivity
TCR	T-cell receptor
CD	class of differentiation
APC	Antigen presenting cell
MHC	Major Histocapatibilty complex
NKT	Natural Killer T
iNKT	Invariant Natural Killer T
α-GalCer	α-galactosylceramide
TH	T-helper
INF	Interferon
IL	Interleukin
WT	Wild type

MyD88	Myeloid differentiation primary response gene (88)
Triff	TIR-domain-containing adapter-inducing interferon
HSQC	Heteronuclear single quantum coherence spectroscopy
COSY	Correlation spectroscopy
HMBC	Heteronuclear multiple-bond correlation spectroscopy
EDCI	1-ethyl-3-(3-dimethylaminopropyl) carbodiimide
DCM	Dichloromethane
DMF	Dimethyl formamide
LAH	Lithium aluminum hydride
THF	Tetrahydrofuran
HOBt	Hydroxybenzotriazol
TDS-Cl	Chloro(dimethyl)thexylsilane
M.S.	Mass spectrometry
RB	Round bottom (flask)
ACN	Acetonitrile
NBS	n-Bromosuccinimide
TBDPS-Cl	tert-butylchlorodiphenylsilane
BODIPY	boron-dipyrromethene
AMP	Antimicrobial peptides
CSA	Cationic steroid antibiotic

Appendix B

NMR Spectra

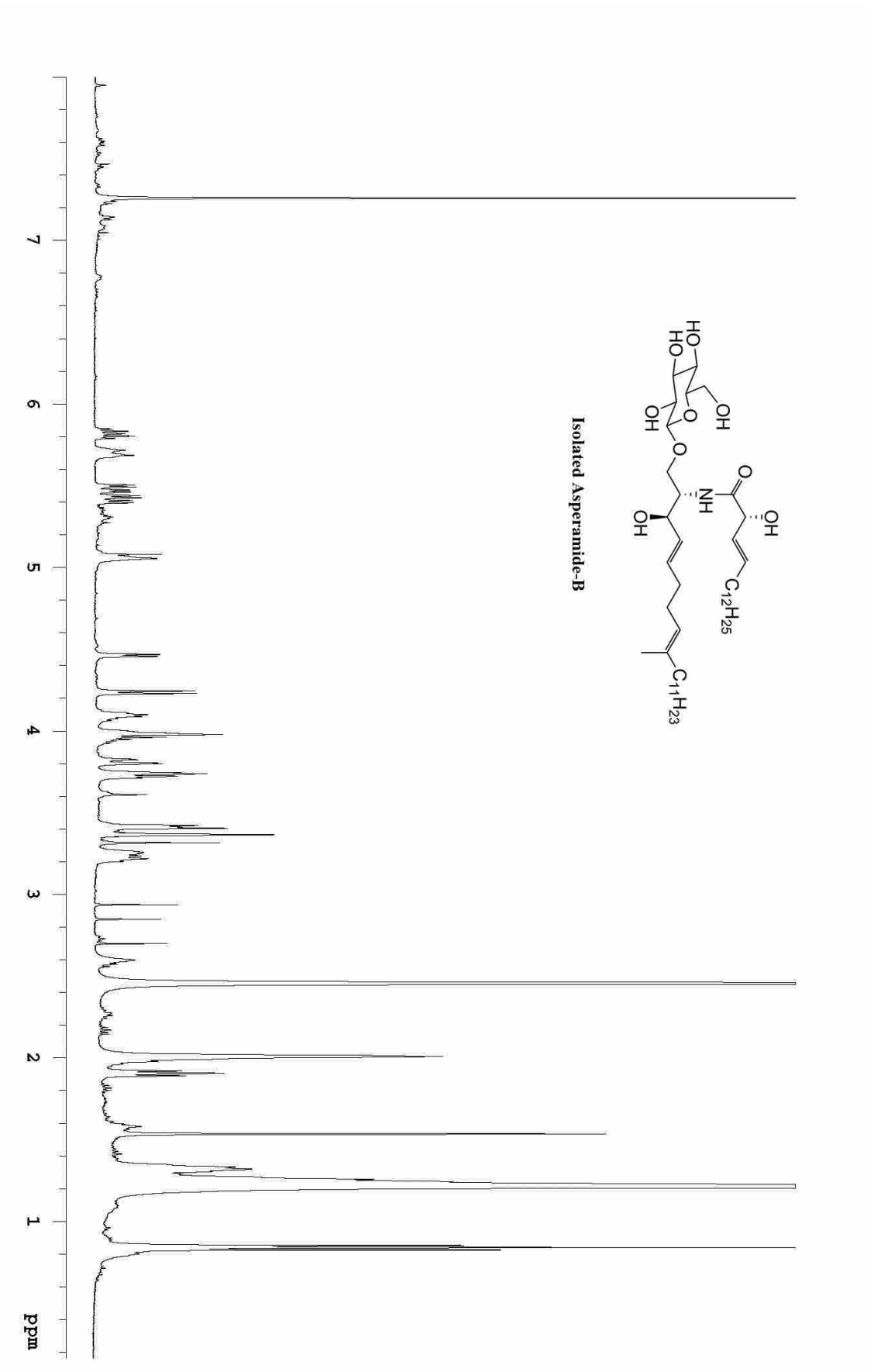
Isolated Asperamide-B
7
6
5
4
3
2
1
ppm

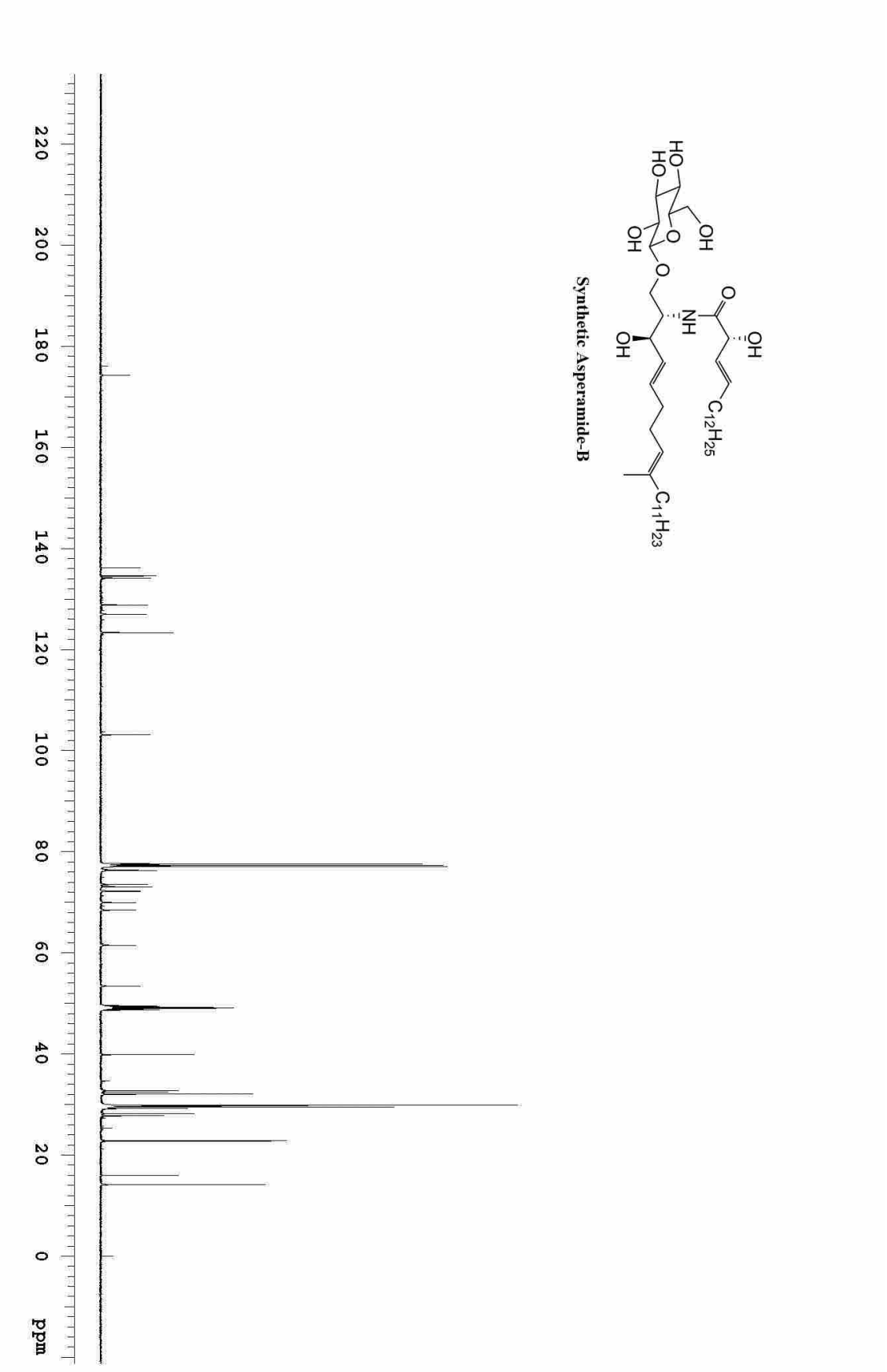
Synthetic Asperamide-B
ppm
220
200
180
160
140
120
100
80
60
40
20
0

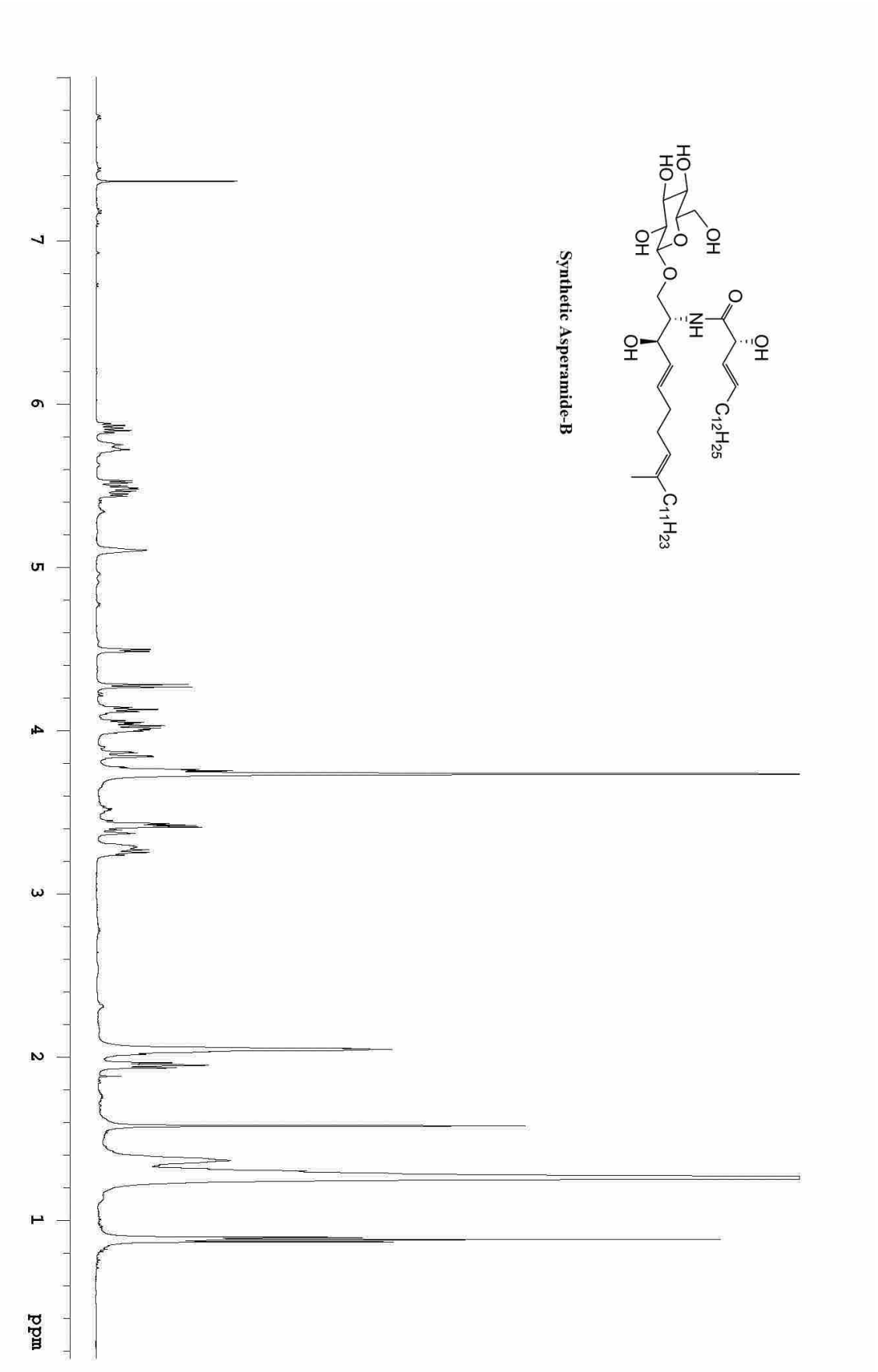
Synthetic Asperamide-B
HO
HO
OH
O
OH
O
NH
OH
OH
$C_{12}H_{25}$
$C_{11}H_{23}$
7
6
5
4
3
2
1
ppm

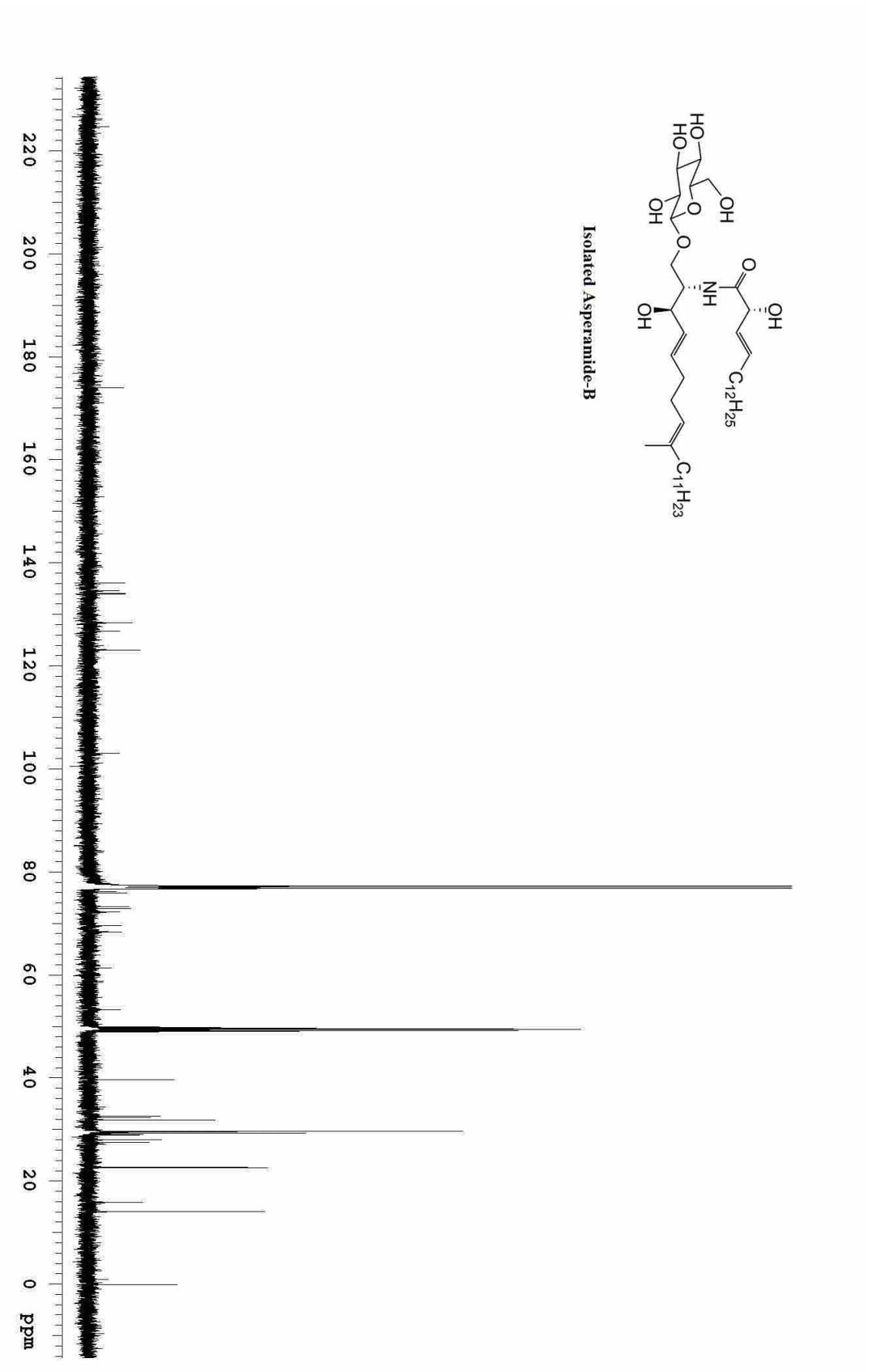
Isolated Asperamide-B
HO
HO
OH
O
OH
O
NH
OH
OH
$C_{12}H_{25}$
$C_{11}H_{23}$
220
200
180
160
140
120
100
80
60
40
20
0
ppm

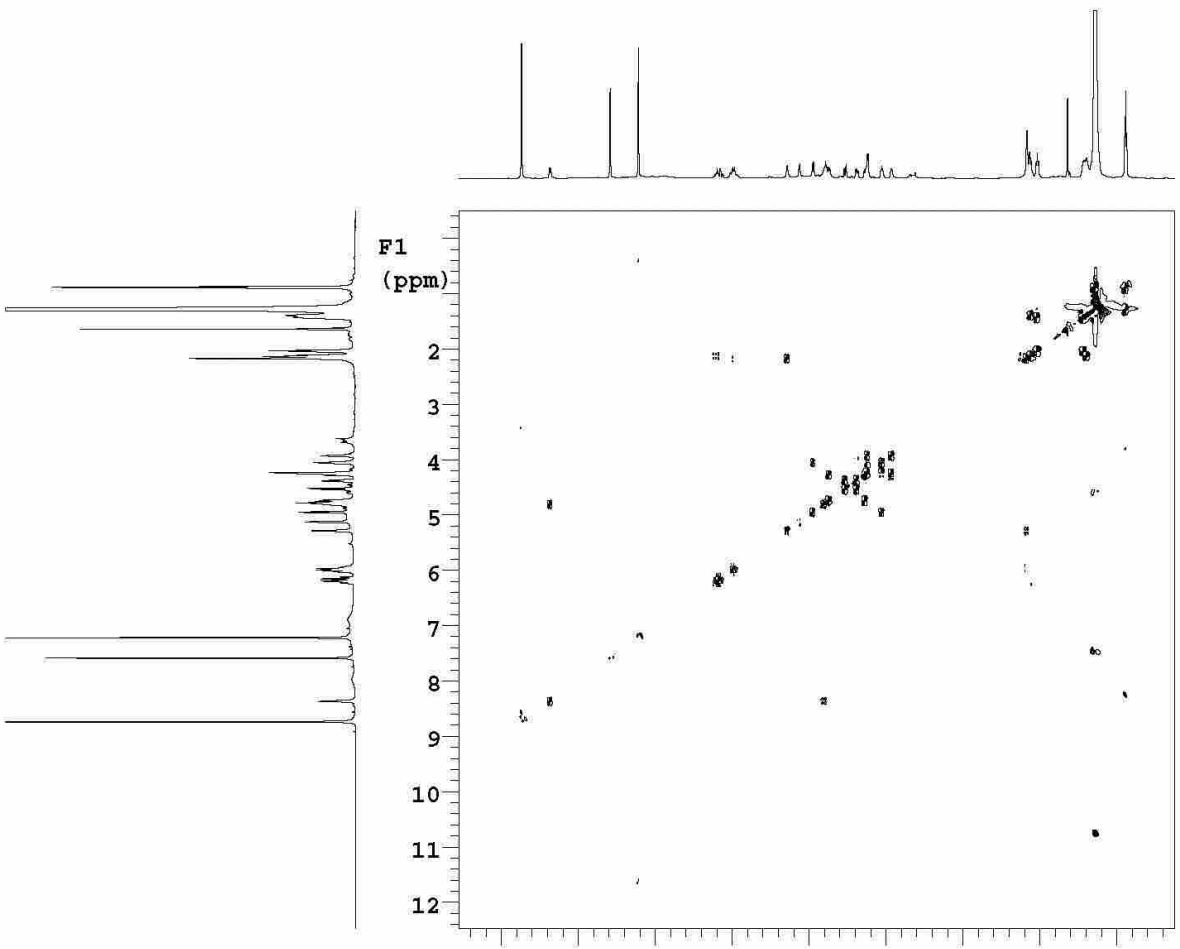

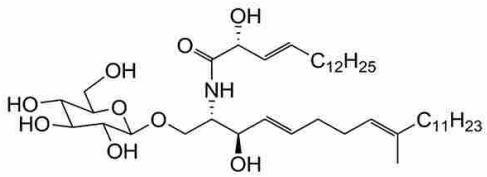

COSY of Isolated Asperamide-B

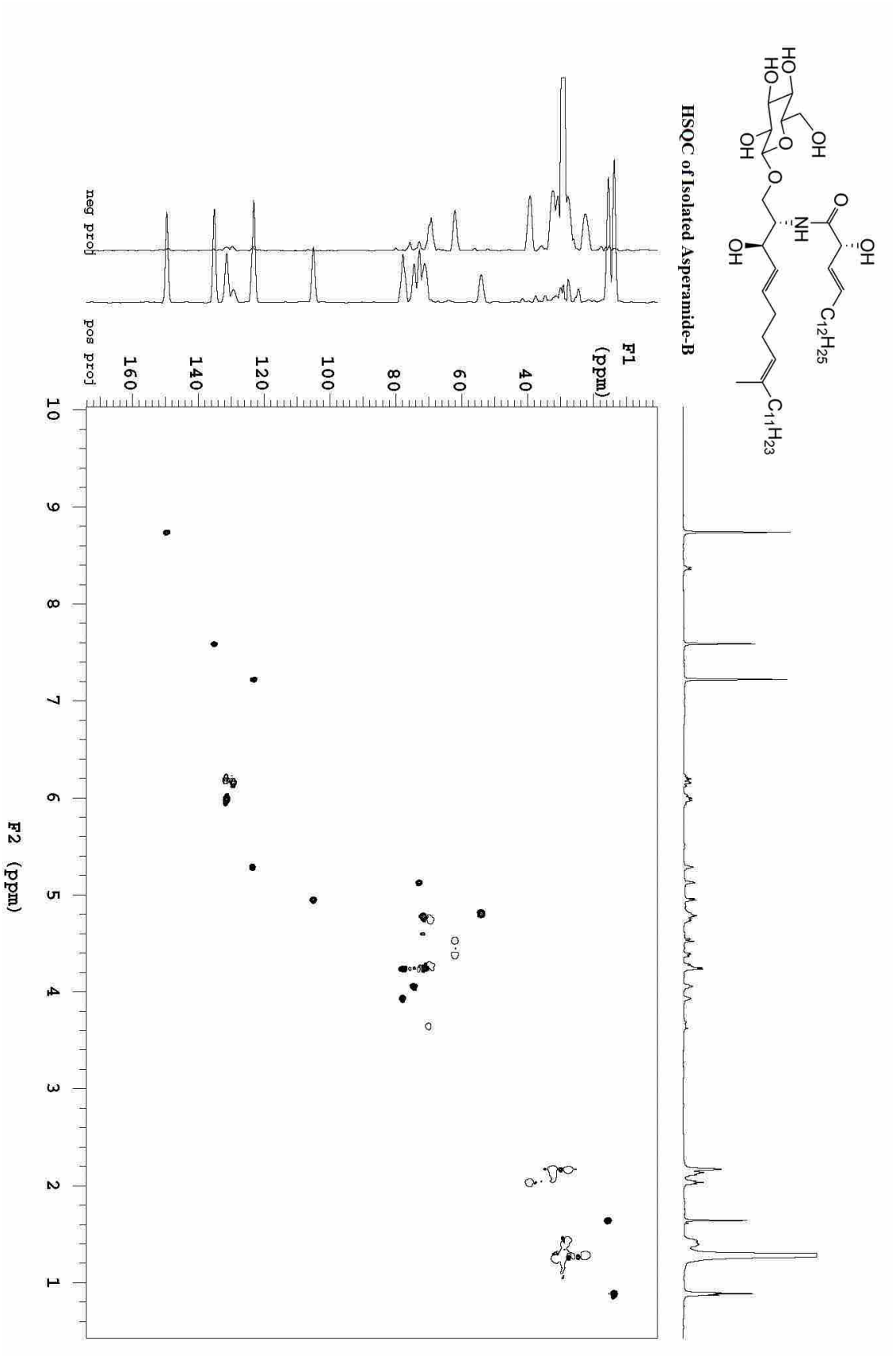
HSQC of Isolated Asperamide-B
F1 (ppm)
F2 (ppm)
pos proj
neg proj

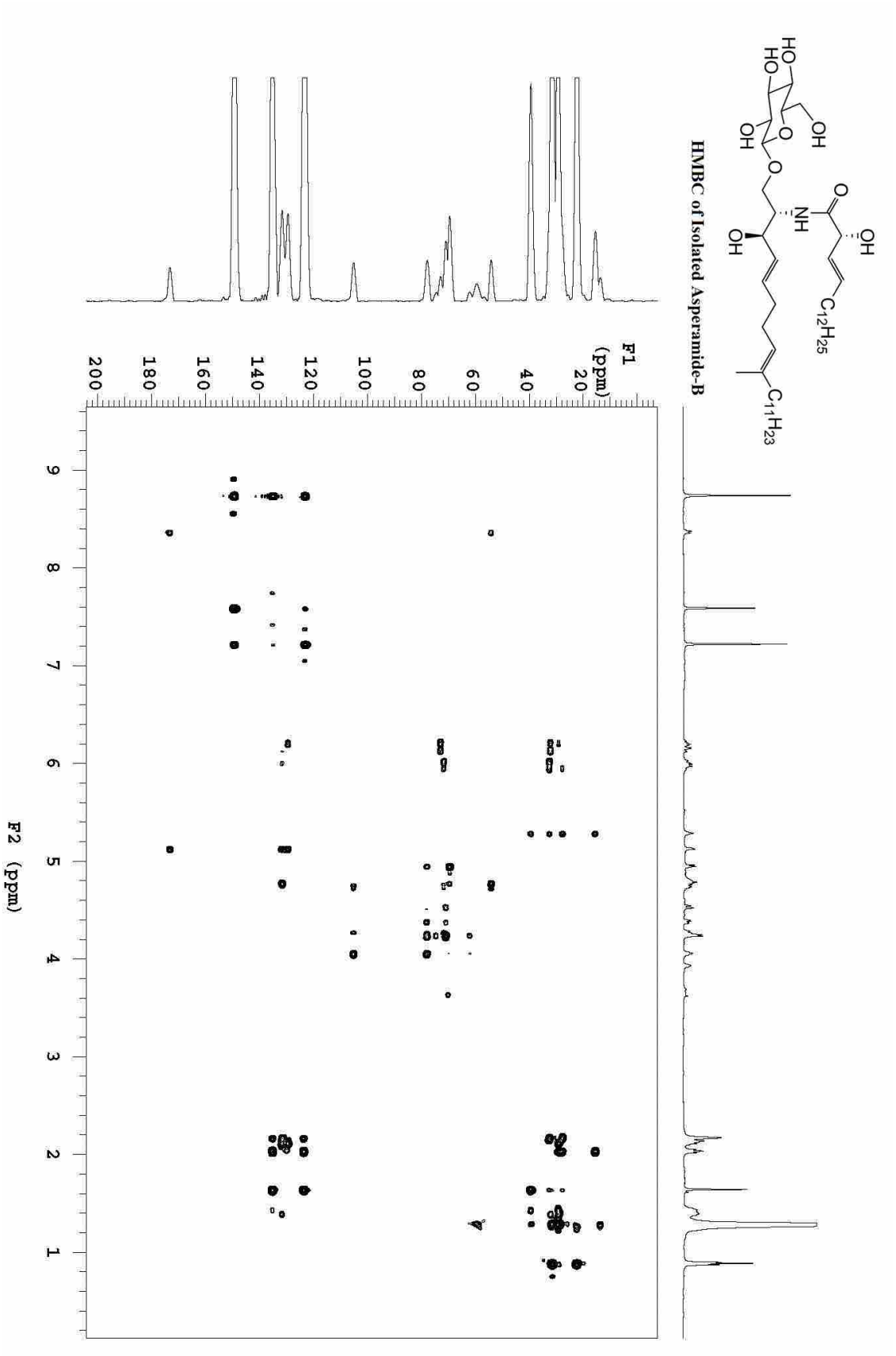
HMBC of Isolated Asperamide-B
F1 (ppm)
F2 (ppm)

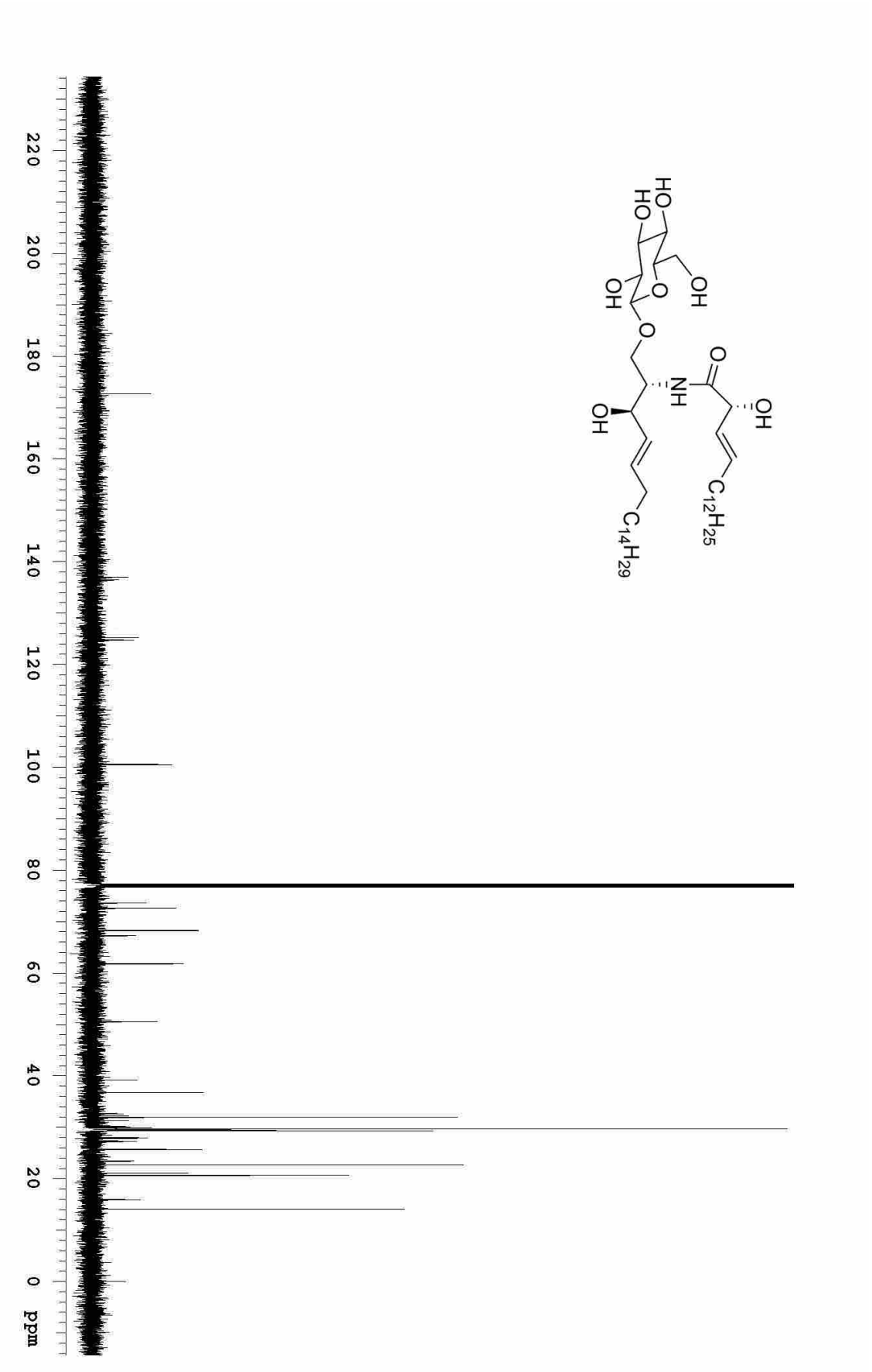
HO
HO
OH
O
OH
O
NH
OH
OH
$C_{12}H_{25}$
$C_{14}H_{29}$
220
200
180
160
140
120
100
80
60
40
20
0
ppm

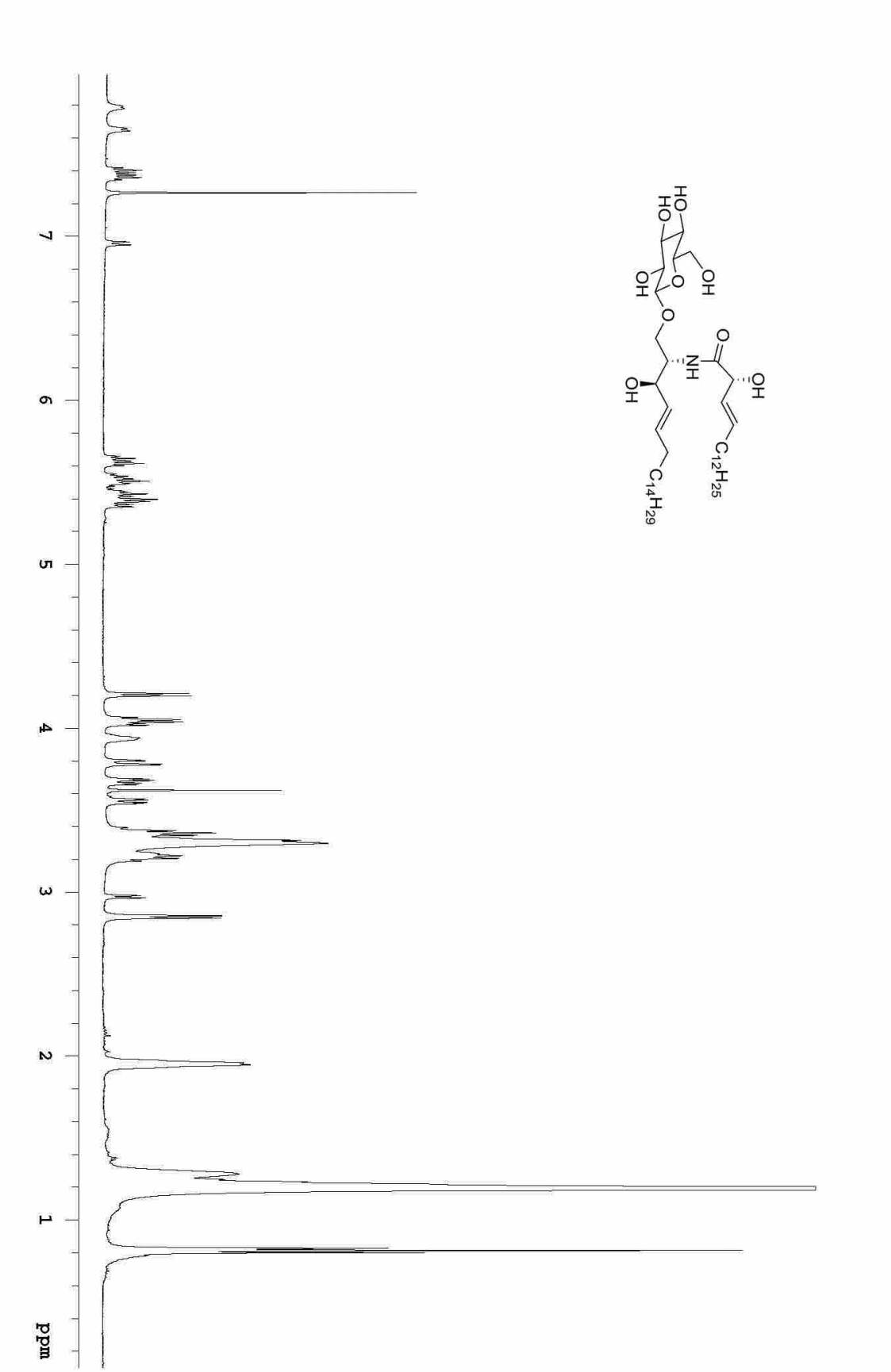
HO
HO
OH
O
OH
O
NH
OH
OH
$C_{12}H_{25}$
$C_{14}H_{29}$
7
6
5
4
3
2
1
ppm

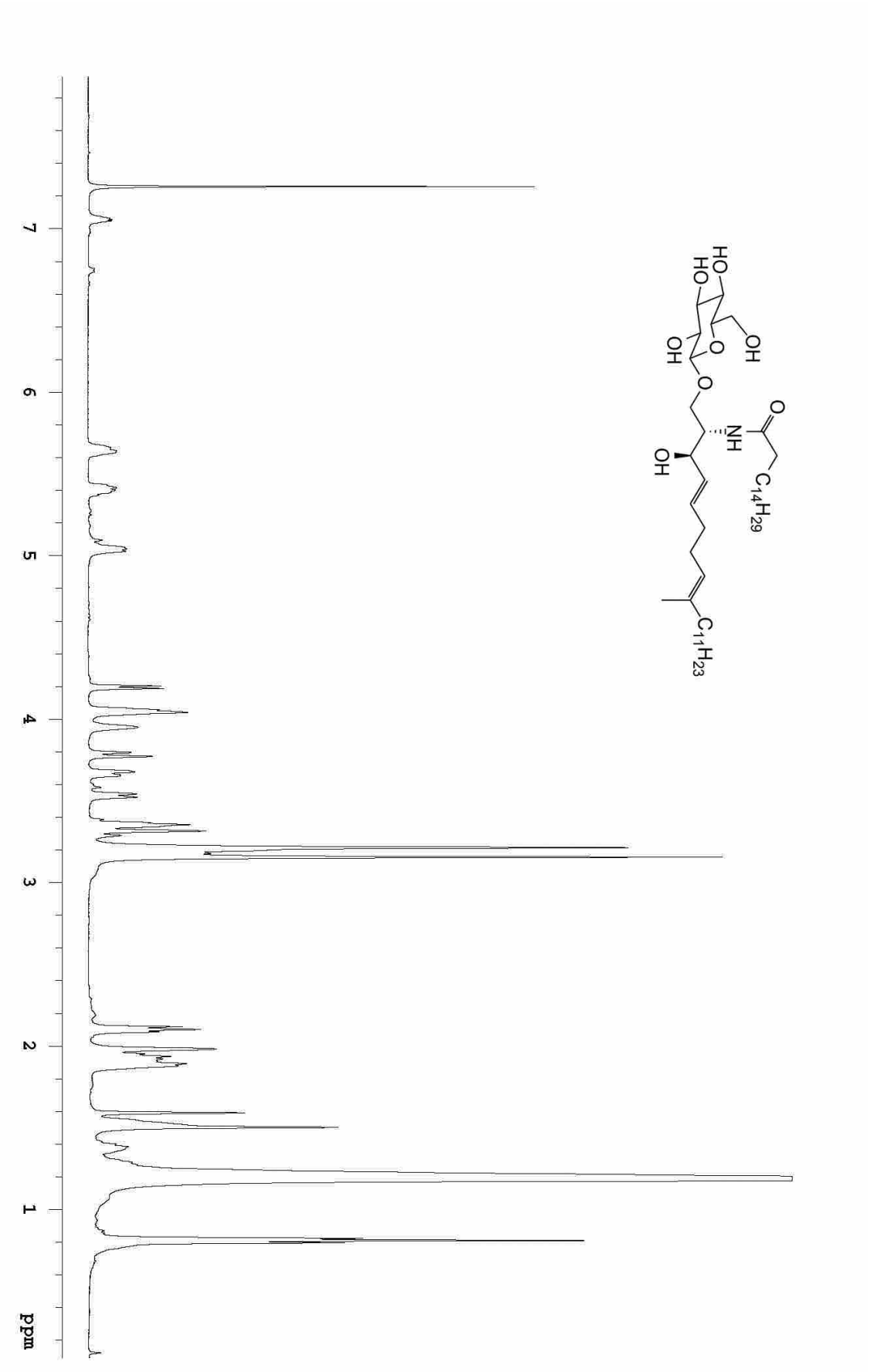
HO
HO
OH
O
OH
O
NH
OH
C14H29
C11H23
7
6
5
4
3
2
1
ppm

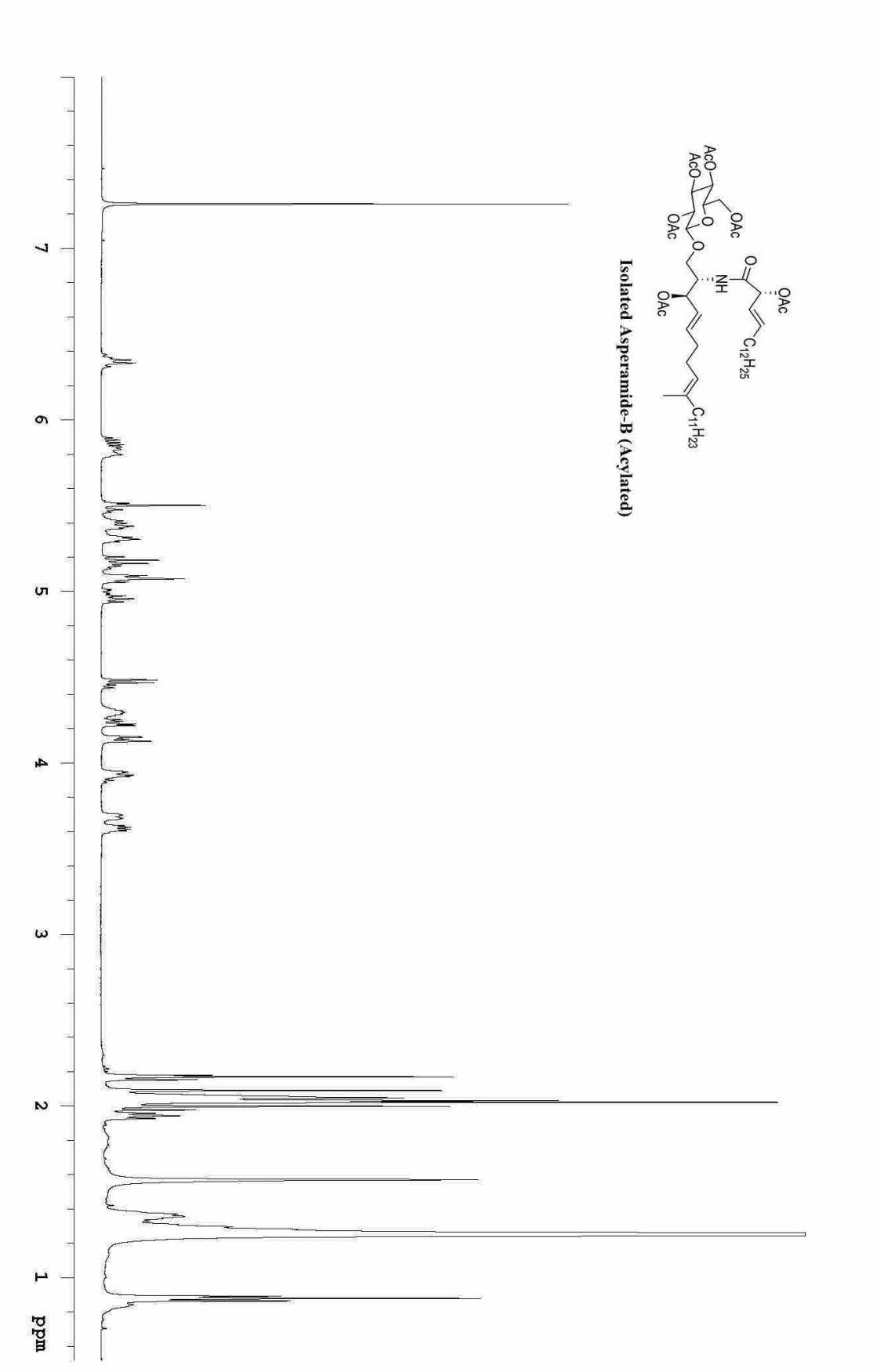
Isolated Asperamide-B (Acylated)
AcO
AcO
OAc
OAc
O
NH
OAc
OAc
$C_{12}H_{25}$
$C_{11}H_{23}$
7
6
5
4
3
2
1
ppm

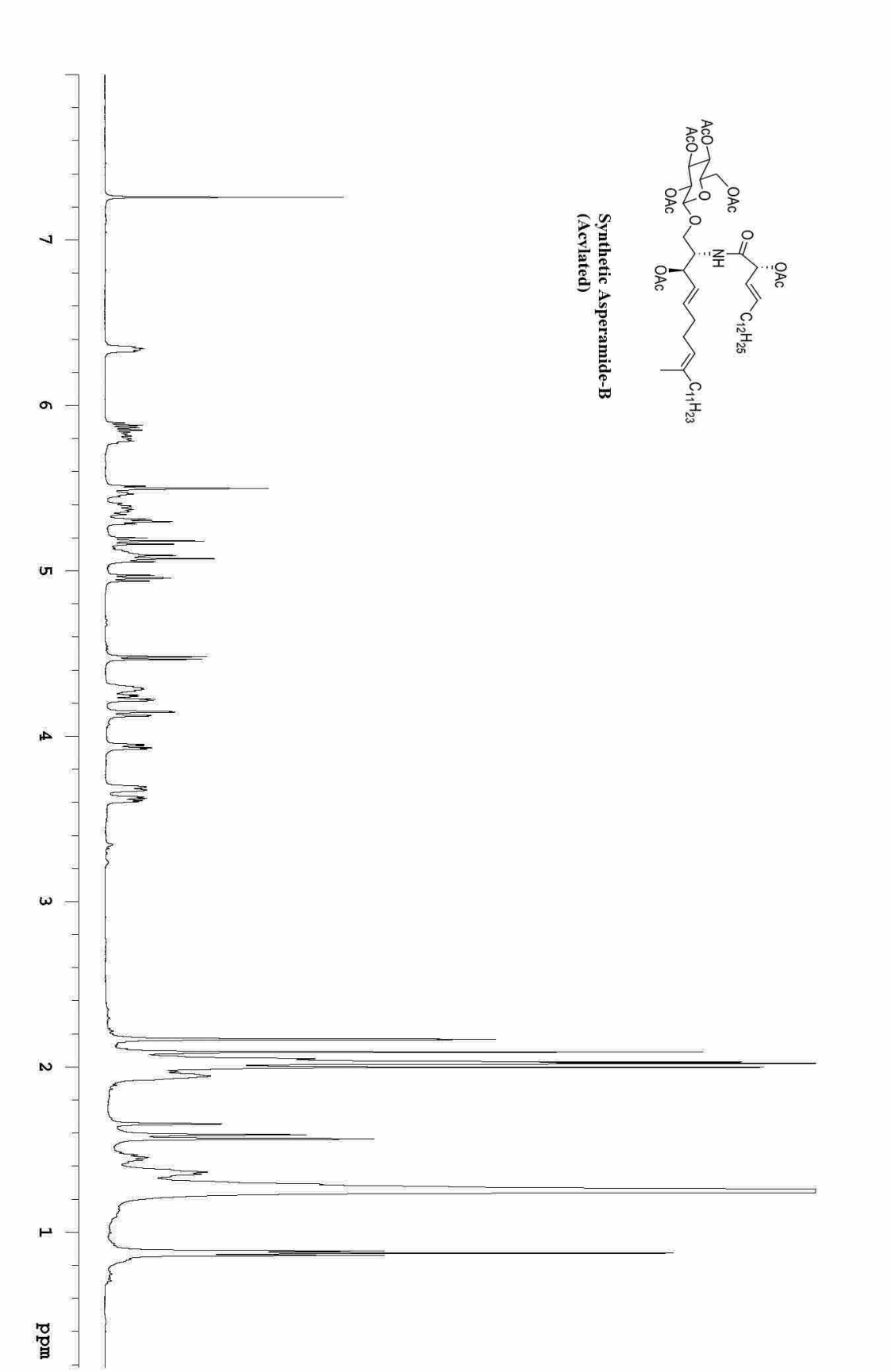
Synthetic Asperamide-B
(Acylated)
AcO
AcO
OAc
OAc
OAc
NH
OAc
OAc
$C_{12}H_{25}$
$C_{11}H_{23}$
7
6
5
4
3
2
1
ppm

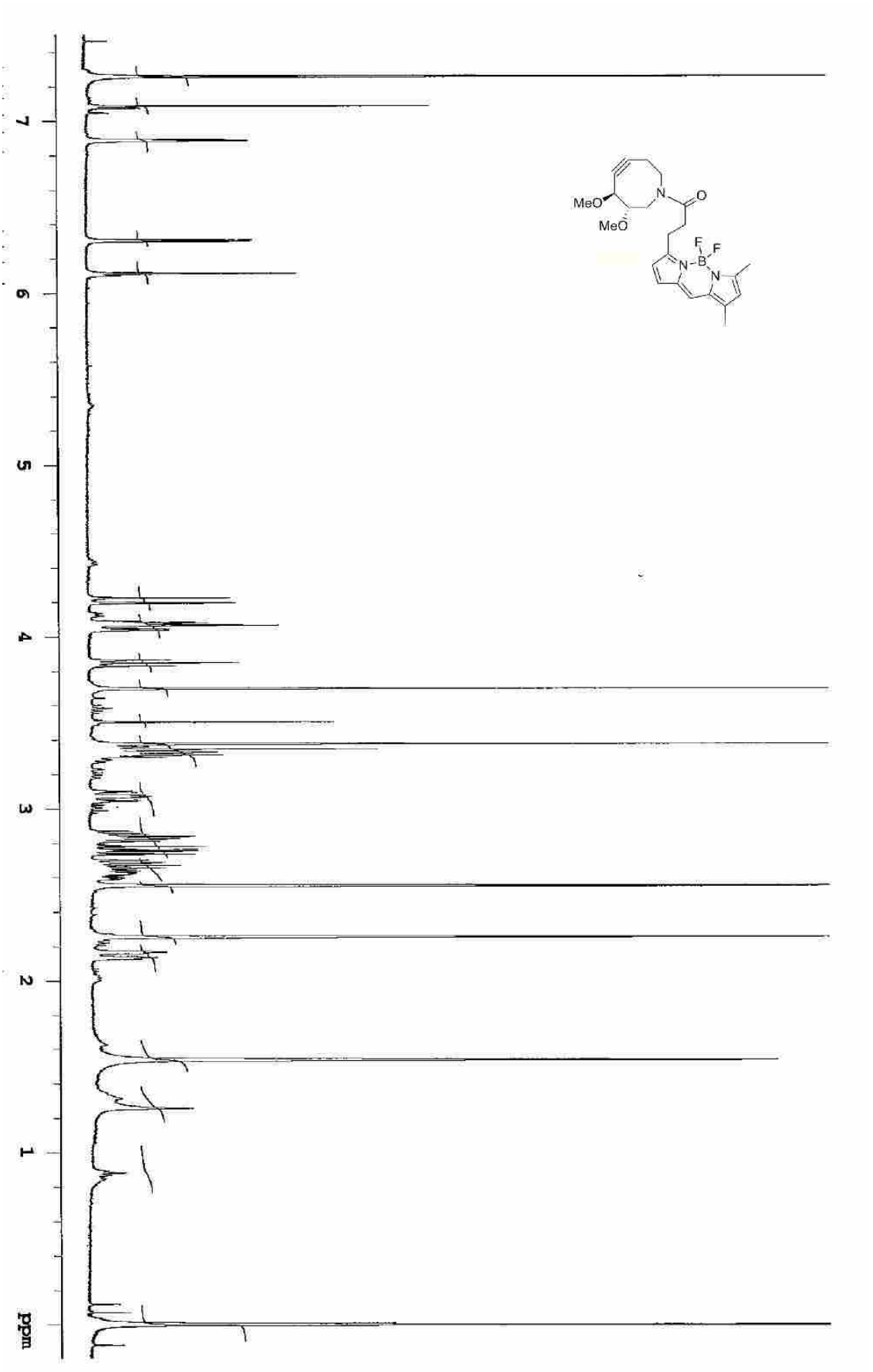
MeO
MeO
N
O
F
F
B
N
N
7
6
5
4
3
2
1
ppm

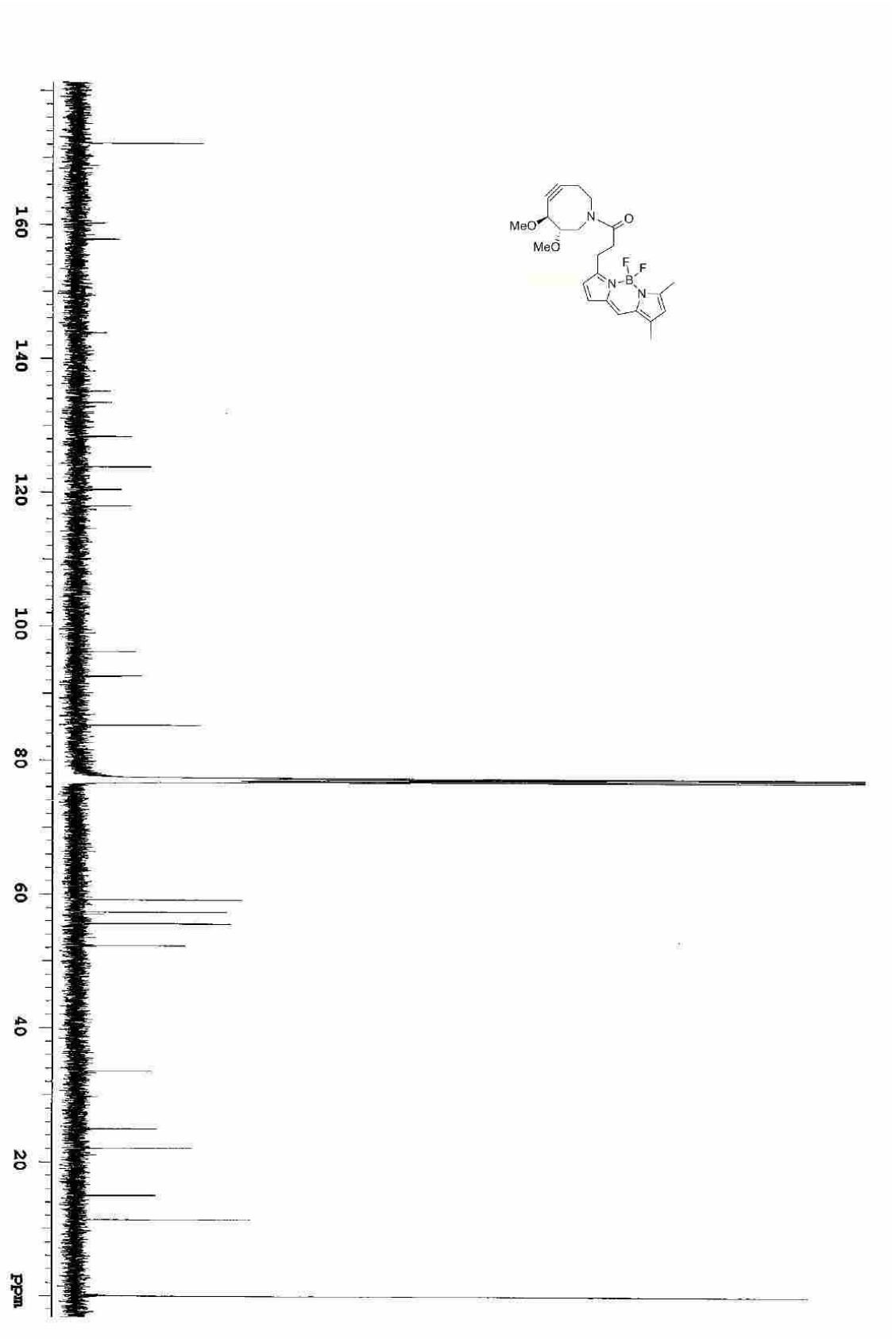
MeO
MeO
N
O
F
F
N
B
N
160
140
120
100
80
60
40
20
ppm